Experimental Investigation of the Acoustic Properties of Perforate using Acoustic Three-Ports

Shail A. Shah

Licentiate Thesis in Vehicle and Maritime Engineering with specialization in Technical Acoustics
School of Engineering Sciences
KTH Royal Institute of Technology
Stockholm, Sweden 2022

Academic thesis with permission by KTH Royal Institute of Technology, Stockholm, to be submitted for public examination for the degree of licentiate in Vehicle and Maritime Engineering, Friday the 28th of October 2022 at 10 hrs, in D3, Lindstedtsvägen 9, Stockholm, Sweden.

TRITA-SCI-FOU 2022:52
ISBN 978-91-8040-381-8

Address:
KTH Royal Institute of Technology
School of Engineering Sciences
Department of Engineering Mechanics
The Marcus Wallenberg Laboratory of Sound and Vibration Research
Teknikringen 8, SE-100 44 Stockholm, Sweden

E-mail:
shail@kth.se

Abstract

This thesis discusses the aero-acoustic characterisation of a perforate sample using a three-port technique. A rectangular T-junction with a flush mounted perforated sample at the intersection form the acoustical three-port. Under acoustic excitation from three different directions a direct method of impedance determination is incorporated to experimentally determine the passive acoustic properties of the perforate. The three-port scattering matrix and the normalised transfer impedance are calculated in the presence of grazing flow and for high-level excitation and the behaviour of these characteristics is studied. Validation of the determined results in the linear range is carried out by comparing it with existing models. Moreover, based on the experimental results for low grazing flow velocities the dependence of the real part of the transfer impedance on the grazing flow parameters as well as dimensionless numbers is described, and a semi-empirical model quantifying the behaviour is proposed.

Furthermore, the thesis explains some experimental errors pertaining to standing wave patterns and operating conditions, and corrections are suggested to reduce the errors.

Keywords:

Duct Acoustics, Acoustical Three-port, Perforated plate, Transfer Impedance, Scattering Matrix, Grazing Flow, High-level Excitation, Non-linear effects, Flow-Acoustic Interaction, Rectangular T-Junction

Sammanfattning

Denna avhandling behandlar aero-akustisk karakterisering av en perforerad platta med en tre-portsteknik. En rektangulär T-formad sidogren med den perforerade plattan monterad över öppningen till sidogrenen bildar den akustiska tre-porten. Med användning av akustisk excitation från tre olika riktningar har en direkt metod för bestämning av de passiva akustika egenskaperna för den perforerade plattan utvecklats. Spidningsmatrisen för den akustika tre-porten och den normaliserade transferimpedansen beräknas för fall med strykande medelströmning och excitation med hög ljudnivå. Variationen hos spidningsmatrisen och transferimpedansen för olika strömningshastigheter och nivåer av akustisk excitering har undersökts. De erhållna resultaten har validerats genom jämförelse med befintliga modeller. Baserat på experimentella resultat för låga strömningshastigheter visas hur transferimpedansens realdel – resistansen - beror av strömningsprofilparametrar och dimensionslösa tal. Baserat på detta föreslås en semi-empirisk modell för resistansen.

Vidare behandlar denna avhandling vissa experimentella fel relaterade till stående vågor och driftsförhållanden, och metoder rekommenderas för att minska felen.

Nyckelord:

Kanalakustik, akustisk tre-port, Perforerad platta, Transferimpedans, Spridningsmatris, Strykande strömning, Excitering med hög ljudnivå, Icke-lineära effekter, Växelverkan mellan ljud och strömning, Rektangulär t-koppling

Licentiate Thesis

This licentiate thesis consists of and introduction with a summary of the following papers:

Paper A

S.A. Shah, H. Bodén, S. Boij, and M.E. D'Elia *Three-port measurements for determination of the effect of flow on the acoustic properties of perforates*, AIAA AVIATION FORUM, August 2021. DOI: 10.2514/6.2021-2269

Paper B

S.A. Shah, H. Bodén and S. Boij, *Nonlinear three-port measurements for the determination of high-level excitation effects on the acoustic properties of perforates*, 28th AIAA/CEAS Aeroacoustics Conference, June 2022. DOI: 10.2514/6.2022-2928

Paper C

S.A. Shah, H. Bodén and S. Boij, *An experimental study on the acoustic properties of a perforate using three-port measurements*, submitted to the Journal of Sound Vibration, October 2022.

Division of work between authors

S.A. Shah performed the experiments, analysis, and produced the papers. The work was supervised, regularly discussed with, and supporting directions were provided by H. Bodén and S. Boij. In Paper A, M.E. D'Elia assisted with the post-processing and analysis. The co-authors also reviewed the papers written.

The content of this thesis has also contributed to the following publications not included here:

- S. Shah, H. Bodén and S. Boij, *Experimental study on the acoustic properties of perforates under flow using three-port technique*, Proceedings of the 27th International Congress on Sound and Vibration, ICSV 2021, Prague (Online), July 2021.

- S.A. Shah, H. Bodén and S. Boij, *Study on the Effect of Operating Conditions on Acoustic Three-Port Measurements of Perforates in presence of Grazing Flow*, Proceedings of the 51st International Congress and Exposition on Noise Control Engineering, Glasgow, August 2022.

- S.A. Shah, H. Bodén and S. Boij, *Flow Acoustic Interaction In A Rectangular T-Junction With Mounted Perforate Using Acoustic Three-Port Measurements*, Proceedings of the 51st International Congress and Exposition on Noise Control Engineering, Glasgow, August 2022.

This work is part of the Marie Skłodowska-Curie Initial Training Network Pollution Know-How and Abatement (POLKA). We gratefully acknowledge the financial support from the European Commission under call H2020-MSCA-ITN-2018 (project number: 813367).

"… the future is in your pen, ink to paper now begin."

-Michael Amott

Contents

Nomenclature

Δp	Acoustic pressure difference across perforate sample, Pa
u	Particle velocity, $m \cdot s^{-1}$
$\Re_x$	Normalised resistance under excitation from duct – x
χ	Normalised reactance
Z	Transfer impedance, $Pa \cdot s \cdot m^{-1}$
$\overline{Z_x}$	Normalised transfer impedance under excitation from duct- x
i	Unit imaginary number $\sqrt{-1}$
t	Perforate Thickness, m
σ	Porosity
d	Hole diameter of perforations, m
M	Mach number
f	Frequency, Hz
u_τ	Skin-friction velocity, $m \cdot s^{-1}$
u_{rms}	Root mean squared value of in-hole particle velocity, $m \cdot s^{-1}$
U	Grazing flow bulk velocity, $m \cdot s^{-1}$
SNR	Signal-to-noise ratio
p	Acoustic pressure, Pa
$p_x^{\pm}$	Propagating wave pressures in duct - x, Pa
k	Wavenumber, m^{-1}
ω	Angular Frequency, $rad \cdot s^{-1}$
c	Speed of sound in air, $m \cdot s^{-1}$
γ_S	Ratio of specific heats
T	In-duct temperature, K
d_{eq}	Equivalent diameter of rectangular cross-section of ducts, mm
Sh	Shear number
L_x	Width of the ducts, 25 mm
L_y	Height of the ducts, 120 mm
Pr	Prandtl Number
s	Microphone distances, m
ΔP_{Flow}	Difference in dynamic and static pressure of the flow field, Pa
ρ_0	Density of air at given temperature, $kg \cdot m^{-3}$
x^+	Normalised distance from duct wall
ν	Kinematic viscosity, $m^2 \cdot s^{-1}$
β_U	Empirical coefficient to determine grazing flow profile in the buffer layer
κ	Von Kármán constant, 0.384

U_{max}	Grazing flow velocity at the centre of the duct cross-section, $m \cdot s^{-1}$
Re_m	Grazing flow Reynolds number
$S - Matrix$	Three-port scattering matrix
ρ_x	Scattering matrix reflection coefficient of duct - x
$\tau_{x \to y}$	Scattering matrix transmission coefficient from duct – x to duct - y
V_{rms}	Root-mean-squared value of excitation voltage, V
S_i	Sensitivity of microphones $mV \cdot Pa^{-1}$
V_{AS}	Auto-Spectrum of the excitation voltage, V^2
L_w	Correction factor for Hanning window
FFT	Fast-Fourier Transform
C_d	Discharge coefficient of the perforate
θ_{DC}	DC flow resistance of the perforate
ΔP_{DC}	Pressure difference across perforate under constant bias flow, Pa
u_{DC}	In-hole constant bias flow velocity through the perforate, $m \cdot s^{-1}$
λ	Wavelength, m
St_u	Strouhal number based on the in-hole particle velocity
C_v	Vena-contracta factor of the perforations
$\Re_{NL}$	Non-linear part of the normalised resistance
$\Re_{Lin}$	Normalised resistance in the linear regime
$\Re_{Flow}$	Linear range normalised resistance in presence of grazing flow
ξ, ζ, ϵ	Empirical coefficients describing resistance in presence of grazing flow
St_U	Strouhal number based on the grazing flow velocity
ψ	Scaling coefficient proposed to account for the relative incidence direction
$\Re_{NL-Flow}$	Non-linear part of the normalised resistance in presence of grazing flow
α, β, γ	Coefficients of the 2nd degree polynomial relationship

Chapter 1: Introduction

1.1 Background

The passive acoustic characterisation of a perforate plate has been studied in this thesis. Perforated plates are an integrated part of noise control systems such as mufflers and acoustic liners. They work on the principle of converting the kinetic energy of incoming acoustic waves into thermal energy using thermo-viscous dissipation. When a sound wave propagating in air passes through a perforate plate, due to a smaller open area of the perforations, a substantial increase in its particle velocity is observed. This results in an increase in the frictional losses, and effectively, a broadband sound attenuation.

Traditionally, in an acoustic liner, a perforated plate in combination with a specific-frequency-designed cavity, targets the tonal noise of an aircraft engine fan. In case of high frequency noise, the wavelength of the incoming sound waves is in the range of the dimensions of the duct. This leads to a higher mode propagation and destructive interferences of the sound waves, leading to higher sound attenuation. However, the challenging part of designing a perforate is to optimise its performance at lower frequencies. Hence it is necessary to characterise the perforate in the plane wave frequency region. Additionally, the acoustic liners are typically attached circumferentially to the nacelle of an aircraft engine. Thus, the standard operating conditions of a perforate involve a grazing flow, and a high-level noise incidence (> 120 dB). It is therefore also necessary to study the effect of these operating conditions on the perforate characteristics.

In presence of grazing flow, there is a formation of a boundary layer over the perforated surface. This results in a complex flow-acoustic interaction in this boundary layer region and affects the passive acoustic response of a perforate. Higher order simulations to map the sound field near the perforate surface require a lot of time and resources. Hence, experimental methods are a cheaper alternative to characterise the perforate in presence of grazing flow. The other operating condition of interest is the behaviour of the perforate under high-level excitation. A high-level incidence results in higher particle velocity of the propagating sound wave. The velocity is further increased due to the smaller open area of the perforated surface, and hence vortex shedding is observed at the edges of the holes [1]. This additional loss of the kinetic energy due to vortices hence results in a non-linear response of the perforate and is necessary to characterise.

A huge increase in commercial air travel over the last few decades has resulted in an extensive study of the acoustic properties of perforates. The acoustic characteristic of interest in this thesis is the real part of the transfer impedance of the perforate. The transfer impedance of a perforate is, as the name suggests, the amount by which the incoming sound wave is impeded, i.e., either reflected or absorbed. Mathematically, it is defined as the ratio of the acoustical pressure difference (Δp) across the sample and the particle velocity ($\hat{u}$) of the sound wave in the direction normal to its surface. It consists of a real part, the resistance ($\Re$), and an imaginary part, the reactance (χ). Physically, the resistance depicts the dissipation of the incoming sound waves, and the reactance depicts the phase change created by the thickness of the perforate, present in the propagation path of the sound waves. At lower frequencies, the wavelength of the incident acoustic waves is comparatively much larger than the thickness of the perforate. As mentioned in the above paragraph, optimisation of the perforate is necessary in the low frequency region. Hence the focus of the thesis is to study attenuation under low frequency acoustic excitation, and the main characteristic of interest in the thesis is only the resistance.

Crandall [2] proposed theoretical models to judge the performance of perforates as early as 1927. Over the years, various measurement techniques and experimental results have studied perforated plates using various approaches and governing equations. This has been done to help design perforated plates and have the required attenuation at the operating conditions. However, till date there are pertaining questions in the scientific community related to passive acoustic characterisation of the perforates. In presence of grazing flow, a difference in the response of the perforate when the excitation is from either the upstream or the downstream direction of the grazing flow is observed. This is a major unresolved question. Additionally, the dependence of the transfer impedance on the excitation frequency, flow profile parameters, as well as the response to high-level acoustic excitation needs further investigation. Hence, a new experimental technique is used in this thesis to contribute experimental results for further investigation. The objective of the thesis is explained in the following subsection.

1.2 Objective

The current research delves into answering the questions regarding the dependence of the perforate resistance under standard operating conditions, on the excitation direction, frequency, and excitation level. The objective of this thesis is to introduce a three-port technique for providing experimental results which can further help understand these dependencies. Usage of the three-port technique helps in characterising the perforate sample under low frequency plane wave excitation from three directions and in presence of grazing flow. Experiments on an empty T-Junctions using the three-port technique have been carried out by Karlsson and Åbom [3] and Holmberg et al. [4]. Using these studies as a foundation, a perforate is flush mounted at the intersection of the T-Junction and the three-port multi-microphone method is used to characterise it. The Scattering matrix ($S - Matrix$) as well as the resistance ($\Re$) of the perforate are experimentally determined. An explanation of the measurement method and the acoustic characteristics is given in the latter sections of this thesis.

Post-processing the acquired experimental data, the characterisation of the resistance in presence of grazing flow with respect to dimensionless numbers is carried out in an effort to study its frequency dependence. Moreover, on the addition of high-level excitation, at lower grazing flow velocities characterisation of the non-linear part of resistance is carried out to show its dependence on the ratio of particle velocity and the grazing flow velocity. Results from the three-port experiments are to provide credible experimental data and further the optimisation of the aero-acoustic performance of perforate.

1.3 Methodology

The characterisation of the perforate sample using the three-port technique has been carried out in this thesis. The methodology follows the flow chart shown in Figure 1. Four testing conditions are considered and results of each are mentioned in section 4.

Firstly, to validate the results obtained using the three-port technique, a reference value of the acoustic characteristics of the perforate is needed. These reference values are experimentally determined by studying the perforate in a geometrically simpler two-port setup of an impedance tube. On comparing the two-port results with the three-port results, in absence of grazing flow and in the linear level excitation range, validation of the results of the three-port technique is done. The next test case considered is the non-linear behaviour of the resistance in absence of grazing flow, the value of the resistance determined in the linear range is used as an input and under high-level excitation the non-linear part of the resistance is compared against a model proposed by Temiz et al. [5].

On addition of the grazing flow, the behaviour of the resistance is studied. A scaling factor is proposed to scale the resistance determined at different grazing flow velocities. Based on the scaled value of resistance, it is shown to be a function of the dimensionless numbers and grazing flow parameters. In the final test case, at three lower grazing flow velocities, non-linear effects are observed under high-level excitation and the behaviour of the non-linear part of the resistance is studied. A dependence of the non-linear part of resistance is seen on the particle velocity, grazing flow velocity and the dimensionless Shear number. Moreover, a limit for the onset of non-linear behaviour in presence of grazing flow is also observed, as discussed in section 4.4.

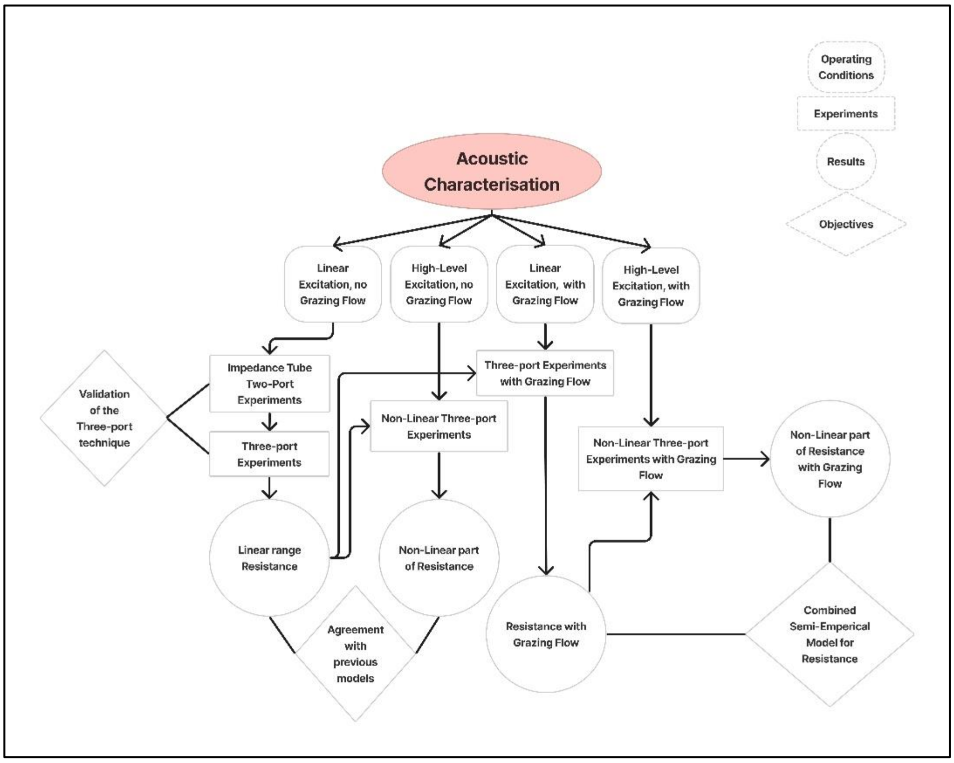

Figure 1 Flowchart of the research methodology

The next section discusses a brief literature review of the research on the acoustic properties of perforates. It should be noted that the research field has been very active over the past 30 years. As a summary of all the research done till date in this thesis is unfeasible, the literature review presented here is only surrounding the objectives of this thesis.

Chapter 2: Literature Review

This section briefly describes the till-date research on the study of the behaviour of the acoustic properties of perforates. Individual effect of the two operating conditions, namely grazing flow and high-level excitation, on the transfer impedance has been studied over the years and the relevant parts of the research, are summarised in the first subsection. The second subsection classifies the experimental methods used over the years to study the perforates into two categories. Advantages and limitations of both categories are discussed and differences in the results of both methods are noted.

2.1 Acoustic Characteristics of a Perforate

The initial research on the use and characterisation of perforates were carried out by Crandall [2], where the perforate is assumed to be a lumped spring-mass system and its behaviour is analytically studied. Sivian [6] a little later in the timeline studied small orifices individually, specifically their non-linear behaviour under high-level excitation. A study by Ingård [7] provided more insight into the experimental determination of perforate properties, namely the transfer impedance (Z) and absorption coefficient. Based on Crandall's theory and Ingård's [7] experiments, Guess [8] proposes a semi-analytical model for the normalised transfer impedance as a function of, among other quantities, the perforate thickness (t), porosity (σ), and the diameter of the perforations (d). The normalisation of the transfer impedance is done with respect to the characteristic impedance of air, in order to make it an independent property of the sample.

As the majority of the perforates applications involve an exposure to grazing flow, various studies model the transfer impedance of the perforate in a variety of setups with grazing flow. The grazing flow creates a shear layer on top of the perforate surface. This shear layer creates an additional pressure on the side of the perforate exposed to the flow. Hence the overall transfer impedance increases in value. Models by Guess [8], Rice [9], and Rao and Munjal [10], propose the real part of the normalised transfer impedance, i.e., the resistance ($\Re$) to have a linear proportionality on the grazing flow Mach number (M), and to be independent of the excitation frequency (f). On the other hand, Kooi and Sarin [11], Kirby and Cummings [12], and Cummings [13] suggest the resistance to be a function of the skin-friction velocity (u_τ), as well as the frequency. A summary of the above-mentioned models is finely presented by Elnady and Bodén [14]. The variety of the experimental results raise the question of which parameter to consider while describing the resistance of the perforate in presence of grazing flow, and its dependence on frequency. This question is discussed in appended Paper C, as well as in section 4.3 in the thesis.

Under high-level excitation, the increase in dissipation is due to the vortex shedding at the perforation edges. This vortex shedding occurs at higher particle velocities and hence, a clear dependence of the resistance on the in-hole particle velocity (u_{rms}) is observed in majority of the research. Results shown by Sivian [6], Ingård [7], Ingård and Ising [15], Melling [16], and Rice [9] are referred to in this thesis. Additionally, all the referred research determines the non-linear part of the transfer impedance and adds it to the transfer impedance determined in the linear range. Temiz et al. [5] summarise the nature of the dependence of the non-linear part of transfer impedance on the in-hole particle velocity in different regimes. They also propose a semi-analytical model in the transition state from a weakly non-linear regime to a strongly non-linear regime. Comparison with this model is shown in the thesis and its limitations are discussed in section 4.2. On the addition of grazing flow at low velocities, the non-linear behaviour under high-level excitation is characterised in Renou [17], as well as Elnady and Bodén [14]. Both the studies individually characterise the effect of high-level excitation and find it to be independent of the grazing flow parameters. However, experimentally determined results, as shown in section 4.4 of this thesis and appended Paper B, show that the non-linear part of the resistance to be also a function of the grazing flow velocity (U).

2.2 Experimental Methods

As the description of the behaviour of the transfer impedance is heavily contested, experimental results in a variety of setups and using multiple measurement techniques have been studied. The majority of the measurement methods are used to study the entire acoustic liner and can be broadly classified into two categories.

The first category includes direct methods, which involve the acquisition of the acoustic pressure difference across the perforate and estimation of the acoustic particle velocity. There is no prediction of the acoustic field near the sample, as well as the usage of any flow-acoustic boundary conditions in determining the transfer impedance of the sample being avoided. In the *in-situ* measurement method, the acquisition of the acoustic pressure above the perforate can be done by a traversing microphone in the direction normal to the perforate plate surface, whereas the pressure below the perforate is measured using a microphone in the backplate of the liner cavity. To compensate for the blocked volume of the traversing microphone in the cavity of the liner, as shown in Bonomo et al. [18], a factor must be introduced in the impedance calculation. This in-situ technique as used by Dean [19], Zandbergen [20], and Gaeta et al. [21] leads to a better signal-to-noise ratio (SNR) in the presence of grazing flow. Another direct method involves using an impedance tube in a branch-type setup. Feder and Dean [22], as well as Dickey et al. [23] determine the transfer impedance using an acquired pressure difference across the perforate and calculate the particle velocity. Under the assumption of linear wave propagation in the branched duct, the two-microphone method is used to determine the particle velocity. Similar to the in-situ method, a higher value of SNR is obtained, however the determined transfer impedance is susceptible to the errors pertaining to the standing wave pattern in the branch. It should be noted that in the branch-type method, acquisition of the acoustic pressure is carried out in the far field, i.e., the propagating field. Hence the presence of the microphone does not affect the acoustic near field of the perforate sample, and unlike the in-situ method, no correction factor is used in the impedance calculation. The direct methods for impedance determination do not involve the estimation of the complex flow-acoustic field in the perforated region, posing it to be a limitation of the method.

The second category of the measurement methods are called indirect methods of impedance eduction, where the acoustic field propagating across the liner surface is modelled using governing equations. An estimated value of the transfer impedance is used as an input to calculate the sound field and based on the difference between the measured sound field and the estimated field, the actual transfer impedance is inversely calculated. This inverse eduction method is used by Watson and Jones [24]. The other eduction method calculates the wave number over the liner sample using an array of microphones on the opposite wall of the liner surface, also known as the Prony technique. Bodén et al. [25] summarises the studies which use the Prony technique and compares the results of different eduction techniques like the straightforward method [26] and the mode matching method [27]. A common boundary condition used in a majority of the indirect methods is the Myers boundary condition [28], which imposes an assumption of the particle displacement in the shear layer of the flow profile. Although popularly used for impedance eduction, usage of this boundary condition is contested as shown by Renou and Aurégan [29], posing to be a major limitation of impedance eduction methods.

Inspired from the sidebranch-type method [22, 23], this thesis discusses a direct method, i.e., the three-port technique for characterisation of the perforate sample. Hence, a richer and more detailed background to summarise all the available indirect eduction methods with their various governing equations, their accompanying boundary conditions and their individual limitations is beyond the scope of this thesis. To know more in detail about the research done using indirect methods till date, the above-mentioned references can be consulted.

Another study by Bodén et al. [30] compares the results of the direct *in-situ* method along with indirect impedance eduction method. The study finds that the impedance determined using the eduction technique is frequency dependent, whereas in case of the *in-situ* technique no frequency dependence is seen. Moreover, higher values of transfer impedance are seen when the excitation is from the direction downstream with respect to the grazing flow. The later observation is also seen in the majority of the research till date, hence making it necessary to discuss the effect of relative grazing flow and acoustic excitation directions.

As mentioned in section 1.2, this thesis attempts to provide experimental results and hypothesis to answer some of the questions pertaining to behaviour of the resistance curves. The three-port measurement method used to determine the results is discussed in the next chapter.

Chapter 3: Measurement Method

The following chapter outlines the experimental technique used in the thesis. The first subsection discusses the theory behind the wave propagation and the determination of the three-port scattering matrix. Following, the next subsection discusses the schematic of the test rig and basic measures taken to reduce the measurement errors, as well as details of the hardware used for the experiments. The third subsection talks about the determination of the flow profile in the test rig. Based on the determined wave propagation inputs, the passive acoustic characteristics of S-Matrix and the resistance are calculated. Moreover, the correlation between both the characteristics is shown. Finally, the validation of the three-port technique is presented. The errors observed on the implementation of the technique and steps taken to reduce the errors are discussed.

3.1 Theory

The propagation of sound waves in ducts is governed by the wavenumber (k). Theoretically, for plane wave propagation, the wavenumber is defined as the ratio of the angular frequency (ω) and the speed of sound (c). However, to account for the thermo-viscous dissipation of the propagating sound waves, the wavenumber is determined using a model proposed by Dokumaci [31]. It is as described in Eq. (1).

$$k_{\pm} = \frac{\omega}{c}\frac{K_0}{1 \pm K_0 M},$$
$$K_0 = 1 + \frac{\left(\frac{(1-i)}{Sh_{duct}}\right)\left(1 + \frac{(\gamma_S - 1)}{\sqrt{Pr}}\right)}{\sqrt{2}} \quad (1)$$

The subscripts $\pm$ indicate the direction of the propagating waves. The notation in case of the three-port is as shown in subsection 3.2. Assuming room temperature, air in the ducts is treated as calorically perfect, i.e., the ratio of the specific heats (γ) is assumed to be 1.4. The speed of sound is determined using the in-duct temperature (T) and following $c = \sqrt{\gamma_S RT}$. The determination of the Shear number (Sh_{duct}) used to calculate the wavenumber follows Eq. (2). The model by Dokumaci [31] is determined for circular ducts, and in order to use it for rectangular ducts, as is the case in this thesis, the equivalent diameter (d_{eq}) is calculated following Eq. (2). The equivalent diameter d_{eq} is determined by taking the ratio between four times the area of the cross-section, and its perimeter. Over an extended path of propagation, this assumption of the d_{eq} is a source of error. However, the maximum propagation length considered in the test rig is less than 300 mm. Hence, this error is negligible and is ignored in the thesis.

$$Sh_{duct} = d_{eq}\sqrt{\omega/4\nu}\ , d_{eq} = 4L_x L_y/\left(2\left(L_x + L_y\right)\right), \quad (2)$$

In Eq. (2), the lengths $L_{x,y}$ are the two dimensions of the cross-section. As per Eq. (1) the wave number is also dependent on the grazing flow Mach number (M). The determination of the Mach number is shown in subsection 3.3.

Using the determined wavenumbers, the decomposed wave pressures can be calculated to depict the propagating pressure amplitudes in each direction. The two-microphone method, as shown in Seybert and Ross [32] calculates the decomposed wave pressures on the basis of the pressure measured by two axially placed microphones and the distance between them. To minimise the error in wave decomposition, Fujimori et al. [33] suggest an overdetermination of the sound field in the ducts. Following the recommendations, three microphones are used in each duct to measure the acoustic pressure. The calculation of the decomposed wave pressures uses the Moore-Penrose pseudo-inverse matrix [34] and is as shown in Eq. (3).

$$\begin{pmatrix} e^{-ik_+s_1} & e^{ik_-s_1} \\ e^{-ik_+s_2} & e^{ik_-s_2} \\ \vdots & \vdots \\ e^{-ik_+s_n} & e^{ik_-s_n} \end{pmatrix} \begin{pmatrix} p^+ \\ p^- \end{pmatrix} = \begin{pmatrix} p_1 \\ p_2 \\ \vdots \\ p_n \end{pmatrix}, \tag{3}$$

where the subscript n represents the n^{th} microphones in the duct and the distances (s_n) are calculated from the origin point of the acoustic multi-port to the n^{th} microphone.

A necessity for calculating the decomposed wave pressures using Eq. (3) is that the distances between the microphones is not equal to half the wavelength of the incoming sound wave. Åbom and Bodén [35] show that when microphone distances are even close to half the wavelength, the wave decomposition method is sensitive to errors. They hence suggest the criterion for the microphone distance to be following Eq. (4)

$$0.1\pi < k(s_x - s_y)/(1 - M^2) < 0.8\pi, \tag{4}$$

where $s_{x,y}$ are the distances from the individual microphones to the acoustic origin point.

Overdetermination of the acoustic pressure and following the above criterion reduces the error pertaining to the standing wave pattern. However, if a pressure node is present at one microphone location, the results are considerably affected by the experimental error. An example of this error is shown in subsection 3.5.

3.2 Test Rig

As shown in Holmberg et al. [4], a rectangular T-junction can be characterised as an acoustic three-port. Figure 2 shows the 3D schematic of the setup where the perforate is mounted at the intersection. The grazing flow passes from duct-1 to duct-2, while the end of duct-3 is closed. This is done to have no mean flow in duct-3. The cross-section dimension of all the three ducts is 25 mm by 120 mm. Each duct has a flush mounted loudspeaker which produces the required plane wave excitation. Three axially placed and flush mounted microphones in each duct acquire the acoustic pressures under plane wave excitation. Two microphones are placed close to each other with a gap of 55 mm and the third microphone is placed 110 mm away from the first microphone in each duct. The microphone closest to the perforate sample is placed 55 mm away from the centre of the sample in duct-1 and duct-2. For duct-3 to minimise the effect of the grazing flow noise, the closest microphone is placed 214 mm away from the sample. Following the criteria of Eq. (4), the frequency range of the experiments was determined to be from 100Hz to 2250 Hz. The cut-on frequency for the first higher order mode at room temperature, based on the 120 mm dimension of the ducts is ≈ 1400 Hz. However, as the microphones are placed in the centre of the longer dimension, we can assume the plane wave propagation limit as ≈ 2800 Hz. Apart from the three microphones in each duct, one additional microphone is flush mounted at the intersection of ducts -1, and 2, i.e., the wall opposite to the perforate, and opposite the centre of the perforate. The pressure acquired by this microphone is used to determine the difference in the acoustic pressure between the two sides of the perforate and to calculate the transfer impedance. This method of impedance calculation is explained in subsection 3.4.

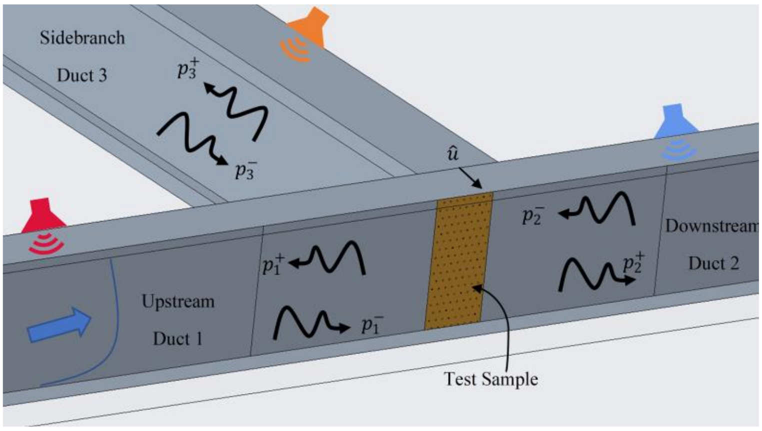

Figure 2 3D schematic of the three-port measurement rig with notations of the acoustic characteristics studied

Using the directly acquired pressure to determine the transfer impedance makes the results susceptible to errors pertaining to the termination reflections. Acoustic reflection from the terminations of the test rig is minimised with mufflers placed at the end of ducts -2 and -3, as a preventive measure. This minimises the errors pertaining to the standing wave pattern at higher frequencies.

Apart from the influence of the standing wave pattern, the presence of flow noise is another major source of error in aero-acoustic measurements. There are two available methods to reduce this random error. The first is to determine the sound field in the ducts with respect to the excitation frequency generated by the loudspeakers. This excitation from the speakers is used as a reference signal and a frequency response function between the microphone and the reference signal is used to determine the sound field in the ducts. The second method is to have an acceptable value of signal to noise ratio (SNR) of the acquired microphone signals. A SNR of at least 20dB was maintained during the measurements at all flow speeds. All the above mentioned remedies are a part of the standard application of the multi-microphone technique and are implemented to improve the quality of the results, as explained in Ref. [36].

The perforate sample studied in this thesis is of glass-fibre material. The perforations are circular in shape with 1.2 mm diameter and have sharp edges. The thickness of the perforate is also 1.2 mm, and the percentage open area approximates 2.54%.

The data acquisition modules used were part of the *National Instruments* CompactDAQ system. The excitation signal was generated using NI 9263 sound card and amplified using the *t. Amp* TSA-4700 amplifier. Loudspeakers of the type *faital PRO* 5FE120 were used. Acquisition of the pressure signals was carried out using 10 calibrated *Brüel and Kjær* ¼- inch 4938 type microphones. Absolute calibration of the microphones was carried out using *Norsonic* Nor1255 calibrator at 114dB and 1000 Hz. The microphone signal was amplified using *Brüel and Kjær* Nexus conditioning amplifiers with a sensitivity of 10 mV/Pa. The acquisition of the amplified microphone signals was done at a sampling frequency of 25.6 kHz using NI 9234 soundcards. Measurements were carried out at room temperature and additionally, the static in-duct temperature in duct-3 was recorded for all the measurements. The temperature was used to determine the speed of sound (c) and for further post-processing. A calibrated K-type thermocouple was used for temperature measurements and the acquisition was done using NI 9213 module. The calibration of the thermocouple was done following the method explained in Peerlings [37] as well as with an in-house resistance temperature detector.

Stepped sine excitation with a resolution of 50 Hz was used as acoustic incidence. For the postprocessing of the acquired signals, the Fast-Fourier Transform (FFT) was used with a Hanning window. The measurement time at each excitation frequency was between 12 to 24 seconds and averaging of the acquired signals was carried out each second. The criteria to select the measurement time, and by extension the number of averages, was to attain a SNR of at least 20dB at each frequency. For the measurements conducted in the linear range, the sound pressure level was maintained to be < 100dB at all frequencies in absence of grazing flow, whereas in presence of grazing flow, the excitation sound pressure level was increased up till 120dB to maintain the desired SNR in presence of flow noise. To determine the absolute root-mean-squared values, a correction factor of the Hanning window was implemented, as shown in Bendat and Piersol [38].

To determine the DC resistance of the perforate (θ_{DC}), as explained in section 4.1, the pressure drop across the perforate sample was measured under constant bias flow. An in-house flowmeter was used to monitor the flow speed and the pressure drop was determined using the *Swema* Man80 micro manometer.

The calculation of the wavenumber also involves an estimated value of the grazing flow Mach number (M). The next subsection discusses the flow profile determination in the ducts which is used to calculate the Mach number.

3.3 Flow Profile

The intended flow profile to study the perforate in presence of grazing flow is turbulent in nature. The flow profile is experimentally determined using a pitot tube with an inner diameter of 1.1 mm, as shown in Figure 3.

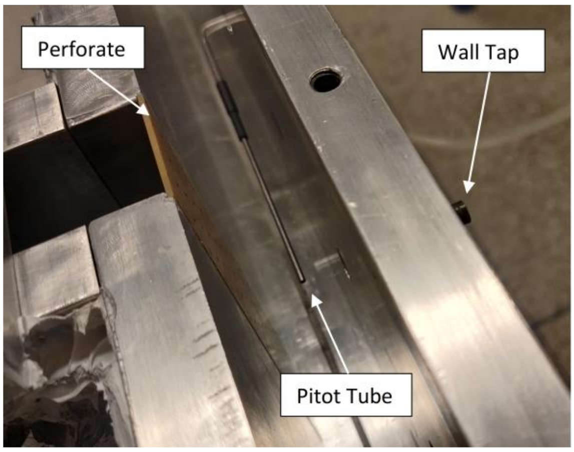

Figure 3 Usage of pitot tube to determine the flow speed upstream of the perforate sample

The pitot tube measures the dynamic pressure in the flow field and the static pressure is acquired using a wall tap at the exact location of the pitot entrance. An extended attachment is used so that the flow profile upstream of the pitot tube is not affected by the traversing mechanism. Based on

Bernoulli's equation and using the density at room temperature, the velocity at each position ($U(x)$) is calculated, where x is the transversal distance of the pitot tube from the duct wall. The calculation is as shown in Eq. (5).

$$U(x) = \sqrt{2\Delta P_{Flow}(x)/\rho_0} \tag{5}$$

The pressure difference ($\Delta P_{Flow}(x)$) is calculated as the difference between the static and the dynamic pressure. The pressure difference is measured using the *Swema* 761430 differential pressure head, and *Swema* 3000 flowmeter.

Flow velocities are measured across half of the 25 mm dimension of the rectangular duct. The bulk velocity (U) of the grazing flow is determined by integrating the half flow profile. The calculated bulk velocity is used to determine the Mach number, and by extension the wavenumber.

The intended grazing flow velocity range for the acoustic measurements is from $\approx$ 10 m/s to $\approx$ 60 m/s. The measurement point of the flow profile closest to the duct wall was at 1.1 mm distance, equivalent to the inner diameter of the pitot tube. Hence the viscous sublayer region of the flow profile, present in the near wall region is outside the range of the measured values of the velocity profile in this thesis. Figure 4 shows the flow profiles measured at the bulk velocity-based Mach numbers of $\approx$ 0.05, 0.1, 0.15, and 0.2. Using the acquired values of the flow velocities, a semi-empirical model of the flow profile was determined following Eq. (6).

$$\begin{gathered} U(x) = 0.0145x^+ + \beta_U,\ for\ \ x^+ < 120 \text{ in the near wall region} \\ U(x)/u_\tau = 1/0.384\, ln(x^+) + 4.27,\ for\ 120 < \ x^+, and\ \eta < 0.3 \text{ in the} \\ \text{logarithmic region} \\ (U_{max} - U(x))/u_\tau = 5.3\left(2x/L_x\right)^2, for\ 0.3 < \eta, \text{ in the outer zone} \end{gathered} \tag{6}$$

where x is the actual distance from the wall. The quantities $x^+ = xu_\tau/\nu$, and $\eta = 2x/L_x$ are the normalised distances from the wall. The normalised distances are used to define the limits of the three different regions of the flow profile. For $x^+ < 120$, an empirical coefficient β_U is determined by matching the experimental results with the modelled profile in the near wall region. Örlü et al. [39] summarises the different limits of the logarithmic region of the flow profile proposed in several studies, and the value of the lower limit of the logarithmic region is in the range of the previous research. The upper limit of η = 0.3 is at a larger value than observed in most of the studies, however, it agrees with the experimental results observed at different flow speeds in the three-port test rig, and matches the value suggested by Pope [40]. The flow velocity in the logarithmic region, is governed by the von Kármán constant (κ =0.384). The values of the constants for the logarithmic region are proposed by the simulated results of Lee and Moser [41], and match well with the experimental results. For the outer zone, i.e., $\eta > 0.3$, a power law is used to describe the flow profile.

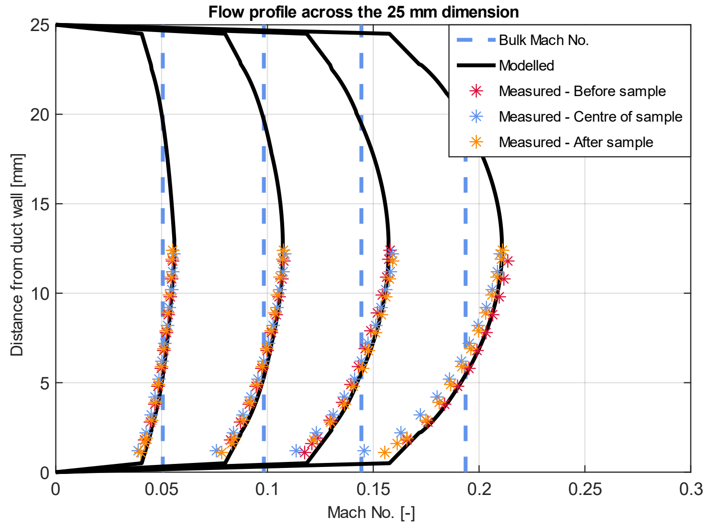

Figure 4 Comparison of the measured and the modelled flow profile

Traditionally, in liners, the flow profile is not assumed to be constant across the lined section. To investigate the deviation in the flow profile, it was also measured at a distance of 55 mm from the sample in the upstream and downstream directions. In case of the perforate sample studied in this thesis, Figure 4 shows the comparison of the flow profile before, at the centre and after the sample. It is observed that the disruption of the flow profile over the perforate surface is negligible, and it is a fair assumption that the bulk flow velocity is constant along the sample length.

The ratio of the experimentally determined bulk velocity to the measured maximum velocity (U_{max}), i.e., the velocity at the centre of the duct cross section, is found to be between 0.908 and 0.918 at all the flow speeds. Hence, for the acoustic measurements, when a simultaneous flow profile measurement was not possible, only the maximum velocity upstream the sample was measured, and the bulk velocity was calculated by multiplying it with the averaged factor of 0.914.

Following the model proposed by Zanoun et al. [42], the skin-friction velocity (u_τ) is also determined using the bulk velocity, following Eq. (7).

$$u_\tau = U\sqrt{0.0743\,(Re_m)^{-0,25}}/2\,, \qquad Re_m = U * L_x/2\nu \tag{7}$$

Using the grazing flow bulk velocity, the measured in-duct temperature, and the pressure signals acquired by the microphones in different operating conditions, post-processing of the data is carried out to determine the passive acoustic characteristics of interest. This determination and the supporting equations are explained in the next subsection.

3.4 Scattering Matrix and Transfer Impedance Estimation

The passive acoustic characteristics of interest in this thesis are the three-port scattering matrix (S-Matrix) and the real part of the normalised transfer impedance, i.e., the resistance ($\Re$). As mentioned in the introduction, Karlsson and Åbom [3] define the three-port S-Matrix. The decomposed wave pressures of the measured total acoustic pressure signals are used and following Eq. (8), the S-Matrix is calculated.

$$\begin{bmatrix} p_1^+ \\ p_2^+ \\ p_3^+ \end{bmatrix} = \begin{bmatrix} \rho_1 & \tau_{2\to1} & \tau_{3\to1} \\ \tau_{1\to2} & \rho_2 & \tau_{3\to2} \\ \tau_{1\to3} & \tau_{2\to3} & \rho_3 \end{bmatrix} \begin{bmatrix} p_1^- \\ p_2^- \\ p_3^- \end{bmatrix}, \tag{8}$$

The notations and the directions of the S-Matrix coefficients are shown in the 2D-schematic of the setup in Figure 5-a, whereas that of the decomposed pressures follows Figure 2.

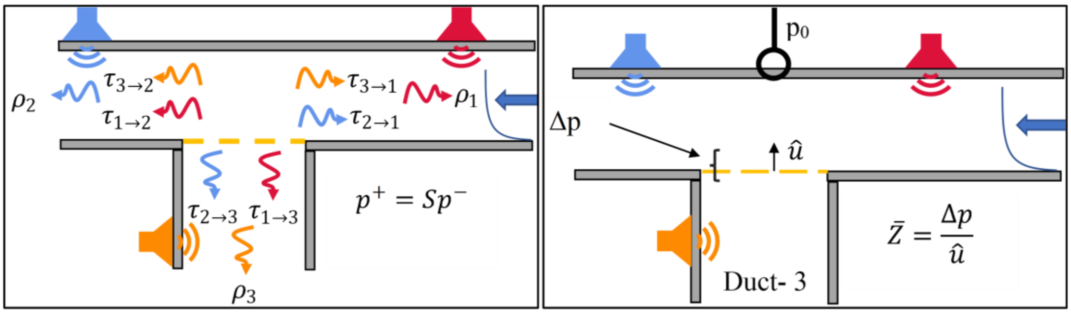

Figure 5 2D-schematic of the three-port test rig with notations for acoustic characterisation. a) S-Matrix components and directions, b) Normalised transfer impedance components and directions.

To solve for a 3X3 scattering matrix, three individual sets of measurements must be carried out to obtain the values of the decomposed wave pressures in all the three ducts. Hence, wave decomposition is carried out under excitation from each duct to solve Eq. (8). Following the determination, the S-Matrix shows the passive acoustic behaviour of the perforate sample in three-different directions.

For an empty T-junction the acoustic origin of the three-port is shifted from the geometrical origin of the setup as shown in Karlsson and Åbom [3]. This shift in the origin is to compensate for the near field effects as well as for the sudden expansion of volume at the opening of the T-junction. However, when a perforate is flush mounted at the intersection of the T-junction, due to a smaller open area, these compensations are not needed, and the acoustical three-port origin is taken as the geometrical centre of the perforate. Validation of the chosen origin point is done by comparing the normalised resistance of the perforate under excitation from three directions in the absence of grazing flow. As shown in subsection 4.1, it is observed that the resistance curves collapse on each other, suggesting that the geometric position of the three-port origin used, is accurate.

Determination of the normalised resistance is carried out by calculating the real part of the normalised transfer impedance. The definition of the transfer impedance of any sample is the difference in the impedance with and without the sample present in the path of propagation. To solely study the property of the sample, independent of the test setup, the transfer impedance is normalised with respect to the characteristic impedance of air ($\rho_0 c$). The normalised transfer impedance has two components, the real part, i.e., the resistance ($\Re$), and the imaginary part, the reactance (χ). Mathematically it is calculated from the experimental data obtained in the three-port test rig using Eq. (9).

$$\bar{Z} = Z/\rho_0 c = \Re + i\chi = \Delta p/u = (p_3 - p_0)/(p_3^- - p_3^+) \quad (9)$$

The notations and the directions follow Figure 5-b, and Figure 2. The quantity p_3 is the total acoustic pressure in duct-3, calculated at the three-port origin, i.e., the centre of the sample. The particle velocity u is in the direction normal to the perforate surface. The normalised value of the particle velocity is used here and it is calculated by taking the difference of the decomposed wave pressures in duct-3 ($p_3^- - p_3^+$), at the three-port origin. To calculate the root-mean-squared value of the in-hole particle velocity (u_{rms}), the magnitude of u is calculated in terms of SI-units, following Eq. (10).

$$u_{rms} = |u| * (V_{rms}/\rho_0 c S_i)/\sigma\,; V_{rms} = \sqrt{V_{AS} * L_w}, \quad (10)$$

where V_{rms} is the r.m.s. value of the incident acoustic signal, i.e., the loudspeaker voltage in the frequency spectrum. V_{rms} is calculated using the acquired auto-spectra (V_{AS}) and the correction factor for the Hanning window used for calculating the FFT (L_w). As mentioned in section 3.2, the frequency response functions (FRF) between the microphone pressure signal and the reference signal is used for post-processing to reduce the random errors. Hence multiplying by V_{rms} converts the FRF back to the acoustic pressure signal. To convert the acoustic pressure difference ($p_3^- - p_3^+$) into the particle velocity, it is divided by the characteristic impedance ($\rho_0 c$). Furthermore, to convert to SI units, the sensitivity (S_i) of the microphones is used. Lastly, to determine the in-hole velocity, an isentropic nature and conservation of mass is assumed, and the SI value of the particle velocity at the perforate surface is divided by the porosity (σ).

In Eq. (9), p_0 is the total acoustic pressure on the opposite side of the perforate and is determined by placing a flush mounted microphone on the wall opposite to the perforate as shown in Figure 5-b. Additionally, it can also be calculated by taking the averages of the total acoustic pressures in duct-1, and 2 determined at the acoustic origin. As shown in subsection 3.5, on comparing the calculated value of the perforate resistance, using the measure microphone pressure (p_0) and the average of p_1, and p_2, a good agreement is found. Hence, it can be assumed that $p_0 = (p_1 + p_2)/2$.

The characterisation of the sample is carried out across a wide frequency range and for twelve different flow speeds. Hence the standing wave pattern in the ducts keeps changing over the entire experimental range. This can result in an acoustic pressure node being present near the microphone position used to measured p_0, an example of such an error is shown in subsection 3.5. To avoid this error and determine the resistance independent of the standing wave pattern, coefficients of the S-Matrix can be used to determine the resistance. The coefficients of the S-Matrix depict the scattering of incoming sound waves by the sample when the termination of each duct is anechoic. Experimentally, as anechoic termination is difficult to attain, the formulation of the S-Matrix is such that the effect of the termination reflections is accounted while calculating the S-Matrix coefficients. Additionally, assuming that the acoustic pressure p_0 is the average of pressures p_1, and p_2, the resistance can be calculated using the S-Matrix coefficients, following Eq. (11). In the case of excitation from duct-1, anechoic termination means $p_{2,3}^- = 0$. Similarly, $p_{1,3}^- = 0$ when the excitation is from duct-2, and $p_{1,2}^- = 0$ when excitation is from duct-3. Modifying Eqs. (8) and (9) with the above-mentioned assumptions, Eq. (11) shows the calculation of resistance under excitation from three ducts.

$$\overline{Z_1} = \left(\frac{1}{2}(p_{1+} + p_{1-} + p_{2+}) - p_{3+}\right) \Big/ p_{3+} \Rightarrow \left\{ \begin{matrix} replacing\ p_{1+}, p_{2+}, and \\ p_{3+}\ as\ per\ Eq. (8) \end{matrix} \right\} \Rightarrow$$

$$\overline{Z_1} = \frac{(\rho_1 + \tau_{1\to 2} + 1)}{2\tau_{1\to 3}} - 1$$

$$\overline{Z_2} = \left(\frac{1}{2}(p_{1+} + p_{2+} + p_{2-}) - p_{3+}\right) \Big/ p_{3+} \Rightarrow \left\{ \begin{matrix} replacing\ p_{1+}, p_{2+}, and \\ p_{3+}\ as\ per\ Eq. (8) \end{matrix} \right\} \Rightarrow \qquad (11)$$

$$\overline{Z_2} = \frac{(\rho_2 + \tau_{2\to 1} + 1)}{2\tau_{2\to 3}} - 1$$

$$\overline{Z_3} = \left(p_{3+} + p_{3-} - \frac{1}{2}(p_{1+} + p_{2+})\right) \Big/ (p_{3-} - p_{3+}) \Rightarrow \left\{ \begin{matrix} replacing\ p_{1+}, p_{2+}, and \\ p_{3+}\ as\ per\ Eq. (8) \end{matrix} \right\} \Rightarrow$$

$$\overline{Z_3} = (1 + \rho_3) \Big/ (1 - \rho_3) - \frac{1}{2}\left(\tau_{3\to 1} + \tau_{3\to 2} \Big/ 1 - \rho_3\right)$$

The resistance calculated using the S-Matrix coefficients improves the results in comparison with the resistance calculated using acquired, as well as estimated pressure p_0, as shown in the appended Paper A, as well as in the next subsection. Hence, for the characterisation of the perforate in the linear excitation range, this formulation is used to calculate the resistance.

In case of high-level excitations, however, the calculation of the resistance was done as per Eq. (9). To study the perforate behaviour under high-level excitation in the three-port test setup the controlling parameter chosen was the root-mean squared value of the in-hole particle velocity (u_{rms}). The experimental range of the controlled particle velocity levels was taken from ≈ 1 m/s to ≈ 10 m/s. As mentioned above, the particle velocity is determined by taking the difference of the decomposed wave pressures in duct-3. In case of excitation from ducts-1, and -2, for the intended frequencies, the loudspeakers used for excitation were unable to generate the desired particle velocity levels. Hence, determination of the S-Matrix, and by extension the resistance following Eq. (11) was not possible. The resistance is therefore determined following Eq. (9). Moreover above 1100 Hz, the particle velocity level reduces significantly and hence the frequency range of the non-linear experiments was limited from 100 to 1100 Hz.

To validate the chosen acoustic origin point of the three-port, as well as the improvement in the results when the S-Matrix coefficients are used to determine the resistance, some initial experiments were carried in the linear range excitation (< 100dB) and no grazing flow. These preliminary results of the three-port technique are shown in the next subsection.

3.5 Validation of the Three-Port Technique

As discussed in the previous subsection, the collapse point of the acoustical three-port, i.e., its origin is determined to be at the centre of the perforate sample. Experiments were conducted under linear range excitation with waves incident from each of the three directions individually, and in absence of grazing flow. Wave decomposition is carried out following Eq. (3), where the distances of each microphone (s_n) is calculated with respect to the chosen origin. Using the decomposed wave pressures, Eq. (8) is solved to determine the S-Matrix, and the magnitude and the phase of the coefficients are shown in Figure 6.

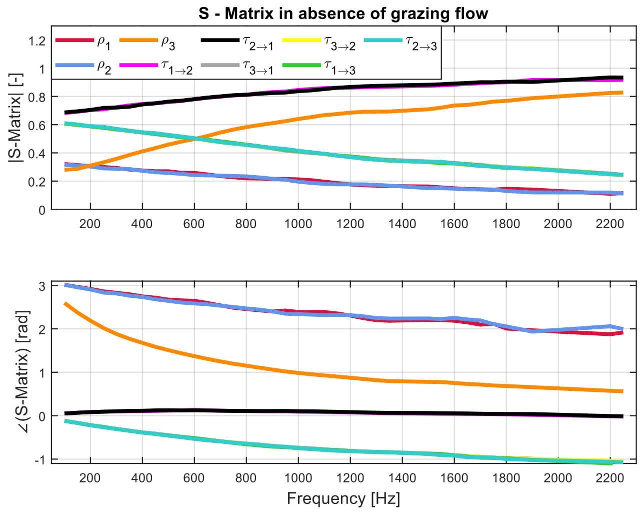

Figure 6 Three-port scattering matrix coefficients of the perforate sample. a) Magnitude, b) Phase angle

As can be seen in the figure, the symmetric behaviour of the perforate sample is apparent from the magnitudes of the coefficients with respect to the duct-1 and duct-2 directions. Additionally, with an increase in frequency, we observe that the magnitude of the reflection coefficient of duct-3 (ρ_3) along with the transmission coefficients between ducts- 1, and 2 ($\tau_{1\to2}, \tau_{2\to1}$), increases. Vice versa, a decrease in the magnitudes of transmission through duct-3 ($\tau_{3\to1,2}, \tau_{1,2\to3}$) with increasing frequency is also seen. This suggests that the degree of acoustic transparency of the perforate is proportional to the ratio of the wavelength and the perforate thickness. Moreover, by extension it also supports the theoretical models suggesting an increase in the normalised resistance with increasing frequency, as summarised in Elnady and Bodén [14].

The determination of the normalised resistance using the three-port technique can be carried out in the three different ways mentioned in the previous subsection. Figure 7 compares the value of the resistance calculated using Eqs. (9), and (11) in absence of grazing flow, as a function of frequency. The acoustic incidence in this case is from duct-3. The comparison of the resistance is shown when the value of p_0 is calculated as the average of p_1, and p_2, as well as taken as the directly measured microphone signal. A good agreement is observed between both the cases, hence the assumption of $p_0 = (p_1 + p_2)/2$ used to determine the resistance using the S-Matrix coefficients is accurate. Additionally, the agreement between the two cases also validates the plane wave propagation above the perforated surface in ducts-1, and 2.

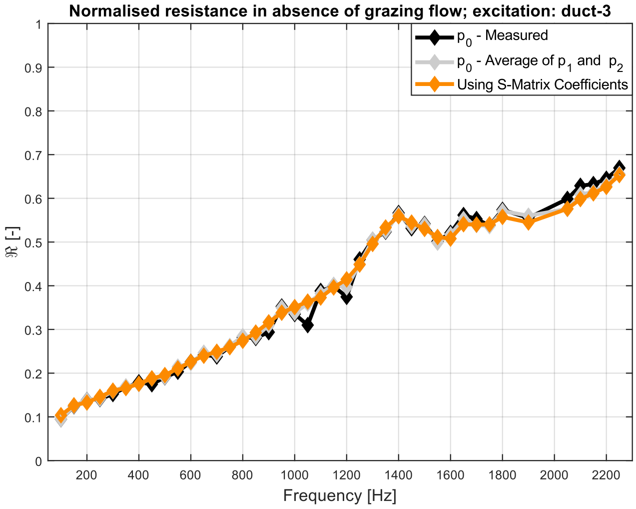

Figure 7 Normalised resistance under excitation from duct-3 and in absence of grazing flow, calculated using three different formulations

Figure 7 also shows the determined resistance using the S-Matrix coefficients. The reduction of error pertaining to standing wave pattern is corrected, as seen at ≈ 1050, 1200 Hz.

An anomaly in the resistance is seen at 1400 Hz. The source of this error is found to be the presence of a pressure node at one of the microphone positions and does not represent a property of the perforate sample. An attempt to shift the position of the pressure node was carried out by rebuilding the test rig and adding absorbing material at the termination of the duct-3 and changing the reflection properties. Three attempts were carried out and the resistance determined in these three cases is shown in Figure 8. Additionally, the perforate sample was studied in an impedance tube, using the traditional two-port technique as shown by Bodén [43], and in Ref. [44]. The resistance of the sample determined in the impedance tube is also shown in Figure 8.

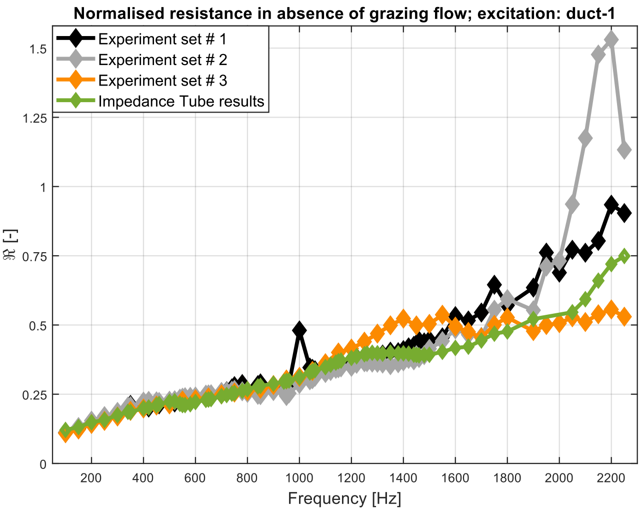

Figure 8 Normalised resistance determined in the impedance tube, and the acoustical three-port with three different termination reflections; excitation from duct-3 and no grazing flow.

As can be seen in the black and the grey lines, the spikes in the resistance are shifted to 1000 Hz and 2200 Hz by changing the termination reflections, but they do not disappear from the entire frequency range. On comparing with the impedance tube results, a better agreement is found in case of test set #3, and hence for the rest of the thesis we look at results calculated with the experimental data from test set #3. It should be noted that on addition of grazing flow, the standing wave pattern in the three-port changes and hence the spike at 1400 Hz is no longer observed in the results determined in presence of grazing flow, as shown in subsection 4.3. Additionally, for the majority of the frequency range, repeatability of the acquired results is observed in the three sets of measurement where the deviation between all the results is found to be in the ±5% range.

After the validation of the experimental technique, the following section discusses the main results of the thesis, investigating the behaviour of the resistance of the perforate sample under different operating conditions.

Chapter 4: Resistance of Perforate

This section discusses the behaviour of the experimentally determined resistance calculated using the three-port measurement technique in presence of acoustic excitation from three different directions, with grazing flow and in the non-linear regime. The resistance under four different operating conditions is presented and discussed in the subsections. Comparison and agreement of the experimental results with existing models is shown. Additionally, using the results at low grazing flow speeds, a semi-empirical model describing the relation between the resistance and dimensionless numbers like the Strouhal number, the Shear number and the Mach number is proposed.

4.1 Resistance under Linear Excitation and No Grazing Flow

In the absence of grazing flow and with an excitation in the linear range, the resistance is determined following Eq. (11), i.e., using the S-Matrix coefficients. The resistance under excitation from three different directions is as shown in Figure 9. As can be seen, the determined resistance is found to be independent of the incidence direction. Moreover, the results also validate the chosen point in the three-port where the entire three-port collapses, i.e., the origin point of the three-port test rig.

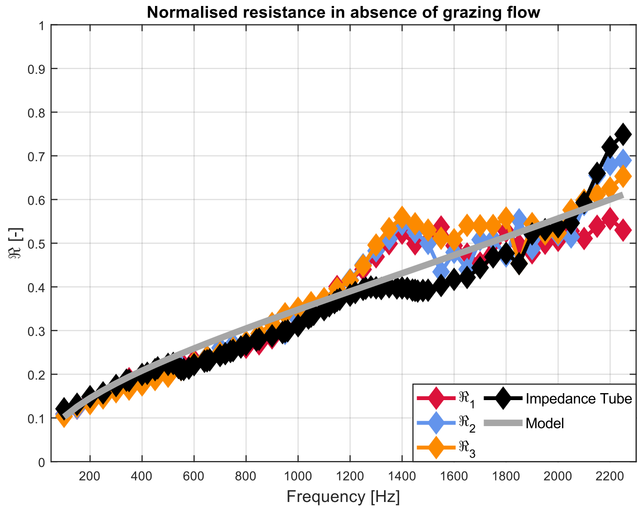

Figure 9 Experimentally determined normalised resistance in absence of grazing flow, using the three-port measurements, the impedance tube (black markers), and as modelled by Guess [8] (grey line).

To characterise the resistance of a perforated plate several models are proposed as mentioned in Section 1. Elnady and Bodén [14] show that the resistance is dependent, among other properties, on the coefficient of discharge (C_d) of the particular perforate plate. The discharge coefficient can be calculated following Eq. (12), as proposed by Betts [45]. Determination of the DC flow resistance (θ_{DC}) of the perforate, i.e., the ratio of the pressure drop (ΔP_{DC}) across the perforate when constant flow is passed through it, and the in-hole velocity of the flow (u_{DC}), is necessary to solve Eq. (12). The pressure drop of the perforate measured at different in-hole velocities is as shown in Figure 10. The in-hole velocity was intentionally kept low to match the root-mean-squared value of the in-hole particle velocity during the linear range acoustical measurements. Comparing the experimental results with that of the Eq. (12), a good agreement is achieved when taking the value of $C_d \approx 0.616$. This agreement is shown in Figure 10.

$$\theta_{DC} = 1/\rho c\,(\Delta P_{DC}/u_{DC}) = 32\nu t/\sigma c d^2 C_d + u_{DC}/2\sigma^2 C_d^2 \tag{12}$$

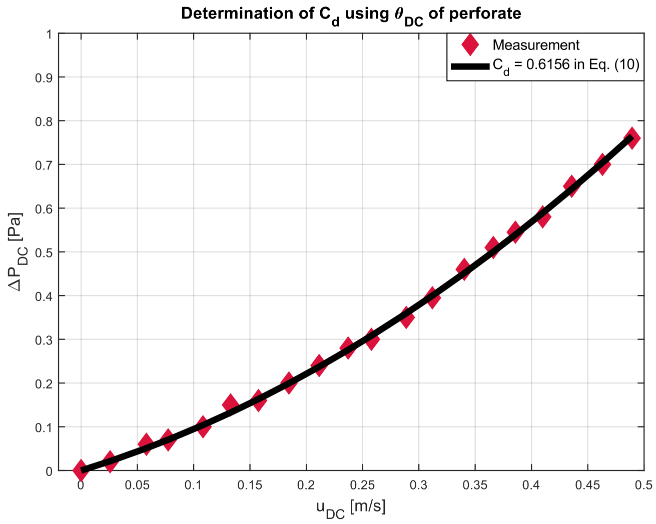

Figure 10 Pressure drop across the perforate under constant bias flow against the in-hole particle velocity

A semi-analytical model proposed by Guess [8] suggests that the resistance is a function of the perforate properties of perforation diameter (d), perforate thickness (t), and porosity (σ). The model by Guess [8], scaled with the discharge coefficient is compared with the experimental results and shown in Figure 9. This model [8, 14] mathematically follows Eq. (13). It should be noted that, in appended Paper A, the radiation impedance ($\rho_0 c/2\,(d/\lambda)^2$) at higher frequencies was not accounted for in the model, and hence the results deviated from the model at higher frequencies. However, the mistake was rectified and as can be seen in Figure 9 , a good agreement is now observed.

$$\Re = (\sqrt{8\nu\omega})t'/\sigma c d C_d + \rho_0 c/2\,(d/\lambda)^2;\ \ t' = t + d \tag{13}$$

In summary, the resistance of the perforate in absence of grazing flow can be described as a function of the perforate properties and the incidence frequency. Although in Figure 9, a deviation between model and experimental results is observed at 1400 Hz, as discussed in section 3.5, this deviation is due to the experimental setup and incorrectly represents the acoustic characteristic. .

4.2 Resistance under High-Level Excitation and No Grazing Flow

Characterisation of the resistance in the non-linear regime is generally done with the help of dimensionless numbers, namely the acoustic particle velocity based Strouhal number (St_u) and the Shear number (Sh). Sh is the ratio of the diameter of the perforation and the Stokes layer thickness. It represents the relative thickness of the oscillating layer responsible for the absorption of the incoming sound waves. On the other hand, St_u is a scaling quantity, which compares the particle displacement inside the perforation with its diameter. When the displacement is relatively higher, vortex shedding occurs near the perforate surface, resulting in acoustic dissipation and an increase in the resistance. Thus, St_u describes the extent of the non-linear behaviour. These numbers are defined following Eq. (14).

$$St_u = \omega d / u_{rms}, \qquad Sh = d\sqrt{\omega/4\nu} \tag{14}$$

Figure 11 shows the resistance at three different frequencies, determined at different levels of u_{rms}, and under excitation from each of the three directions. The values are determined in absence of grazing flow. As can be seen, the value of $\Re$ at different in-hole particle velocity levels is found to be independent of the excitation direction. Additionally, as seen for the results under 650, and 1100 Hz acoustic incidence the maximum value of the in-hole particle velocity is attained when excitation is from duct-3. Similar observations are also observed in the presence of low velocity grazing flow, as shown in the appended Paper B. Hence for the analysis of the non-linear part of the resistance, only the results under excitation from duct-3 are considered in the following.

Additionally, it should be noted that the value of the resistance at different frequencies when the value of u_{rms} is controlled to be 1 m/s, match that of results in Figure 9. This suggests that the resistance determined at 1 m/s of in-hole particle velocity level is equivalent to the resistance determined in the linear range.

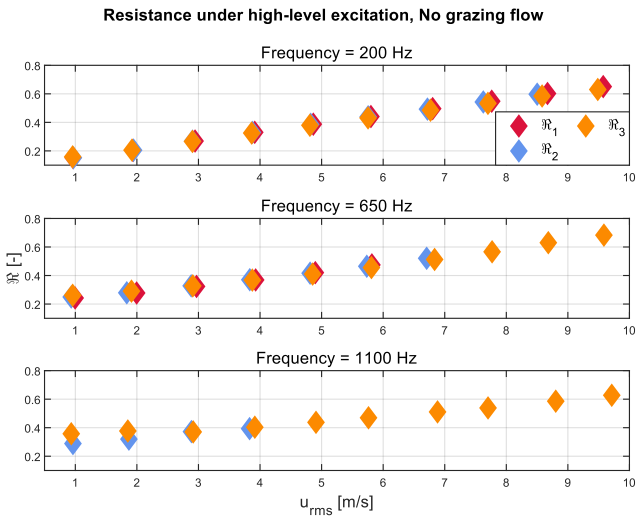

Figure 11 Experimentally determined resistance at higher levels of in-hole particle velocity, in absence of grazing flow. a) Excitation frequency = 200 Hz, b) Excitation frequency = 650 Hz, c) Excitation frequency = 1100 Hz

To only study the non-linear part of the resistance ($\Re_{NL}$), resistance determined in the linear range ($\Re_{Lin}$) is subtracted from the determined resistance under high-level excitation. There are several models that predict the non-linear behaviour of the resistance as discussed in section 2.1. For the experimental results obtained using the three-port technique, a transition state model proposed by Temiz et al. [5] agrees well. The model proposed by Temiz is scaled by the vena-contracta factor (C_v) of the perforation. For sharp edged perforations, the value of C_v is taken as 0.6, and the model is calculated as per Eq. (15).

$$\Re_{NL} = F_c(St_u, Sh)\rho u_{rms}\sigma/2C_v^3,$$
$$F_c(St_u, Sh) = 1/\left(1 + 2St_u\left(1 + 0.06e^{3.74/Sh}\right)\right) \quad (15)$$

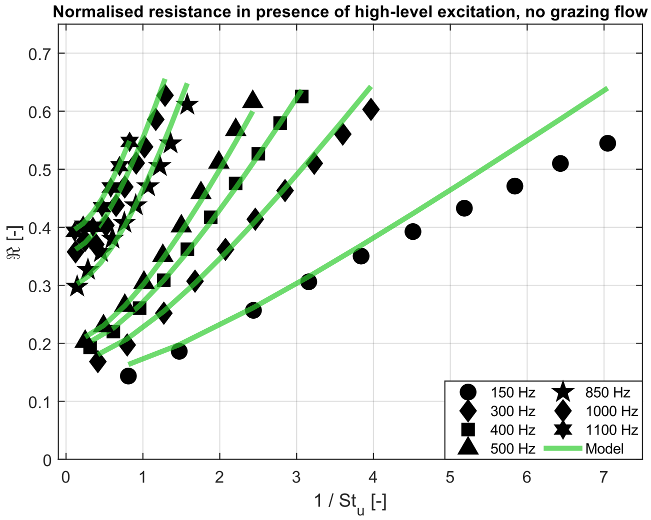

Figure 12 Experimentally determined resistance at higher in-hole particle velocity levels compared with model from Eq.(15), in absence of grazing flow

The comparison at selected frequencies is shown in Figure 12, where the experimental results and the model [5] of the total resistance ($\Re_{NL} + \Re_{Lin}$) is compared and shown as a function of the inverse Strouhal number ($1/St_u$). For $1/St_u >\approx 3$, the transition state model starts deviating from the experimental results. In this strongly non-linear regime, the particle displacement is very high resulting in a jet-type expulsion of the vortices, as explained in Temiz et al. [5]. In this range the behaviour of the resistance is linearly dependent on the particle velocity and follows the observations in the research of Melling [16].

The agreement of the experimental results with existing models shown in the subsections above further validates the results of the three-port technique. In order to further study the perforate, another standard operating condition, i.e., the presence of grazing flow, is now considered. The behaviour of resistance is discussed, first in the linear range of acoustic excitation and then under high-level excitation.

4.3 Resistance under Linear Excitation and Grazing Flow

This subsection discusses the behaviour of the resistance in the presence of linear range excitation and grazing flow. Earlier, extensive research has been carried out using direct and indirect experimental methods to study the behaviour of resistance, as summarised in section 2. Results discussed below are a part of the appended Paper A, and appended Paper C.

The following points regarding the resistance are currently under discussion in the scientific community:

- Grazing flow parameter which best describes the resistance, and the dependence of resistance on the frequency of incident acoustic waves.

- Behaviour of the resistance when the acoustic incidence is from different directions with respect to the grazing flow.

The study of the first point, as discussed in section 2.1, involves two types of models. The ones proposed by Kooi and Sarin [11], Kirby and Cummings [12], and Cummings [13] follow Eq. (16). In these models, the resistance under grazing flow ($\Re_{Flow}$) is a function of the skin-friction velocity (u_τ), the frequency of excitation (f), and the empirically defined coefficients (ξ, ζ).

$$\Re_{Flow} = (\xi u_\tau - \zeta \omega d)/c \tag{16}$$

The other type of models, as proposed by Rao and Munjal [10], Guess [8], and Rice [9] follow Eq. (17) and show the resistance to be solely a function of grazing flow Mach Number (M), and the porosity (σ).

$$\Re_{Flow} = \epsilon M/\sigma \tag{17}$$

The characterisation of the experimentally determined resistance in the three-port is done with respect to the grazing flow velocity based Strouhal number (St_U). The definition of St_U follows that of Eq. (14), but instead of the in-hole particle velocity (u_{rms}), the grazing flow bulk velocity (U) is used.

The proposed model by Kooi and Sarin [11] has a limit of validity. This limit is the ratio u_τ/fd to be of a value greater than 0.2. They propose that when $u_\tau/fd < 0.2$, the effect of the grazing flow on the resistance is almost non-existent, and the resistance can be estimated using the no grazing flow models. The value of $u_\tau/fd \approx 0.2$ corresponds to a St_U of ≈ 0.7. Figure 13 shows the determined resistance, under excitation from duct-3 in the presence of low grazing flow velocities, compared with the results from the model proposed using Eq. (16). The values of ξ are given in the legend of the figure, and the value of ζ is taken as 0.54. These values are empirically chosen to match with the experiments and show the resemblance in the behaviour of the experimental and modelled results.

The behaviour of the resistance with respect to the St_U is, as shown, completely different before and after the $St_U \approx 0.7$ region. Another important point of observation is that even for $St_U > 0.7$, the resistance keeps increasing with an increase in flow velocities, suggesting a limitation of the Kooi and Sarin model. The behaviour of the resistance after the St_U limit is similar to that in the absence of grazing flow, however, it is still dependent on the flow profile parameters.

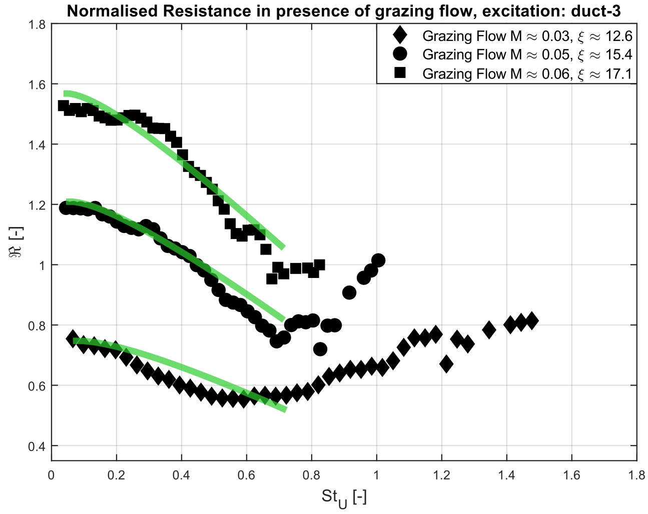

Figure 13 Experimentally determined normalised resistance at low grazing flow velocities (black markers) compared against model following Eq. (16) (green lines)

Based on the results of Figure 13, it can be observed that to concurrently study the resistance determined at different flow velocities, a scaling of the determined resistance with respect to flow profile parameters is needed. Furthermore, studying the results, it is also observed that an empirically determined scaling coefficient (ψ) can be used to account for the different values of resistance when the incidence direction is different with respect to the grazing flow direction, i.e., to propose a solution for the second bullet point mentioned above. Hence, a scaling factor of $1/\psi * (M^{1.17}(1+St)^{1.75})$ is determined to compare the experimental results at different flow speeds and different incidence directions. For $\Re_1$, the value of ψ is 1, for $\Re_2, \psi$ = 0.92, and for $\Re_3, \psi$ = 0.85.

Figures 14, 15, and 16 show the scaled value of resistance under different excitation directions determined in presence of eleven different flow velocities.

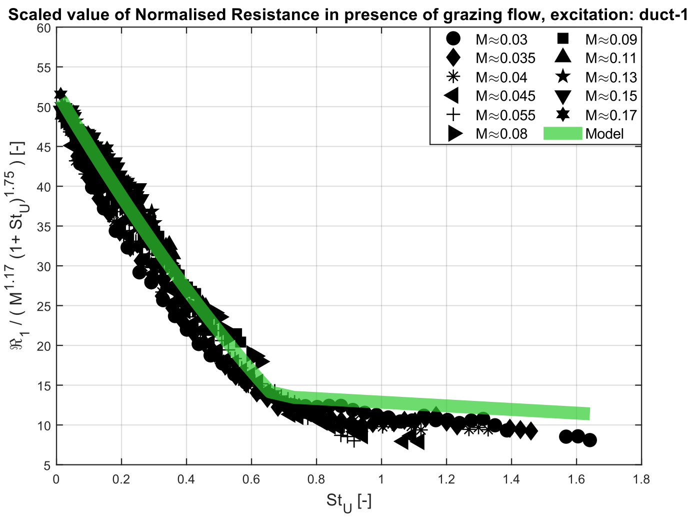

Figure 14 Experimentally determined resistance in presence of linear range excitation from duct - 1, and eleven grazing flow velocities is compared with the model proposed in Eq.(18)

For $St_U < \approx 0.7$, the scaled resistance as a function of St_U have a 2nd degree polynomial relationship, and for higher values of St_U, the relationship is linear in nature. Quantification of the relationship is shown in the model proposed in Eq. (18).

$$
\begin{aligned}
&for\ St_U < 0.7, \Re_{Flow} = 1/\psi * M^{1.17}\ (1 + St_U)^{1.75}\ (17.9\ St_U^2 - 69.2\ St_U + 51.9) \\
&for\ St_U > 0.7, \Re_{Flow} = 1/\psi * M^{1.17}\ (1 + St_U)^{1.75}\ \big((-440M + 10.9)St_U + 311M + 5.8\big)
\end{aligned} \tag{18}
$$

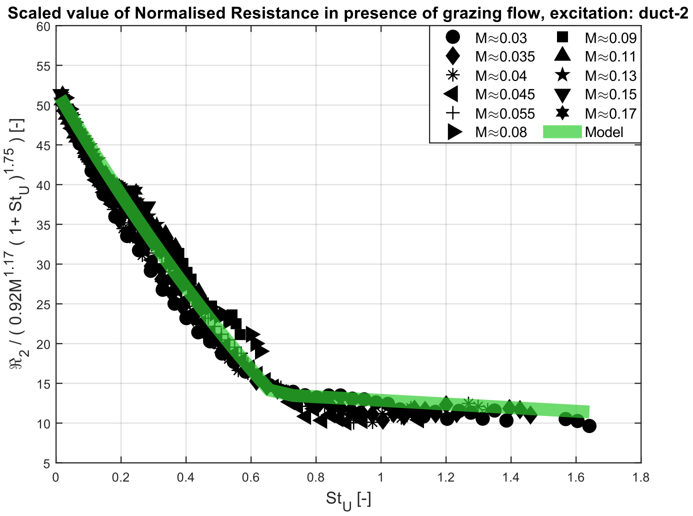

Figure 15 Experimentally determined resistance in presence of linear range excitation from duct - 2, and eleven grazing flow velocities is compared with the model proposed in Eq.(18)

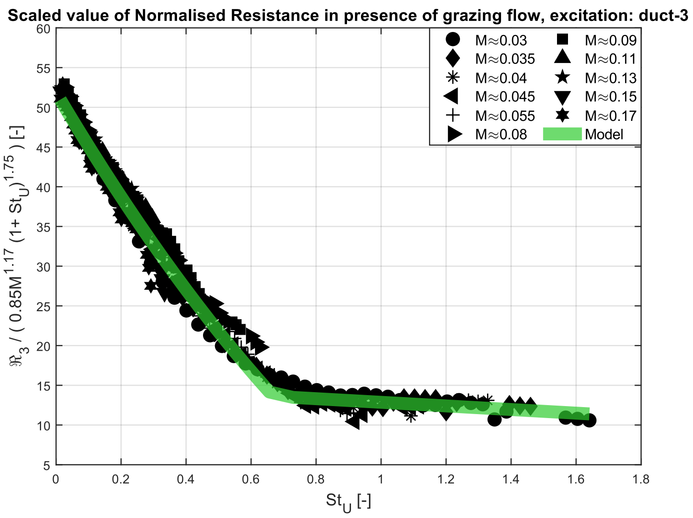

Figure 16 Experimentally determined resistance in presence of linear range excitation from duct - 3, and eleven grazing flow velocities is compared with the model proposed in Eq.(18).

The comparison of this proposed model with the experimental results is also shown in Figures 14, 15, and 16, and as can be seen a good agreement is observed. In the figures, for $St_U <\approx 0.7$ the relationship between the scaled value of resistance and St_U appears to be linear. However, as shown in appended Paper C, on individually comparing the results at different flow velocities, a good agreement between the modelled and the experimentally determined resistance is observed, and the relationship with respect to St_U can be clearly seen as of a 2nd degree polynomial in nature.

The different empirical coefficients used in the model can be dependent on perforate properties like the thickness, porosity, and the diameter of perforations. However, as only one sample is studied in this thesis, further study of these coefficients is necessary, but beyond the scope of this thesis.

The final subsection determines the result of the addition of high-level excitation with grazing flow. The model proposed in this subsection is appended with the effect of high-level excitation to give a combined model depicting the experimentally determined resistance in operating conditions similar to that of its application in acoustic liners.

4.4 Resistance under High-Level Excitation and Grazing Flow

Non-linear effects are observed in the experimentally determined resistance values when the perforate is exposed to high-level acoustic excitation in the presence of low velocity grazing flow ($M <\approx 0.05$). The magnitude of the resistance is observed to increase on increasing the in-hole particle velocity (u_{rms}). The characterisation of this non-linear behaviour of the resistance is done by comparing it against a dimensionless ratio of the in-hole particle velocity and the grazing flow velocity (u_{rms}/U). Referred studies regarding the non-linear behaviour in presence of grazing flow, namely Renou [17], and Elnady and Bodén [14] observe the non-linear effects on the resistance in presence of the grazing flow to be only dependent on the particle velocity levels and independent of the grazing flow velocity. However, in the three-port experimental results, the non-linear part of the resistance ($\Re_{NL-FLow}$) is observed to be a function of the ratio of u_{rms}/U. $\Re_{NL-FLow}$ is calculated by subtracting the linear range resistance from the resistance under high level excitation at the same grazing flow velocity. Following the observations discussed in subsection 4.2, the linear range resistance is defined to be the resistance determined when the in-hole particle velocity is controlled to be 1 m/s.

Figure 17 shows the values of $\Re_{NL-FLow}$ under excitation from duct-3 at three grazing flow velocities, and at different frequencies. Similar results were also observed when the excitation was from ducts-1, and 2. From Figure 17, the relation of $\Re_{NL-FLow}$ with the ratio of velocities can be defined as parabolic in nature. The relation is shown in Eq. (19).

$$\Re_{NL-Flow} = \alpha(u_{rms}/U)^2 + \beta(u_{rms}/U) + \gamma \tag{19}$$

On increasing the flow velocity, the non-linear effects reduce significantly. Moreover, despite the steps taken to reduce the effect of flow noise, the quality of the results is affected at the comparatively higher grazing flow velocity of Mach number ≈ 0.05. In comparison the results at lower grazing flow velocities are observed to be of a better quality. Nevertheless, the behaviour of $\Re_{NL-FLow}$ still follows Eq. (19) at grazing flow Mach ≈ 0.05.

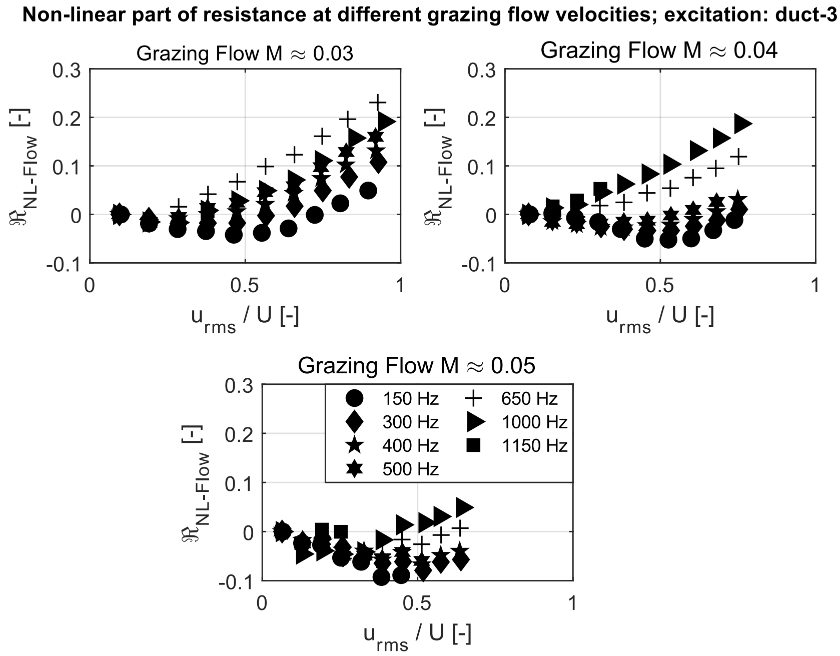

Figure 17 Experimentally determined resistance under high-level excitation and in presence of grazing flow compared against the ratio of in-hole velocity and grazing flow velocity;
a) Grazing flow M ≈ 0.03, b) Grazing flow M ≈ 0.04, c) Grazing flow M ≈ 0.05.

It can be seen from the experimental results that the values of $\Re_{NL-FLow}$ are observed to be negative for two simultaneous cases:

- Lower excitation frequencies, and
- Lower values of the u_{rms}/U ratio.

Hence, it is necessary to characterise $\Re_{NL-FLow}$ with respect to frequency and the grazing flow velocity. A natural choice for characterisation would be the flow velocity based Strouhal number (St_U). However, on comparing results under different grazing flow velocities, it was found that $\Re_{NL-FLow}$ is a function of the square root of frequency, and the grazing flow velocity. Hence another dimensionless ratio of the shear number with the grazing flow Mach number (Sh/M) was chosen to characterise the behaviour. Interpolation of the experimentally determined values of $\Re_{NL-FLow}$ was carried out to determine the values of α, β, and γ. The values of these interpolated coefficients were found to be linearly dependent on the Sh/M ratio, as shown in Figure 18.

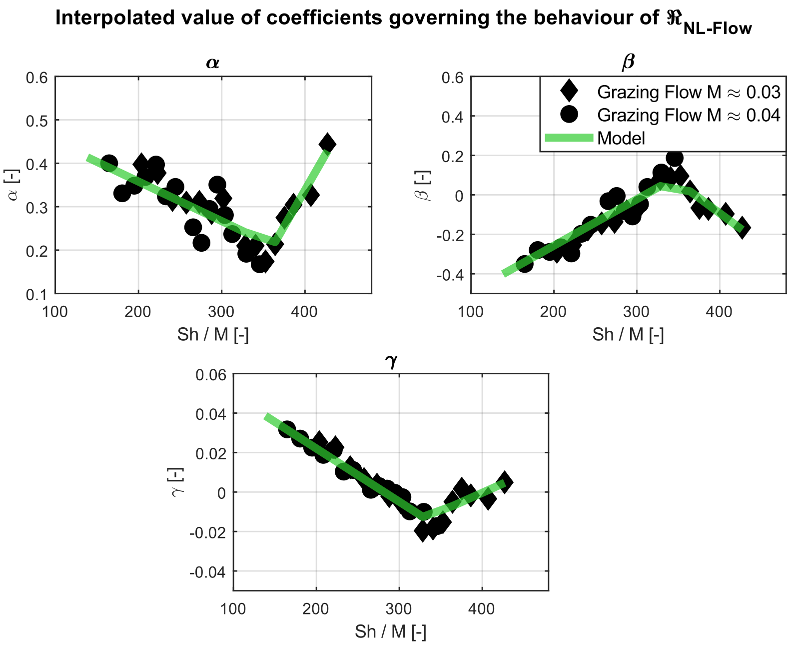

Figure 18 Interpolated values of the coefficients used to calculate the non-linear part of resistance in presence of grazing flow; a) Value of α, b) Value of β, c) Value of γ.

From Figure 18, in a small region where the Sh/M value is between ≈ 300 and ≈ 380. The value of β is positive, which is the region of the onset of positive values of $\Re_{NL-Flow}$. For values of $Sh/M >\approx 380$, although the values of β become negative, the values of $\Re_{NL-Flow}$ stays positive due to the positive values of α and γ. However, if the trends continue, the values at higher frequencies would show negative values of $\Re_{NL-Flow}$. This observation, and the definition of Shear number suggests that the positive $\Re_{NL-Flow}$ values are dependent on the oscillating Stoke layer thickness and the displacement generated by the grazing flow. Moreover, it can also be observed that the behaviour of the coefficient values is completely opposite before and after the value of ≈ 344. Eq. (20) quantifies this relation mathematically and calculates the value of α, β, and γ with respect to Sh/M.

$$
\begin{aligned}
&when\ Sh/M <\approx 344; \quad \begin{matrix}\alpha\\ \beta\\ \gamma\end{matrix} = \begin{cases} -9.1\times10^{-4}(Sh/M)+0.54 \\ 2.3\times10^{-3}(Sh/M)-0.73 \\ -2.7\times10^{-4}(Sh/M)+0.076 \end{cases}, \\
&when\ Sh/M >\approx 344; \quad \begin{matrix}\alpha\\ \beta\\ \gamma\end{matrix} = \begin{cases} 3.3\times10^{-3}(Sh/M)-0.99 \\ -3.1\times10^{-3}(Sh/M)+1.15 \\ 1.9\times10^{-4}(Sh/M)-0.075 \end{cases}
\end{aligned}
\tag{20}
$$

Addition of the model predicting the resistance in the linear range and in presence of grazing flow with the model for the non-linear part of resistance, i.e., Eqs. (18), (19), and (20), a combined model for the resistance is proposed. The comparison of the model with the experimental results at three different flow speeds and two different in-hole particle velocity levels is shown in Figure 19.

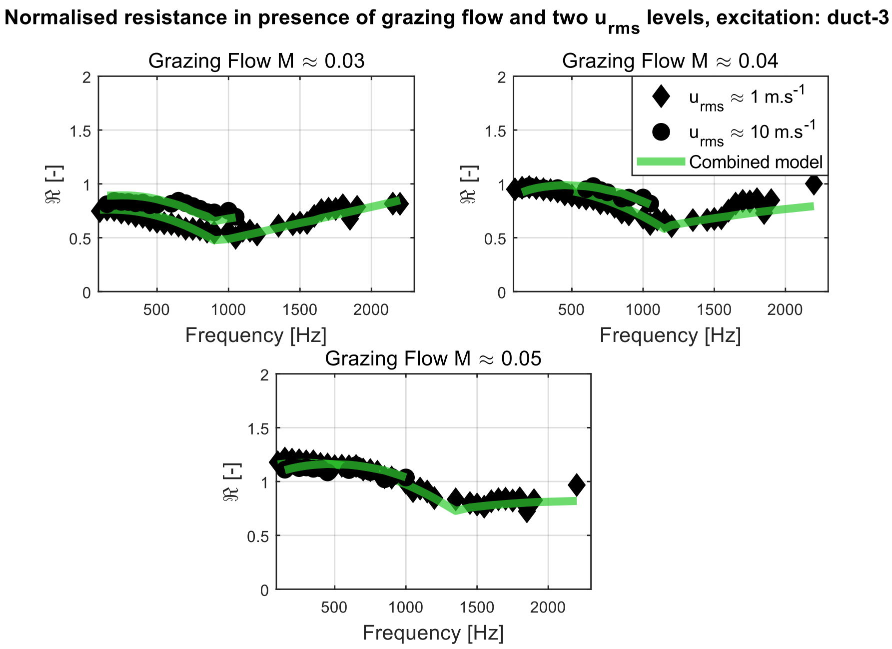

Figure 19 Comparison of the experimentally determined resistance with the combined model at two different pin-hole particle velocity levels and three grazing flow speeds; a) Grazing flow M ≈ 0.03, b) Grazing flow M ≈ 0.04, c) Grazing flow M ≈ 0.05.

Summary of Papers

Paper A: ***Three-port measurements for determination of the effect of flow on the acoustic properties of perforates***

Acoustic behaviour of the perforate sample is experimentally studied in a three-port setup with linear-level excitation from three different directions, and in presence of grazing flow. Incorporating the scattering matrix coefficients to determine the normalised resistance, errors due to the standing wave pattern in the duct are reduced. The flow profile in the rectangular T-junction is determined and a formulation of the determined normalised resistance in terms of skin-friction velocity is shown. On observing similarities in the determined resistance of an open T-junction and the perforate sample, an hypothesis regarding the behaviour of resistance of the perforate is proposed. The validation of the hypothesis requires expansion of the testing parameters, which is carried out in future publications.

Paper B: ***Nonlinear three-port measurements for the determination of high-level excitation effects on the acoustic properties of perforates***

Three-port measurements are carried out under high-level excitation to observe the non-linear effects on the resistance of the perforate. The discharge coefficient of the perforate sample is determined and is used to validate the resistance determined experimentally in the linear range in absence of grazing flow, by comparing it with an existing model. Moreover, validation of the experimental results under high-level excitation is carried out by comparing the non-linear part of the resistance with an existing model. A clear dependence of the resistance on the in-hole particle velocity, Shear number and Strouhal number is observed. At low grazing flow speeds, a relationship is observed between the non-linear part of the resistance and the ratio of in-hole particle velocity and the grazing flow velocity.

Paper C: ***An experimental study on the acoustic properties of a perforate using three-port measurements***

Following the observations of Paper A, an expansion of the experimental parameters is carried out to further study the perforate in the three-port setup. In the presence of grazing flow, a change in the acoustic response of the perforate is observed before, and after a particular Strouhal number based on the grazing flow velocity. A scaling of the determined resistance is proposed to derive a semi-empirical model of the resistance as a function of incidence direction, Strouhal number and the grazing flow Mach number. Under high-level excitation, the polynomial relation observed in Paper B is further studied and a dependence of the coefficients of a polynomial relation is found with the grazing flow Mach number and the incident wave Shear number. A model is proposed showing the non-linear part of resistance as a function of in-hole particle velocity, grazing flow velocity, and the Shear number. Combined with the effect of grazing flow, a comparison between the determined model and the experimental results is shown with a deviation within the 5% range.

Conclusions and Future Work

A detailed investigation of the acoustic characteristics of a perforate sample is carried out using a three-port measurement technique in this thesis. Characterisation of the passive acoustic properties of the sample in the presence of grazing flow and high-level excitation is done. The contribution of this thesis, in terms of experimental results and hypothesis derived from it, intends to help the scientific community better understand the response of a perforate plate at the operating conditions of an acoustical liner. Steps taken to improve the quality of the results by minimising experimental errors are discussed, a prime example being determination of the normalised resistance of the perforate using the three-port scattering matrix coefficients. This reduces the effect of termination reflections and the standing wave pattern on the results. Studying the perforate across a wider parameter range than its application-based operating range has given a deeper understanding of its response. For example, in case of the resistance calculated in presence of the grazing flow, at higher Strouhal numbers, a completely different dependence on the grazing flow parameters is seen as compared to lower Strouhal numbers. Additionally, studying the resistance at low grazing flow velocities, and for high-level excitation has shown the non-linear part of the resistance to be also dependent on grazing flow parameters like the flow velocity. The combined empirical model proposed describes the resistance to be a function of the Strouhal number, grazing flow Mach number, Shear number. and the in-hole particle velocity. A good agreement with the experimental results is seen. Studying a relatively smaller perforate has allowed the assumption of an undisrupted grazing flow over the perforated surface and negligible near field acoustic propagation. The described behaviour however needs to be validated over a longer perforated surface, as the flow acoustic interaction over a larger surface area can influence the results. Moreover, as a single sample is studied, and dependence of the empirically defined coefficients on the perforate properties like the diameter, thickness and the porosity still need to be studied.

The future work should focus on the above-mentioned points. Additionally, the effect of the relative flow and acoustic incidence directions is still a question and needs to be studied further on.

References

[1] Maa, D.-Y. *Microperforated panel at high sound intensity*. in *InterNoise*. 1994. Yokohama.
[2] Crandall, I.B., *Theory of vibrating systems and sounds*. 1927.
[3] Karlsson, M. and Åbom, M., *Aeroacoustics of T-junctions-an experimental investigation*. Journal of Sound and Vibration, 2010. **329**: p. 1793-1808.
[4] Holmberg, A., Karlsson, M. and Åbom, M., *Aeroacoustics of rectangular T-junctions subject to combined grazing and bias flows - An experimental investigation*. Journal of Sound and Vibration, 2015. **340**: p. 152-166.
[5] Temiz, M.A., Tournadre, J., Arteaga, I.L. and Hirschberg, A. , *Non-linear acoustic transfer impedance of micro-perforated plates with circular orifices*. Journal of Sound and Vibration, 2016.
[6] Sivian, I.J., *Acoustic impedance of small orifices*. Journal of the Acoustical Society of America 1935. **7**.
[7] Ingård, U., *On the theory and design of acoustic actuators*. Journal of the Acoustical Society of America, 1953. **25**: p. 1037-1061.
[8] Guess, A.W., *Calculation of Perforated Plate Liner Parameters from Specified Acoustic Resistance and Reactance*. Journal of Sound and Vibration, 1975. **40**: p. 119-137.
[9] Rice, E.J. , *A Model for the acoustic impedance of a perforated plate liner with multiple frequency excitations* in *NASA Technical Memorandum*. 1971.
[10] Rao, N. and Munjal, M., *Experimental evaluation of Impedance of perforates with Grazing Flow* Journal of Sound and Vibration, 1986.
[11] Kooi, J.W. and Sarin, S.L., *An experimental study of the acoustic impedance of Helmholtz resonator arrays under a turbulent boundary layer*, in *7th AIAA Aeroacoustics Conference*. 1981.
[12] Kirby, R. & Cummings, A., *The impedance of perforated liners subjected to grazing flow and backed by porous media*. Journal of Sound and Vibration, 1998.
[13] Cummings, A., *The effects of Grazing Turbulent Pipe-Flow on the Impedance of an Orifice*. Acoustica, 1986. **61**: p. 233-242.
[14] Elnady, T. and Bodén, H. *On the modelling of the acoustic impedance of perforates with flow*. in *9th AIAA/CEAS Aeroacoustics Conference*. 2003.
[15] Ingård, U. and Ising, H., *Acoustic nonlinearity of an orifice*. Journal of the Acoustical Society of America, 1967. **42**.
[16] Melling, T.H., *The acoustic Impedance of Perforates at Medium and High Sound Pressure Levels*. Journal of Sound and Vibration, 1973.
[17] Renou, Y. , *Impédance des traitements acoustiques absorbants en conduit : effets de l'écoulement rasant et de la couche limite*, in *Laboratoire d'Acoustique de l'Université du Mans*. 2010, Le Mans University.
[18] Bonomo, L.A., Quintino, N.T., Spillere, A., Cordioli, J.A. and Murray, P.B. *A Comparison of In-Situ and Impedance Eduction Experimental Techniques for Acoustic Liners with Grazing Flow and High SPL*. in *28th AIAA/CEAS Aeroacoustics Conference*. 2022. Southampton, UK.
[19] Dean, P.D., *An In-Situ method of wall acoustic impedance measurements in flow ducts*. Journal of Sound and Vibration, 1974. **34**: p. 97-130.
[20] Zandbergen, T., *On the Practical Use of Three-Microphone Techniqe for In-Situ Acoustic Impedance Measurements on Double Layer Flow Duct Liners*, in *7th AIAA Aeroacoustics Conference*. 1981.
[21] Gaeta, R.J., Mendoza J.M. and Jones M.G., *Implementation of in-situ impedance techniques on a full scale aero-engine system*, in *13th AIAA Aeroacoustics Conference*. 2007.
[22] Feder, E. and Dean, L. W., *Analytical and Experimental Studies for Predicting Noise Attenuation in Acoustically Treated Ducts for Turbofan Engines NASA Contractor Report CR-1373* 1969.

[23] Dickey, N.S., Selamet, A. and Ciray, M.S., *An experimental study of the impedance of perforated plates with grazing flow*. Journal of Acoustical Society of America, 2001. **110**: p. 2360-2370.
[24] Watson, W.R., and Jones, M.G., *New Numerical Procedure for Impedance Eduction in Ducts Containing Mean Flow*. AIAA Journal, 2012. **49**(10).
[25] Bodén, H., Zhou, L., Cordioli, J., Medeiros, A. and Spillere, A., *On the effect of flow direction on impedance eduction results*, in *22nd AIAA Aeroacoustics Conference*. 2016.
[26] Jing, X., Peng, S., and Sun, X. , *A straightforward method for wall impedance eduction in a flow duct*. The Journal of the Acoustical Society of America, 2008. **124**(227).
[27] Zhou, L., Bodén, H., Lahiri, C., Bake, F., Enghardt. L and Elnady T. , *Comparison of impedance eduction results using different methods and test rigs*, in *20th AIAA/CEAS Aeroacoustics Conference*. 2014: Atlanta, GA.
[28] Myers, M.K., *On the Acoustic Boundary Condition in the presence of Flow*. Journal of Sound and Vibration, 1980. **71**: p. 429-434.
[29] Renou, Y. and Aurégan, Y., *Failure of the Ingard–Myers boundary condition for a lined duct: An experimental investigation*. The Journal of the Acoustical Society of America, 2011. **130**: p. 52-60.
[30] Bodén, H., Cordioli, J.A., Spillere, A., and Serrano, P. *Comparison of the effect of flow direction on liner impedance using different measurement methods*. in *23rd AIAA/CEAS Aeroacoustics Conference*. 2017. Denver, Colorado.
[31] Dokumaci, E., *A Note on Transmission of Sound in a Wide Pipe with Mean Flow and Viscothermal Attenuation*. Journal of Sound and Vibration, 1997. **208**: p. 653-655.
[32] Seybert, A. F., and Ross, D. F., *Experimental determination of acoustic properties using a two-microphone random-excitation technique*. Journal of the Acoustical Society of America, 1977. **61**: p. 1362-1370.
[33] Fujimori, T., Sato, S., and Miura, H. *An automated measurement system of complex sound pressure reflection coefficients*. in *Internoise 84*. 1984.
[34] Dahlquist, G. and Björck, Å., *Numerical Methods*. 1974: Prentice Hall Inc.
[35] Åbom, M. and Bodén, H. , *Error analysis of two-microphone measurements in ducts with flow*. The Journal of the Acoustical Society of America, 1988. **83**.
[36] Holmberg, A. , *Experimental determination of aeroacoustic sources in low mach number internal flows*. 2010, KTH Royal Institute of Technology: Stockholm, Sweden.
[37] Peerlings, L., *Assessing precision and accuracy in acoustic scattering matrix measurements*. 2017, KTH Royal Institute of Technology.
[38] Bendat, J. S. and Piersol, A.G. , *Engineering Applications of Correlation and Spectral Analysis*. 2nd ed. 1980: Wiley Interscience
[39] Örlü, R., Fransson, J.H.M., Alfredsson, H., *On near wall measurements of wall bounded flows - The necessity of an accurate determination of the wall position*. Progress in Aerospace Sciences, 2010. **46**: p. 353-387.
[40] Pope, S., *Turbulent Flows*. 2000, Cambridge, UK: Cambridge University Press.
[41] Lee, M., and Moser, R.D. , *Direct numerical simulation of turbulent channel flow up to Reτ ≈ 5200*. Journal of Fluid Mechanics 2015. **774**: p. 395-415.
[42] Zanoun, E-S, Nagib,H. and Durst, F., *Refined cf relation for turbulent channels and consequences for high-Re experiments*. Fluid Dynamics Research, 2009. **41**.
[43] Bodén, H. *Simulation of high acoustic excitation level harmonic interaction effects for perforates and liners*. in *25th AIAA/CEAS Aeroacoustics Conference*. 2019. Delft, Netherlands.
[44] Shah, S., Bodén, H. and Boij, S., *Experimental study on the acoustic properties of perforates under flow using three-port technique*, in *27th International Congress on Sound and Vibration*. 2021: Prague.
[45] Betts, J.F., *Experiments and Impedance Modeling of Liners Including The Effect of Bias Flow*. 2000, Virginia Polytechnic Institute and State University.

Appended Papers

PAPER A

AIAA AVIATION Forum
August 2-6, 2021, VIRTUAL EVENT
AIAA AVIATION 2021 FORUM

10.2514/6.2021-2269

Three-port measurements for determination of the effect of flow on the acoustic properties of perforates

Shail Shah[1], Hans Bodén[2] and Susann Boij[3]
Marcus Wallenberg Laboratory for Sound and Vibration Research, KTH Royal Institute of Technology, SE- 10044 Stockholm, Sweden

Massimo D'Elia[4]
Laboratoire d'Acoustique de l'Universit´e du Mans, Le Mans, 72000, France

A major discussion in the scientific community is the effect of the acoustic propagation direction being relative to the mean flow direction on the acoustic boundary condition posed by perforated liners. The reason being that the results from liner-impedance-eduction measurements show acoustic propagation upstream or downstream to the flow direction giving different resulting acoustical impedances. This paper contributes to this continuing effort to gain confidence in results obtained under different acoustical excitation and flow configurations. Instead of a traditional two-port configuration, by placing a perforate sample in a T-junction, this paper presents a three-port measurement technique. The transfer impedance of the perforate is determined under grazing as well as under normal incidence. Moreover, to study the effect of acoustic incidence relative to the flow directions, transfer impedance is also determined under the presence of grazing flow. A comparison of the measurement results with existing analytical and semi empirical models is also presented. An attempt to determine the nature of the transfer impedance under normal acoustic incidence is carried out and an analogous behavior between an empty T-junction and the perforated sample is proposed.

I. Introduction

Perforates are used for noise control of aircraft engines as well as for other vehicles and machines. Their properties and noise reduction are known to depend on the mean flow field and other external parameters such as temperature and acoustic excitation level. Many test techniques for determining liner impedance under grazing flow conditions have therefore been developed [1-13]. There are many test rigs around the world and a number of different techniques for extracting the liner impedance from measurements have been developed. The dominating techniques, at least in terms of numbers of publications, are the so-called inverse impedance eduction techniques [1-10]. In order to gain confidence in the results, which may depend on both the test rig used and on the impedance education method, some comparative studies have been initiated [1, 4, 5, 8]. The in-situ impedance measurement technique [11], in which the liner is instrumented, has also been successfully applied to measure the liner impedance [12]. To study only the impedance of the perforated top sheet, methods using an impedance tube located in a side branch [14, 15] have also been used.

In this study, a three-port method similar to that proposed in Refs. [16, 17] is used to study the effect on perforate acoustic properties for different combinations of flow direction and acoustic excitation. Similar to the in-situ

[1] Ph.D. Student, Department of Engineering Mechanics; shail@kth.se.
[2] Professor, Department of Engineering Mechanics, AIAA Member; hansbod@kth.se.
[3] Associate Professor, Department of Engineering Mechanics, AIAA Member; sboij@kth.se.
[4] Ph.D. Student, Laboratoire d'Acoustique de l'Universit´e du Mans ; massimo_emiliano.delia.etu@univ-lemans.fr

impedance measurement technique and the side branch method, the disparities related to the Ingard-Myers boundary condition [18] are not applicable while discussing the results of the three-port method, as the boundary condition is not used for determination of the sound field in the main duct.

Acoustic properties of the sample studied here are the real part of the normalized transfer impedance, i.e., the resistance ($\Re$), and the three-port scattering matrix (S-Matrix). These properties are determined with and without the presence of grazing flow. A validation of the three-port results in the absence of flow by comparing with an existing model [19] and the experimental results from impedance tube measurements [20], is presented. In the presence of grazing flow, the behavior of the calculated resistance values are compared with existing semi-empirical models [21, 22]. Moreover, similar to Ref. [17], experiments to determine the properties of an empty T-junction (test setup in the absence of a perforated sample) are also presented. This is done to determine the transfer impedance of the perforate and provide a possible explanation for the behavior of the perforate resistance in the presence of grazing flow.

II. Experimental Technique

A. The three-port technique

The test setup for the three-port technique can be described as an impedance tube placed in a side branch, and is inspired by studies [11, 14] which have used this type of configuration to investigate the effect of grazing flow on the impedance of perforates. The three-port measurement uses a test rig according to Figure 1, where the ducts 1, 2, and 3 intersect and form a T-junction. A perforate sample was placed covering the opening of duct 3 at the intersection of ducts 1 and 2. The end of the duct 3 was sealed to avoid leakage of grazing flow. The acoustic pressure in all three ducts was determined using the multi-microphone method [17]. Plane wave propagation over the perforated plate was assumed given that the comparison between the calculated results using the measured pressure signal and decomposed wave amplitudes at position P_0, showed good agreement. Hence, it was assumed that the total acoustic pressure at point P_0 is given by $P_0 = {(P_1 + P_2)}/{2}$, where P_1 and P_2 are the total acoustic pressures at that point determined using wave decomposition in ducts 1 and 2, respectively.

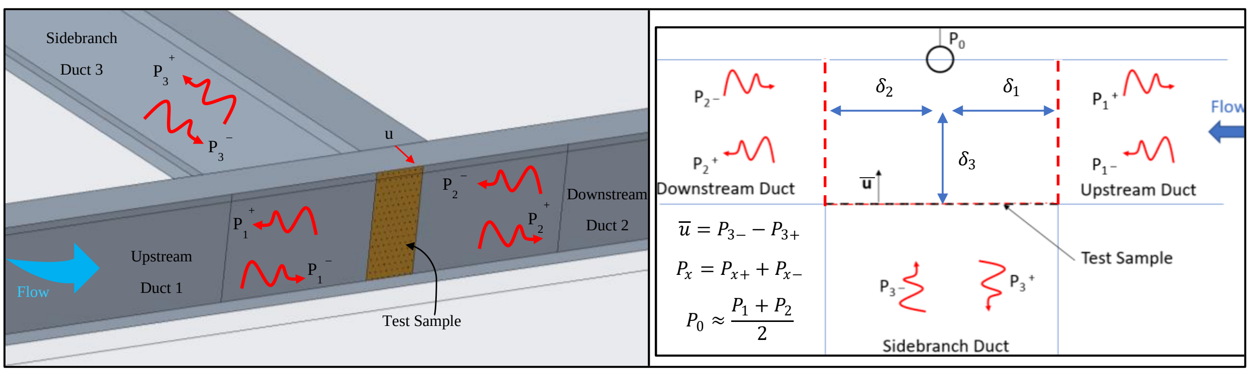

Figure 1 Schematic of the experimental setup

Using the decomposed wave pressure amplitudes, the scattering matrix (S-Matrix) of the three-port is defined as per the Eq. (1) [16]:

$$\begin{bmatrix} P_{1+} \\ P_{2+} \\ P_{3+} \end{bmatrix} = \begin{bmatrix} \rho_1 & \tau_{2\to1} & \tau_{3\to1} \\ \tau_{1\to2} & \rho_2 & \tau_{3\to2} \\ \tau_{1\to3} & \tau_{2\to3} & \rho_3 \end{bmatrix} \begin{bmatrix} P_{1-} \\ P_{2-} \\ P_{3-} \end{bmatrix}, or\ \mathbf{P}^+ = \mathbf{S}\mathbf{P}^-, \tag{1}$$

where $P_{x\pm}$ describes the decomposed wave pressure amplitudes in duct x. The direction $'+'$ is taken outwards, and $'-'$ is taken inwards as shown in Figure 1. ρ and τ stand for the reflection and transmission coefficients, respectively, and the subscripts represent the respective duct. To study the properties of the sample placed in the T-junction, the origin point of the acoustical three-port must be determined. In Refs. [16, 17] the origin point is defined for an empty T-junction by studying the phase angle of transmission coefficients in absence of external flow. The geometric origin of the three-port is shifted and the alteration δ, as shown in Figure 1, is calculated using Eq. (2) [17].

$$-2(\delta_i + \delta_j) = c\ mean\left(\frac{\Delta\theta(\tau_{ij}) + \Delta\theta(\tau_{ji})}{2\pi f}\right), (i \neq j), \tag{2}$$

where i, j represent the three ducts, $\delta_{i,j}$ are the added alterations for the respective ducts and $\Delta\theta(\tau_{ij,ji})$ is the deviation of the phase angle of the transmission coefficients from zero. In the case when the sample is placed in the T-Junction, a modification of this method is proposed in Ref. [20]. The value of δ is then calculated by comparing the transmission coefficients of duct 3 with the results from an impedance tube. As the sample, when viewed from duct 3, is placed in the same way as it is placed in an impedance tube, the phase angle of the transmission coefficients in both cases should be equal. Thus $\Delta\theta(\tau_{ij,ji})$ in Eq. (2) is now changed to represent the difference between the phase angles when the sample is placed in the impedance tube, and when it is placed in the T-Junction, respectively. For the perforate sample used, the values of δ_1, δ_2, and δ_3 were calculated to be 15.95, 14.95 and 8.35 mm, respectively.

B. Determination of the Transfer Impedance

The normalized transfer impedance ($\bar{Z}$) of the test sample was calculated to study the acoustic properties of the sample under excitation from all three ducts, respectively. The normalization was done with respect to the characteristic impedance of air.

In the case of plane wave excitation, given that the sample is acoustically compact, it can be assumed that the normalized particle velocity (u) is equal on both the sides of the sample. The normalized transfer impedance $\bar{Z}$ can then be determined by taking the ratio of the pressure difference across the perforate and the acoustic particle velocity u at the sample surface, as shown in Eq. (3).

$$\bar{Z} = \frac{\Delta P}{u} = \frac{P_3 - P_0}{P_{3-} - P_{3+}} = \frac{(P_{3+} + P_{3-}) - \frac{1}{2}(P_{1+} + P_{1-} + P_{2+} + P_{2-})}{P_{3-} - P_{3+}}, \tag{3}$$

where P_3 is the total acoustic pressure determined at δ_3 distance from the perforate.

Acoustic reflection from the terminations creates standing wave patterns in all the ducts, leading to the creation of nodes at the T-junction at certain frequencies. The transfer impedance calculated using Eq**.** (3) is dependent on the pressure at point P_0, and the presence of nodes in the vicinity of P_0 lead to measurement errors [23]. The S-Matrix of the three-port describes the properties of the sample properties, independent of any termination reflections. Hence Eq. (3) can be modified to calculate $\bar{Z}$ without the influence of termination and incorporate the S-Matrix coefficients as shown in Eqs. (4) to (6).

1) Considering non-reflecting terminations, in case of excitation from duct 1, we can say that $P_{3-} = P_{2-} = 0$. Applying it to Eq. (3) and using Eq. (1), we get:

$$\begin{aligned}\overline{Z_1} &= \frac{\frac{1}{2}(P_{1+} + P_{1-} + P_{2+}) - P_{3+}}{P_{3+}} = \begin{Bmatrix} replacing\ P_{1+}, P_{2+}, and \\ P_{3+}\ as\ per\ Eq. (1) \end{Bmatrix} \\ &= \frac{(\rho_1 P_{1-} + P_{1-} + \tau_{1\to2} P_{1-})}{2\tau_{1\to3} P_{1-}} - 1 \Rightarrow \overline{Z_1} = \frac{(\rho_1 + \tau_{1\to2} + 1)}{2\tau_{1\to3}} - 1\end{aligned} \tag{4}$$

2) Similarly, under excitation from duct 2, we can say $P_{3-} = P_{1-} = 0$, and transform Eq. (3) into:

$$\begin{aligned}\overline{Z_2} &= \frac{\frac{1}{2}(P_{1+} + P_{2-} + P_{2+}) - P_{3+}}{P_{3+}} = \begin{Bmatrix} replacing\ P_{1+}, P_{2+}, and \\ P_{3+}\ as\ per\ Eq. (1) \end{Bmatrix} \\ &= \frac{(\rho_2 P_{2-} + P_{2-} + \tau_{2\to1} P_{2-})}{2\tau_{2\to3} P_{2-}} - 1 \Rightarrow \overline{Z_2} = \frac{(\rho_2 + \tau_{2\to1} + 1)}{2\tau_{2\to3}} - 1\end{aligned} \tag{5}$$

3) Lastly, for excitation from duct 3, we assume $P_{1-} = P_{2-} = 0$, converting Eq. (3) into:

$$\begin{aligned}\overline{Z_3} &= \frac{(P_{3+} + P_{3-}) - \frac{1}{2}(P_{1+} + P_{2+})}{P_{3-} - P_{3+}} = \begin{Bmatrix} replacing\ P_{1+}, P_{2+}, and \\ P_{3+}\ as\ per\ Eq. (1) \end{Bmatrix} \\ &= \frac{(\rho_3 P_{3-} + P_{3-} - \frac{1}{2}(\tau_{3\to1} P_{3-} + \tau_{3\to2} P_{3-})}{\rho_3 P_{3-} + P_{3-}} \Rightarrow \overline{Z_3} = \frac{1 + \rho_3}{1 - \rho_3} - \frac{1}{2}(\frac{\tau_{3\to1} + \tau_{3\to2}}{1 - \rho_3})\end{aligned} \tag{6}$$

It should be noted that under the assumption of no absorption by the sample, Eqs. (4) to (6) can be further simplified, and theoretically give the same results.

The transfer impedance of the perforate can also be determined by calculating Eq. (3) with and without the perforate present in the T-Junction. Theoretically in the absence of flow, the value of $\bar{Z}$ should be zero for an empty T-Junction. Experimentally, marginal errors were observed when comparing the calculated transfer impedance by Eq. (3) and the above-mentioned method.

As discussed in Ref. [20], an analytical model proposed by Guess [19] shows good agreement with the experimentally determined resistance of the sample in absence of external flow. The proposed model follows Eq. (7).

$$\Re = \frac{\sqrt{8\nu\omega}t'}{\sigma c d C_D}, t' = t + d, \tag{7}$$

where $\Re$ is the resistance (real part of $\overline{Z}$), ν is the kinematic viscosity, ω the angular frequency, d is the diameter of perforation, σ is the porosity, c is the speed of sound, C_D is the discharge coefficient and t is the thickness of the sample. The variable t' is the corrected length proposed and taken as the sum of t and d [19].

In the presence of grazing flow, some semi-empirical models [14, 21, 24, 25] suggest a relationship between the normalized resistance, the skin friction velocity (u_τ), and the frequency (f). The model proposed by Kooi and Sarin [21] was used in this study as a reference, following Eq. (8).

$$\Re = \Re_{noflow} + \left(\frac{5 - {}^{t}/_{d}}{4\sigma c}\right)(9.9u_\tau - 3.2fd), \tag{8}$$

where $\Re_{noflow}$ is the calculated resistance in absence of external flow as per Ref. [21].

For the case of a fully developed flow boundary layer, several models are proposed where the perforate resistance is described as a function of the mean Mach number (M) and the porosity (σ) [19, 22, 26]. The model proposed by Rao and Munjal [26] was considered in this study, following Eq. (9).

$$\Re = \frac{0.53M}{\sigma} \tag{9}$$

In Ref. [10], results obtained using a number of different impedance eduction methods and test rigs were discussed. It was demonstrated that different transfer impedance values are obtained for upstream and downstream acoustic excitation measured for different liner samples and in different test rigs. In general, the resistance under upstream excitation shows an almost frequency-independent behavior, agreeing with the model proposed in Eq. (9). In the case of downstream excitation, a clear frequency-dependent behavior can be noted, with an almost constant decrease of the resistance with frequency, as seen in Eq. (8). Overall, the data sets show a clear difference between educed liner resistance for upstream and downstream conditions.

C. The Flow Profile

To determine the transfer impedance under the effect of grazing flow, characteristics of the flow profile in ducts 1 and 2 were determined. Flow speeds were controlled to give bulk velocities of Mach No. ≈ 0.05, 0.1, 0.14, and 0.19. Measurement of the in-duct flow profile was carried out using a pitot tube of 0.5 mm inner diameter. The flow velocity profile across ducts 1 and 2 was measured to determine the profile at three different positions vis-à-vis the sample, namely 55 mm upstream, at the center, and 55 mm downstream. Deviations of <2% were observed between the measured velocity profiles at the three different positions. This suggests that the flow profile was not significantly affected by the presence of the sample. The bulk flow velocity (u_{bulk}) as well as the skin-friction velocity (u_τ) was determined using Eq. (10) [27]. Moreover, the displacement thickness (δ^*) and the momentum thickness (θ) of the profile were determined using the Eq. (11) [28].

$$u_{bulk} = \frac{1}{H}\int_0^H u(x)dx\,;\ Re_m = \frac{u_{bulk} * H}{\nu};\ u_\tau = \frac{u_{bulk}\sqrt{0.0743\ (Re_m)^{-0{,}25}}}{2}, \tag{10}$$

$$\delta^* = \int_0^H \left(1 - \frac{u(x)}{u_{bulk}}\right)dx;\ \theta = \int_0^H \frac{u(x)}{u_{bulk}}\left(1 - \frac{u(x)}{u_{bulk}}\right)dx, \tag{11}$$

where H is the duct width, x is the distance from the smooth boundary wall, and Re_m is the Reynolds number.

The test sample under consideration is a square-edged perforate with a hole diameter and plate thickness of 1.2mm. The sample is 25 mm long in the axial direction of duct 1 and 2, 120 mm wide, and has a porosity of 2.5%. The cross section of all the three ducts is also 25 mm by 120 mm. All the measurements were performed at room temperature with deviation in the speed of sound <0.1%. The frequency range of the measurements was 300-1500 Hz. The wave numbers considered for plane wave decomposition were calculated using a model proposed by Dokumaci [29]. NI 9234 modules were used for data acquisition at a sampling frequency of 25.6 kHz. Stepped sine excitation was used as input and reference signal. The upper limit of the incident sound pressure level was set to 120 dB to have a minimal effect of non-linearities. The frequency response function (FRF) between the measured pressure signal and the reference signal was used for the entire analysis to reduce measurement errors due to external noise. Moreover, a relative calibration of the microphones was performed to remove bias errors in the data acquisition system. A signal-to-noise ratio of >40 dB was maintained during measurements conducted in the presence of grazing flow.

III. Results

A. Three port results for the no flow case

The magnitude of the S-Matrix coefficients are shown in Figure 2-a. A clear symmetry in ducts 1 and 2 can be seen. Moreover, with an increase in frequency, an increase in the reflection and subsequently a decrease in the transmission from duct 3 is observed. As per Eqs. (4) to (6), this suggests an increase in resistive behavior of the sample with an increase in frequency.

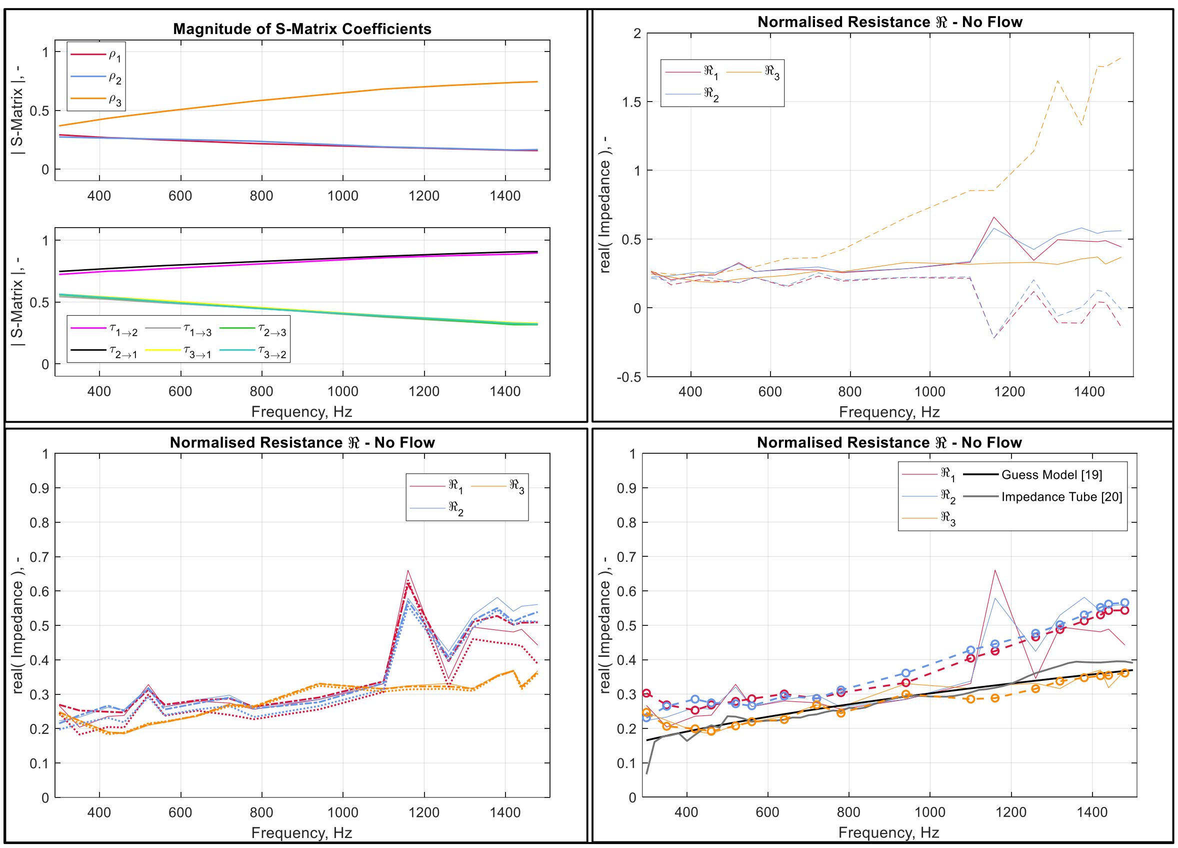

Figure 2 a) Magnitude of the reflection and transmission coefficients; b) Comparison between calculated normalized resistance, solid lines: with $\delta_{I,II,III}$ from Eq. (2), dashed lines: with $\delta_{I,II,III}$= 0; c) Comparison between normalized resistance calculated using Eq. (3), solid lines: pressure at P_0 is determined using microphone signal, Dash-dot lines: pressure at P_0 is determined as average of P_1 and P_2, dotted lines: Difference of the calculated $\Re$ with and without the perforate in the T-junction; d) Comparison between calculated normalized resistance and models [19, 20], solid lines: calculated using Eq. (3), circles: calculated using Eqs. (4) to (6).

Figure 2-b portrays the effect of shifting the origin of the three-port, by $\delta_{1,2,3}$, on the real part of the normalized transfer impedance of the perforate i.e., $\Re$. $\Re$ is determined under excitation from all three ducts to give $\Re_1$, $\Re_2$, and $\Re_3$, respectively. In absence of these added alterations, calculated as per Eq. (2), a clear difference in the behavior of the resistance curves under excitation from different directions is observed. Moreover, in case of excitations from ducts 1 and 2, the resistance appears to be negative for frequencies >1100 Hz, suggesting incorrect results without the addition of the calculated alterations.

As mentioned in Section II-A, to validate the accuracy of the plane wave decomposition over the perforated section a comparison of resistance is done, as shown in Figure 2-c. Calculation of $\Re$ is done using Eq. (3), where in one case the value of total acoustic pressure at P_0 is measured using a microphone, and in the other case it is taken as the average of the decomposed wave amplitudes in duct 1 and 2, which are evaluated at P_0. Moreover, determination of $\Re$ is also done by taking the difference of calculated resistance with and without the perforate present in the T-junction. The resistance calculated using all the above-mentioned three methods exhibit good agreement. Given the small deviation over the frequency range, plane wave decomposition can be used for the determination of the sound field in the perforated section. The large deviations observed in the resistance curves, e.g., at ≈ 520, 1150 Hz can be attributed to the experimental errors caused due to standing wave patterns in the duct.

A comparison between the normalized resistance calculated using Eqs. (3) to (6) is shown in Figure 2-d. It should be noted that for frequencies >1100 Hz, the resistance values calculated by Eq. (3) under excitation from ducts 1 and 2 are smoothened by using the S-Matrix coefficients. This is due to the removal of the effect of the termination reflections, and subsequently the measurement error due to the presence of nodes near the position P_0. A good agreement is observed between all the calculation methods, the model proposed in Eq. (7), and the resistance calculated from the impedance tube measurements [20].

B. Flow Profile Results

Figure 3 displays the measured flow Mach Numbers. The displayed measurement data are the average of the values determined at three different positions with respect to the perforate. An empirical model for the measured profile is proposed in Eq. (12).

$$\begin{aligned} u(x) &= 0.0145x^+ + \beta, && for\ 11 < x^+ < 350\ in\ the\ buffer\ layer \\ \frac{u(x)}{u_\tau} &= \frac{1}{0.384} ln(x^+) + 4.27, && for\ 350 < x^+ < 830\ in\ the\ logarithmic\ layer \\ \frac{u_{max} - u(x)}{u_\tau} &= 6.3\left(\frac{x}{H/2}\right)^2, && for\ 830 < x^+\ in\ the\ outer\ zone \end{aligned} \tag{12}$$

where $x^+ = \frac{xu_\tau}{\nu}$ is the normalized distance from the hard wall, u_{max} is the maximum velocity (observed at the center of the cross section), and β is a constant determined by curve fitting of the measured data. The limits of x^+ for the buffer and the logarithmic layer are defined using Ref. [30] and [31].

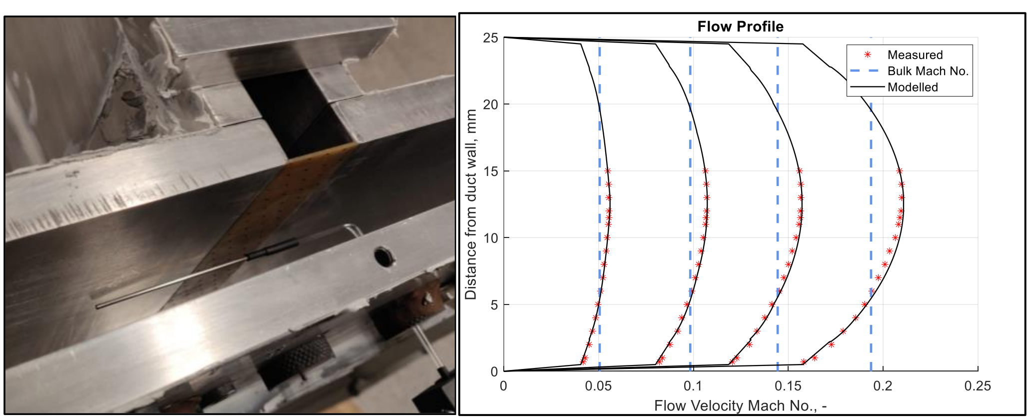

Figure 3 a) Flow profile measurements using pitot tube; b) Comparison between the measured and the modelled flow velocity profiles

Based on Eqs. (10) and (11), the skin friction velocity along with the different flow profile characteristics were calculated as shown in Table 1.

Mach Number	u_{max} (m/s)	u_{bulk} (m/s)	u_τ (m/s)	δ^* (mm)	θ (mm)
0.05	19.19	17.21	0.90	9.44	2.25
0.1	36.99	33.33	1.63	6.62	3.05
0.14	54.22	48.92	2.28	3.94	2.64
0.19	72.68	65.55	2.96	1.08	0.90

Table 1 Flow profile characteristics

C. Three port results under grazing flow

The magnitude of the S-Matrix coefficients and the normalized resistance calculated in the presence of grazing flow is as shown in Figure 4. On observing the scattering matrix coefficients in Figure 4-a, it can be clearly seen that with increasing flow velocity, the transmission from and into the duct 3 decreases and its reflection increases. This effect is due to an increase in the overall resistance of the perforate.

As displayed in Figure 4-b, as the flow speed increases, the resistance calculated under acoustic excitation from the grazing direction i.e., $\Re_{1,2}$ increase. Moreover, an increase in the flow speeds also show the resistance becoming increasingly independent of the frequency. The behavior of the curves starts following the Rao and Munjal model [26]. However, under incidence from duct 3, the resistance curve i.e., $\Re_3$ displays a dependence on the frequency as well as the flow speed, following the behavior seen in Ref. [21]. The reason for the discrepancy of the resistance under normal and grazing incidence with increasing flow speeds is unknown.

Moreover, on comparing with the results from impedance eduction methods [10], it is found that the distinguishing behavior of the resistance curves under upstream and downstream excitation is absent in the three-port results presented here. However, the behavior portrayed under normal incidence is similar to that of the resistance calculated using impedance eduction under downstream incidence.

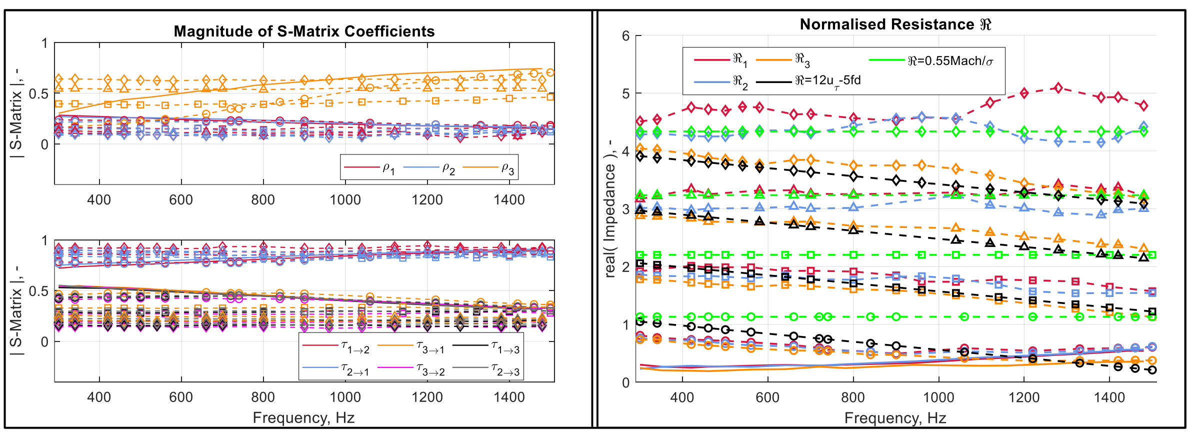

Figure 4 a) Magnitude of S-Matrix coefficients in presence of grazing flow; b) Normalized resistance calculated in the presence of external flow compared against proposed models, solid lines: No grazing flow, circles: Mach No. ≈ 0.05, squares: Mach No. ≈ 0.1, triangles: Mach No. ≈ 0.14, diamonds: Mach No. ≈ 0.19.

A modification to the semi-empirical model of Kooi and Sarin [21] is proposed to match the experimental results of calculated resistance. Resistance calculated as per Eq. (13) agrees well with the experimental results under normal acoustic incidence as can be seen in Figure 4-b. Similarly, modifying Rao and Munjal [26], Eq. (14) describes the resistance calculated under grazing incidence at higher flow speeds of Mach No. ≈ 0.14 and 0.19,

$$\Re = \frac{12u_\tau - 5fd}{\sigma c} \tag{13}$$

$$\Re = \frac{0.55Mach}{\sigma} \tag{14}$$

In order to understand the flow acoustic interaction effect on the properties of the test sample under normal incidence, the transmission coefficient and the resistance of the empty T-Junction were calculated with grazing flow and the results were compared. Scaling of the experimentally determined quantities with respect to the flow speeds was done by using Strouhal number (St) which is calculated using Eq. (15).

$$St = {}^{f d_{eq}}/_{U}, \tag{15}$$

where U is taken as the bulk flow velocity, and d_{eq} is taken as the equivalent diameter of the rectangular pipes in case of an empty T-Junction. When the sample is placed in the T-junction, d_{eq} is taken as the diameter of the perforations. It should be noted that the diameter and the thickness of the perforated sample under consideration is equal, hence the length scaling factor is calculated using only the diameter in the analysis of the sample.

The transmission coefficients as well as the resistance of the empty T-junction calculated under normal acoustic incidence at all flow speeds is shown in Figure 5-a. As observed in Ref. [17], the transmission coefficients of the empty T-junction show oscillating variation with respect to the Strouhal number, indicating amplification and attenuation of the incident sound at particular Strouhal numbers. The Strouhal numbers where an amplification is displayed corresponds to intervals where the calculated resistance decreases to negative values as shown in Figure 5-b. Moreover, it can also be seen that the Strouhal numbers at which the resistance values equal zero are 2^n multiples of a principle Strouhal number, i.e., the resistance decreases to cross zero at $St \approx 0.44, 0.86, 1.67$.

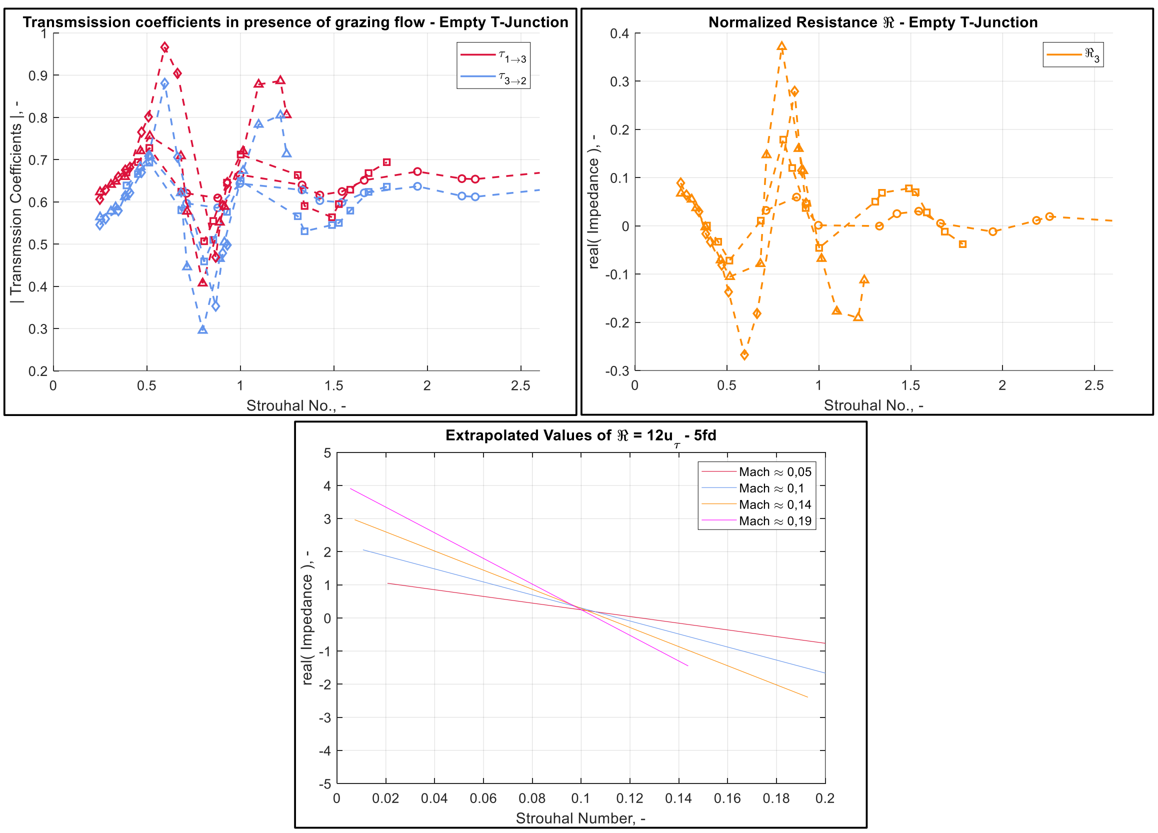

Figure 5 a) Magnitude of the transmission coefficients of the empty T-Junction; b) Normalised resistance of the Empty T-junction calculated under normal acoustic incidence; circles: Mach No. ≈ 0.05, squares: Mach No. ≈ 0.1, triangles: Mach No. ≈ 0.14, diamonds: Mach No. ≈ 0.19; c) Extrapolation of resistance calculated using Eq. (13) to determine the zero resistance Strouhal number.

To compare with the perforated sample, Figure 5-c shows the extrapolated resistance of the perforated plate. This extrapolation is done adhering to Eq. (13), with the aim of determining the Strouhal number where the resistance of the perforated sample in presence of grazing flow becomes zero. The Strouhal Number is determined to be roughly 0.11. In case of the empty T-junction experiments, for the given frequency range all the determined Strouhal numbers are > 0.25. On expanding the frequency range to include lower Strouhal numbers, if a fundamental is observed at $St \approx 0.11$, it suggests a similarity in the flow-acoustic field of an empty T-junction and a perforate under normal acoustic incidence. Moreover, in case of the perforate an approach towards an oscillating behavior, like the one observed in the empty T-junction, can also be investigated by expanding the Strouhal Number range. If observed, these similarities in the flow-acoustic field under normal acoustic incidence can be the reason for the behavior of the perforate resistance curve.

IV. Concluding Remarks

To study the transfer impedance of a perforated plate, an experimental three-port technique is presented in this study. Using the three-port, the acoustic properties of the perforate are studied with and without the presence of grazing flow, and under acoustic incidence from the normal and the grazing directions. To reduce the errors occurring due to termination reflections, incorporation of the scattering matrix coefficients in the calculation of the transfer impedance is displayed. In the absence of flow, agreement between the calculated resistance and an existing analytical model is found. On the addition of grazing flow, determination of the flow profile characteristics is carried out. A clear dependency of the flow velocity on the value of normalized resistance is seen and the resemblance between the behavior of the three-port results and existing semi-empirical models is shown. Modifications in the constants of the existing models are suggested to fit the experimental results. Similarities in the flow-acoustic field of an empty T-junction and a perforated section are shown. Moreover, a possible reason for the behavior of the calculated resistance curve under normal acoustic incidence is proposed. Future works include expanding the Strouhal number range to study the possibly oscillating amplification and attenuation by the perforate sample, and study the discrepancy observed in the calculated resistance under excitation from normal and grazing directions.

Acknowledgments

This work is part of the Marie Skłodowska-Curie Initial Training Network Pollution Know-How and Abatement (POLKA). We gratefully acknowledge the financial support from the European Commission under call H2020-MSCA-ITN-2018 (project number: 813367).

References

[1] Jones, M. G., Parrott, T. L., and Watson, W. R., *Comparison of Acoustic Impedance Eduction Techniques for Locally-Reacting Liners*, in *9th AIAA/CEAS Aeroacoustics Conference*. 2003: Hilton Head, South Carolina. p. 1837-1847.

[2] Watson, W. R. and Jones, M. G. , *Comparison of Convected Helmholtz and Euler Model for Impedance Eduction in Flow*, in *12th AIAA/CEAS Aeroacoustics Conference*. 2006: Cambridge, Massachusetts.

[3] Jones, M.G., Watson, W.R., and Nark, D.M., *Effects of Flow Profile on Educed Acoustic Liner Impedance*, in *16th AIAA/CEAS Aeroacoustics Conference*. 2010: Stockholm, Sweden.

[4] Jones, M.G. , Watson, W.R., Howerton, B.M. and Busse-Gerstengarbe, S., *Comparative study of Impedance Eduction Methods, art 2: NASA Tests and Methodology*, in *19th AIAA/CEAS Aeroacoustics Conference*. 2013.

[5] Watson, W.R., and Jones, M. G, *A Comparative Study of Four Impedance Eduction Methodologies Using Several Test Liners*, in *19th AIAA/CEAS Aeroacoustics Conference*. 2013: Berlin, Germany.

[6] Elnady, T., Bodén, H., and Elhadidi, B., *Validation of an Inverse Semi-Analytical Technique to Educe Liner Impedance.* AIAA Journal, 2009. **47**: p. 2836-2844.

[7] Busse-Gerstengarbe, S., Richter, C., Lahiri, C., Enghardt, L., Roehle, I., Thiele, F., Ferrante, P., and Scofano, A., *Impedance Eduction Based on Microphone Measurements of Liners under Grazing Flow Conditions.* AIAA Journal, 2012. **50**: p. 867-879.

[8] Zhou, L., Bodén, H., Lahiri, C., Bake, F., Enghardt, L. and Elnady, T., *Comparison of impedance eduction results using different methods and test rigs*, in *20th AIAA/CEAS Aeroacoustics Conference*. 2014: Atlanta, GA.

[9] Kabral, R., Bodén, H. and Elnady, T., *Determination of Liner Impedance under High Temperature and Grazing Flow Conditions*, in *20th AIAA/CEAS Aeroacoustics Conference*. 2014: Atlanta, GA.

[10] Bodén, H., Zhou, L., Cordioli, J., Medeiros, A. and Spillere, A., *On the effect of flow direction on impedance eduction results*, in *22nd AIAA Aeroacoustics Conference*. 2016.

[11] Dean, P.D., *An In-Situ method of wall acoustic impedance measurements in flow ducts.* Journal of Sound and Vibration, 1974. **34**: p. 97-130.

[12] Zandbergen, T., *On the Practical Use of Three-Microphone Techniqe for In-Situ Acoustic Impedance Measurements on Double Layer Flow Duct Liners*, in *7th AIAA Aeroacoustics Conference*. 1981.
[13] Gaeta, R.J., Mendoza J.M. and Jones M.G., *Implementation of in-situ impedance techniques on a full scale aero-engine system*, in *13th AIAA Aeroacoustics Conference*. 2007.
[14] Dickey, N.S., Selamet, A. and Ciray, M.S., *An experimental study of the impedance of perforated plates with grazing flow.* Journal of Acoustical Society of America, 2001. **110**: p. 2360-2370.
[15] Feder, E. and Dean, L. W., *Analytical and Experimental Studies for Predicting Noise Attenuation in Acoustically Treated Ducts for Turbofan Engines NASA Contractor Report CR-1373* 1969.
[16] Karlsson, M. and Åbom, M., *Aeroacoustics of T-junctions-an experimental investigation.* Journal of Sound and Vibration, 2010. **329**: p. 1793-1808.
[17] Holmberg, A., Karlsson, M. and Åbom, M., *Aeroacoustics of rectangular T-junctions subject to combined grazing and bias flows - An experimental investigation.* Journal of Sound and Vibration, 2015. **340**: p. 152-166.
[18] Myers, M.K., *On the Acoustic Boundary Condition in the presence of Flow.* Journal of Sound and Vibration, 1980. **71**: p. 429-434.
[19] Guess, A.W., *Calculation of Perforated Plate Liner Parameters from Specified Acoustic Resistance and Reactance.* Journal of Sound and Vibration, 1975. **40**: p. 119-137.
[20] Shah S., Bodén H. and Boij, S., *Experimental Study on the Acoustic Properties of Perforates under Flow using Three-Port Technique*, in *27th International Congress on Sound and Vibration*. 2021 (unpublished).
[21] Kooi, J.W. and Sarin, S.L., *An experimental study of the acoustic impedance of Helmholtz resonator arrays under a turbulent boundary layer*, in *7th AIAA Aeroacoustics Conference*. 1981.
[22] Rice, E.J. , *A Model for the acoustic impedance of a perforated plate liner with multiple frequency excitations* 1971.
[23] Åbom, M. and Bodén, H. , *Error analysis of two-microphone measurements in ducts with flow.* Journal of Acoustical Society of America, 1988. **83**: p. 2429-2438.
[24] Kirby, R. & Cummings, A., *The impedance of perforated liners subjected to grazing flow and backed by porous media.* Journal of Sound and Vibration, 1998.
[25] Cummings, A., *The effects of Grazing Turbulent Pipe-Flow on the Impedance of an Orifice.* Acoustica, 1986. **61**: p. 233-242.
[26] Rao, N. and Munjal, M., *Experimental evaluation of Impedance of perforates with Grazing Flow* Journal of Sound and Vibration, 1986.
[27] Zanoun, E-S, Nagib,H. and Durst, F., *Refined cf relation for turbulent channels and consequences for high-Re experiments.* Fluid Dynamics Research, 2009. **41**.
[28] Schlichting, H., *Boundary Layer Theory*. 1968: McGraw-Hill Inc.
[29] Dokumaci, E., *A Note on Transmission of Sound in a Wide Pipe with Mean Flow and Viscothermal Attenuation.* Journal of Sound and Vibration, 1997. **208**: p. 653-655.
[30] Lee, M. and Moser, R., *Direct numerical simulation of turbulent channel flow up to* $Re_\tau \approx 5200$. Journal of Fluid Mechanics, 2015. **774**: p. 395-415.
[31] Zhou, L., *Acoustic characterization of orifices and perforated liners with flow and high-level acoustic excitation*, in *MWL Sound and Vibration*. 2015, KTH Royal Institute of Technology.

PAPER B

Aeroacoustics Conferences
June 14-17, 2022, Southampton, UK
28th AIAA/CEAS Aeroacoustics 2022 Conference

10.2514/6.2022-2928

Nonlinear three-port measurements for the determination of high-level excitation effects on the acoustic properties of perforates

Shail A. Shah[1], Hans Bodén[2] and Susann Boij[3]
Marcus Wallenberg Laboratory for Sound and Vibration Research, KTH Royal Institute of Technology, SE- 10044 Stockholm, Sweden

The effect of high-level excitation on the acoustic properties of perforates, and formulation of the non-linear part of the impedance is under scientific discussion. Analytical models including the non-linear properties, as well as various experimental studies give varying results for the acoustic impedance. This paper aims to provide detailed results obtained under high-level excitation with different acoustic wave incidence and flow configurations. Contrary to the well-established two-port configuration, here, a three-port measurement technique is used to observe the acoustic impedance of the perforated plate using excitation from the three different directions. Plane wave propagation is considered and physical quantities such as in-hole particle velocity, which is calculated at the perforate sample, are used as the controlling parameters. This paper is an attempt to study the effect of high-level excitation on the acoustic behavior of the perforates with grazing and normal acoustic incidence. Moreover, the non-linear behavior of the perforate determined in presence of an external grazing flow is also discussed.

I. Introduction

The study of nonlinear acoustic properties of perforates and orifice plates dates back to 1935 [1]. Since then, many papers have been published on the subject, e.g., Ref. [1-9]. Perforates are of interest in many technical applications such as automotive mufflers and aircraft engine liners where they are exposed to a combination of high acoustic excitation levels and either grazing or bias flow. To study the impedance of the perforated top facesheet alone, a method using an impedance tube located in a side branch [10, 11] has been used. The present work intends to study the effect of high-level excitation in such a three-port configuration, used by Karlsson and Holmberg et. al. [12, 13]. This gives the possibility to investigate the nonlinear influence of normal and grazing acoustic incidence on the impedance. Moreover, the effect of the combination of grazing mean flow and high-level excitation is also studied.

In order to study the effect of a certain acoustic level and achieve a result that is independent of the test setup, the level of the excitations was controlled by maintaining the same in-hole particle velocity of the perforate sample for incidence from each of the three duct parts. This allowed to check the dependence of the acoustic incidence direction on the determined characteristics as a function of the in-hole particle velocity. Similar to Refs. [12-14], normalized transfer impedance in the plane wave frequency range is studied in this paper. Results in absence of grazing flow were compared with the models proposed in Refs. [1, 15-18]. A good agreement between the experimental results of this study and that of Temiz et. al. [15] is observed in a majority of the measurement range.

With the addition of grazing flow, effects of high-level excitation are observed in this study for a flow speed up to Mach number ≈ 0.05. Previous research on liners suggests the non-linear part of the resistance to be independent of the flow field and only dependent on the particle velocity, e.g. Refs. [17, 18]. However, in this study, the determined non-linear part of the resistance under high-level excitation and in presence of grazing flow is compared against a non-dimensional ratio of particle and grazing flow velocity. A second-degree polynomial relation is observed between

[1] Ph.D. Student, Department of Engineering Mechanics; shail@kth.se
[2] Professor, Department of Engineering Mechanics; hansbod@kth.se
[3] Associate Professor, Department of Engineering Mechanics; sboij@kth.se

them. This suggests an influence of the flow field on the non-linear part of the resistance, as explained in section III-D. Moreover, observations related to the behavior of the determined coefficients of the polynomial relationship with other experimental factors are also pointed out. For grazing flow speeds of Mach number higher than 0.05, the non-linear effects can no longer be seen with the level of excitation used in this study.

II. Experimental Technique

Inspired by Ref. [12], the three-port technique has been previously used for characterizing the behavior of a perforate in presence of grazing flow in Refs. [14, 19]. The schematic of the three-port used in this work is as shown in Fig. 1, with the perforate sample mounted flush at the opening of pipe III. Three condenser microphones are placed in each of the test ducts I, II and III to perform plane wave decomposition. Moreover, an extra microphone is placed in the duct wall opposite to the perforate sample. A perforate sample with hole diameter and plate thickness 1.2 mm and 2.54 % open area is placed covering the opening of duct III at the intersection of ducts I and II. The dimensions of the sample are: 25 mm in the axial direction of duct I and II and 120 mm wide. The duct height is 25 mm.

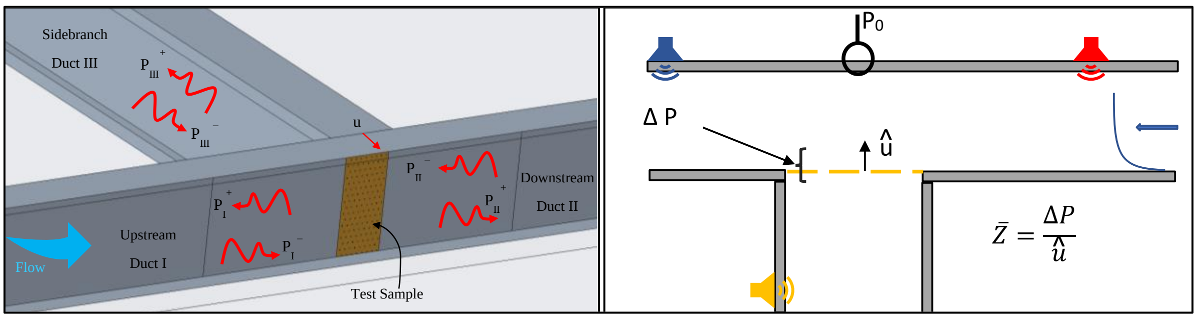

Fig. 1 a) Schematic of the three-port technique [14]; b) Calculation of the transfer impedance

The real part of the transfer impedance (Z) is normalized with the characteristic impedance of air (ρc) to give the normalized resistance ($\Re$). It is the main characteristic of interest in this study and is defined as the ratio of the pressure difference across the perforate (ΔP), and the particle velocity at the perforate surface ($\hat{u}$) as shown in the following equation [14]:

$$\Re = \frac{1}{\rho c} real(Z) = \frac{1}{\rho c} real\left(\frac{\Delta P}{\hat{u}}\right) = real\left(P_{III} - P_0 \big/ P_{III}^{-} - P_{III}^{+}\right), \tag{1}$$

where P_{III} is the total acoustic pressure at the sample surface in duct III, P_0 is the total acoustic pressure measured by the flush mounted microphone on the opposite duct wall of the perforate, as shown in Fig. 1. Lastly, $P_{III}^{\pm}$ are the decomposed wave amplitudes. Results of Ref. [14] suggest that a good estimate of the total acoustic pressure in the perforated section of the T-Junction is given by the pressure signal P_0 and hence it can be directly used to determine the transfer impedance.

In order to classify the calculated results, dimensionless numbers, namely the Strouhal Number (*St*), and the Shear Number (*Sh*) are used. They are defined as per the Eq. (2).

$$Sh = d\sqrt{\frac{\omega\rho}{4\mu}};$$
$$St = \frac{\omega d}{u}, \tag{2}$$

where d is the diameter of the perforation, ω is the angular frequency, ρ is the density, μ is the dynamic viscosity, and u is the root-mean-squared (RMS) value of the in-hole particle velocity. Temiz et al. in Ref. [15] defines a model for the non-linear behavior of the perforated plate, which is classified into different regimes using these dimensionless numbers. The model is defined semi-empirically for the measurement range of $0.05 < St, Sh < 10$. The measurement range of this study is from $0.1 < St < 8$ and $5 < Sh < 12$. Hence there exists a good overlap of the experimental data between both the studies. The model proposed in Ref. [15] follows Eq. (3).

$$\Re = \Re_{Lin} + \frac{F_c(St, Sh)\rho u}{2C_v^2\sigma};$$
$$F_c(St, Sh) = \frac{1}{1 + 2St[1 + 0.06e^{3.74/Sh}]}, \tag{3}$$

where $\Re_{Lin}$ is the resistance in the linear range, C_v is the vena contracta factor and σ is the open area of the perforated plate.

The calculated value of the resistance in the linear range ($\Re_{Lin}$) follows the model proposed by Guess [20], as shown in Ref. [14, 19]. The model is as shown in Eq. (4), and the validation of this calculated value of resistance is shown in the results section.

$$\Re_{Lin} = \frac{(\sqrt{8\nu\omega})t'}{\sigma c d C_d}, \qquad t' = t + d, \tag{4}$$

where ν is kinematic viscosity, t is the thickness of the perforate, and c is the speed of sound. Here t' is defined as the corrected length of the perforations by Guess in Ref. [20], and accordingly is equivalent to the sum of the thickness of the perforated plate and the perforation diameter (d). C_d is the coefficient of discharge and is determined using the DC flow resistance of the perforate (θ_{DC}), following the Eq. (5) and as described in Ref. [21].

$$\theta_{DC} = \frac{1}{\rho c}\frac{\Delta P}{u_{DC}} = \frac{32\nu t}{\sigma c d^2 C_d} + \frac{u_{DC}}{2\sigma^2 C_d^2}, \tag{5}$$

where in the above equation, ΔP is the DC pressure difference across the perforate when the surface velocity in the direction normal to the perforate surface is u_{DC}. Measurement of the velocity and the pressure difference is carried out and following Eq. (5), the value of C_d is determined.

For the experiments conducted in presence of grazing flow, similar to the in-situ impedance measurement technique [22] and the side branch method [10, 11], the three-port post processing method does not use the Ingard-Myers boundary condition. To characterize the experimental results against a dimensionless number describing both the flow field and the sound field in the three-port, the results are compared with respect to the ratio of the RMS value of the in-hole particle velocity (u) and the grazing flow bulk velocity (U).

The determination of the grazing flow bulk velocity is carried out by integrating the flow profile as shown in Ref. [14]. The flow profile was measured using pitot tubes up- and downstream of the perforate sample, with negligible deviation between the cases. The in-duct temperature was monitored using thermocouples and was used for post-processing. The wavenumber used for performing the wave decomposition follows the model proposed by Dokumaci in Ref. [23]. Acquisition of the sound pressure was carried out using flush mounted Brüel and Kjær ¼- inch 4938 type condenser microphones and NI 9234 DAQ modules.

III. Results

A. Resistance in the linear range and Coefficient of Discharge

Experimental determination of the coefficient of discharge (C_d) was carried out as explained in the above section. Following Eq. (5), a value of C_d = 0.62 was calculated. Fig. 2-a shows the comparison between the experimental and the calculated values of pressure drop over the perforate at different levels of in-hole DC velocity. A good agreement between both the cases can be clearly seen. Implementing the value of C_d, Fig. 2-b shows a comparison between the calculated resistance in the linear range using the model in Eq. (4), and the experimentally determined value of resistance following Eq. (1).

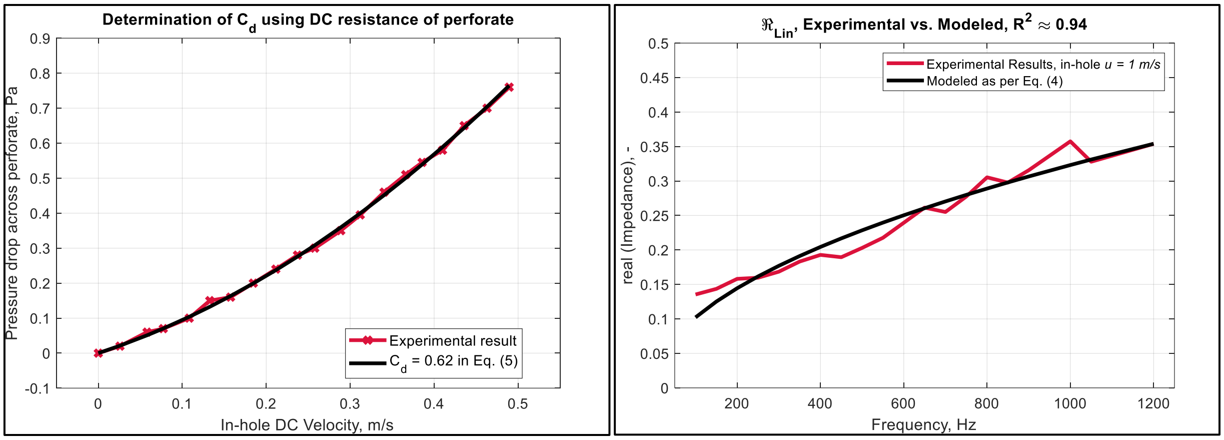

Fig. 2 a) Determination of C_d using DC Resistance of perforate; b) Normalized resistance of perforate in linear range

The RMS value of the in-hole particle velocity is controlled to be equal to 1m/s in the experimental results, suggesting it to be in the linear range. The coefficient of determination (R^2) value between the model and experimental results is ≈ 0.94, suggesting a good fit.

B. Results under high-level excitation from three incidence directions

Experiments under high-level excitation were conducted, where the in-hole particle velocity was controlled across the frequency range. Fig. 3 displays the behavior of the perforate resistance with respect to the direction of acoustic incidence. The resistance $\Re_x$ compared against the in-hole particle velocity, is determined under excitation from each of the three duct parts (duct-*x*). Classification in different frequency regions is depicted by the Shear number (*Sh*).

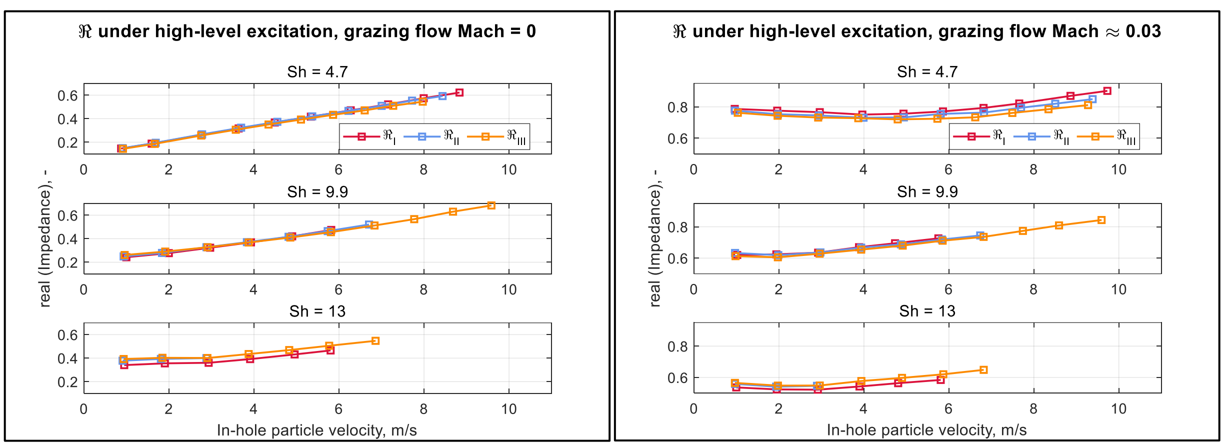

Fig. 3 Independence of normalized resistance from acoustic incidence direction: a) No grazing flow; b) Grazing flow Mach No. ≈ 0.03

The curves overlap with each other suggesting that the resistance is completely independent of the incidence direction. The same independence is also observed in presence of grazing flow in the three-port. Hence, for the rest of this study, results only from duct-III excitation are studied.

The particle velocity at different frequencies is dependent on the standing wave pattern in the three-port. Due to the hardware limit of the loudspeaker used for the experiments, for the highest shear number in Fig. 3, the maximum attainable in-hole velocity was 7m/s.

The behavior of the resistance with respect to the increasing particle velocity in Fig. 3-a, displays a linear increase and is as observed in Ref. [1] as well as in the majority of the research carried out on the non-linear properties of perforates till date.

C. Results under high-level excitation in absence of grazing flow

To study the behavior of the calculated resistance with no grazing flow, comparison of the experimental results with existing models in Refs. [2, 15-18] was carried out. It was found that for the measurement range, perforate properties, and the calculated resistance of this study, a scaled version of the model proposed in Ref. [15] matches well with the results. The scaling of the model was carried out with respect to the porosity of the perforate and the vena contracta factor (C_v). As per Flügge in Ref. [24], the value of C_v is approximately equal to that of the coefficient of discharge, however, empirically a $C_v \approx 0.57$ was chosen to give a better fit with the model. The comparison between the experimental results and the discussed model against the inverse Strouhal number ($1/St$) is as shown in Fig. 4.

It can be seen from the result that for a Strouhal number < ≈ 0.3, i.e., for inverse Strouhal > ≈ 3, the model starts deviating from the experimental results. A possible reason is that the model is designed in Ref. [15] for a 'transition state' where the Strouhal number value is close to 1. For higher values of $1/St$ i.e., for St << 1, it can be seen in Fig. 4 that rather than the transition state model, the resistance follows a linear relation with respect to the inverse Strouhal number, and by extension, the in-hole particle velocity, as seen in Ref. [1].

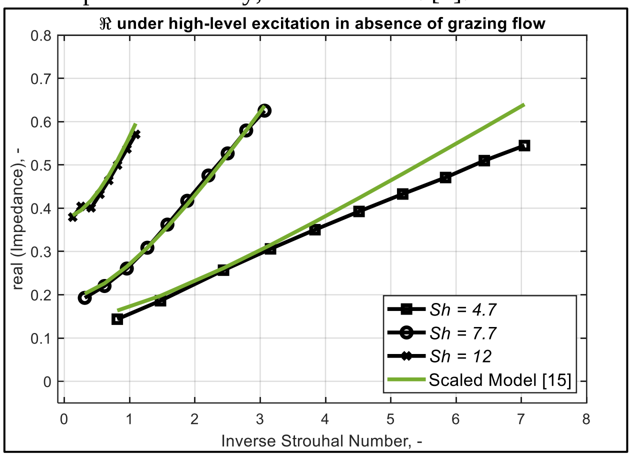

Fig. 4 Normalized Resistance under high-level excitation in absence of grazing flow compared with the scaled existing model by Temiz et. al. [15]

D. Results under high-level excitation in presence of grazing flow

In order to study the effect of high-level excitation in the presence of grazing flow, the calculated non-linear part of the resistance is compared against the ratio of the in-hole particle velocity and the bulk velocity of the grazing flow (u/U). The non-linear part of the resistance at three different flow speeds and for three different shear numbers (frequency regions) can be seen in Fig. 5. The non-linear part of the resistance ($\Re_{NL}$) is determined by taking the resistance calculated under high-level excitation and subtracting the linear part of the resistance, i.e., the resistance determined when the in-hole particle velocity is controlled to be 1 m/s across all the frequencies. Hence by this definition, for the lowest value of u/U in Fig. 5, the non-linear part of resistance is equal to zero.

It can be seen that for low values of the u/U ratio the non-linear part of the resistance has a negative value. The physical reason for that is currently unknown. However, with increasing Shear number, the ratio of u/U where $\Re_{NL}$ is negative, decreases. This suggests that along with the particle velocity and grazing flow velocity, there is a dependance of $\Re_{NL}$ on the frequency. A second-degree polynomial model between $\Re_{NL}$ and u/U appears to fit well with the experimental results, following Eq. (6).

$$\Re_{NL} = A\left(\frac{u}{U}\right)^2 + B\left(\frac{u}{U}\right) + C, \tag{6}$$

where *A*, *B*, and *C* are empirically defined polynomial coefficients. The relationship of the coefficients with respect to other experimental parameters, e.g., shear number and Strouhal number is currently under study.

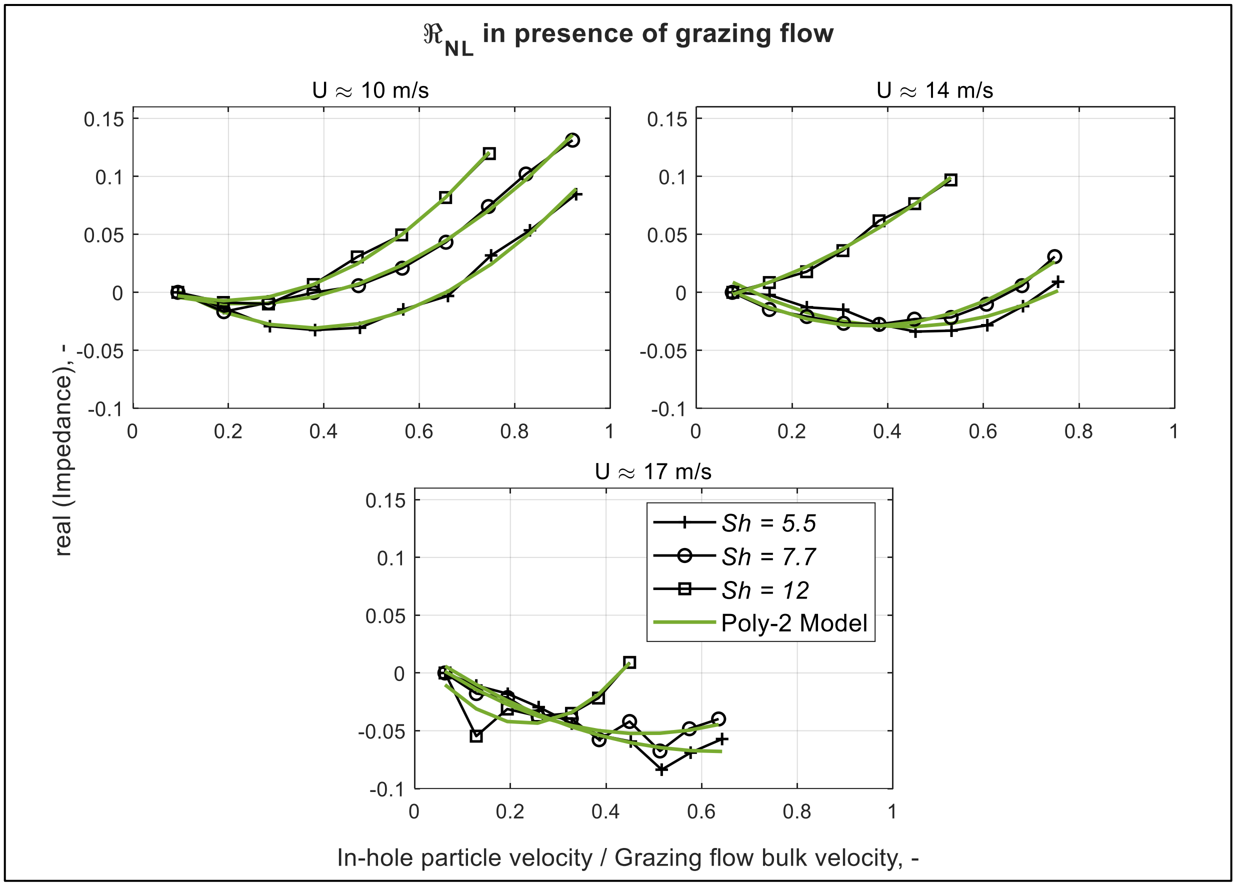

Fig. 5 Non-linear part of the calculated resistance in presence of grazing flow compared against a model, a) Grazing flow bulk velocity = 10 m/s; b) Grazing flow bulk velocity = 14 m/s; c) Grazing flow bulk velocity = 17 m/s

IV. Concluding Remarks

Non-linear behavior of a perforated plate is studied using high-level excitation in an acoustical three-port configuration. Characterization of the perforate using the real part of the normalized transfer impedance, i.e., the resistance, is carried out for a range of values of dimensionless quantities like shear and Strouhal numbers. Validation of the determined resistance in the linear range is done by comparing the experimental results with existing semi-empirical models. Independence of the resistance with respect to the direction of the high-level acoustic incidence is shown in different frequency regions in the plane wave propagation range. Moreover, the resistance calculated in absence of grazing flow in the three-port is compared with existing models and up to a Strouhal number lower limit, a good agreement is observed. In presence of grazing flow, contrary to previous research, a relation between the flow field characteristic, namely the bulk velocity of the grazing flow, and the non-linear part of the determined resistance is observed. A second-degree polynomial model is proposed to describe the relationship. Future work includes a study of the coefficients describing the above-mentioned polynomial relationship, and explanations regarding the physical behavior of the non-linear part of the resistance of the perforate in presence of grazing flow in the three-port.

Acknowledgments

This work is part of the Marie Skłodowska-Curie Initial Training Network Pollution Know-How and Abatement (POLKA). We gratefully acknowledge the financial support from the European Commission under call H2020-MSCA-ITN-2018 (project number: 813367).

References

[1] Sivian, I.J., *Acoustic impedance of small orifices.* Journal of the Acoustical Society of America 1935. **7**.

[2] Ingård, U. and Ising, H., *Acoustic nonlinearity of an orifice.* Journal of the Acoustical Society of America, 1967. **42**.

[3] Rice, E.J. , *A Model for the acoustic impedance of a perforated plate liner with multiple frequency excitations* 1971.

[4] Melling, T.H., *The acoustic Impedance of Perforates at Medium and High Sound Pressure Levels.* Journal of Sound and Vibration, 1973.

[5] Cummings, A., *Acoustic nonlinearities and power losses at orifices.* AIAA Journal, 1984. **22(6)**.

[6] Bodén, H., *Acoustic properties of perforates under high level multi-tone excitation*, in *19th AIAA/CEAS Aeroacoustics Conference*. 2013.

[7] Bodén, H., *The effect of high level multi-tone excitation on the acoustic properties of perforates and liner samples*, in *18th AIAA/CEAS Aeroacoustics Conference*. 2012.

[8] Bodén, H., *One-sided multi-port techniques for characterisation of in-duct samples with nonlinear acoustic properties.* Journal of Sound and Vibration, 2012. **331**.

[9] Bodén, H., *Two-Sided Multi-Port Techniques for Characterisation of In-Duct Samples with Non-Linear Acoustic Properties.* Acta Acustica united with Acustica, 2013. **99**.

[10] Dickey, N.S., Selamet, A. and Ciray, M.S., *An experimental study of the impedance of perforated plates with grazing flow.* Journal of Acoustical Society of America, 2001. **110**: p. 2360-2370.

[11] Feder, E. and Dean, L. W., *Analytical and Experimental Studies for Predicting Noise Attenuation in Acoustically Treated Ducts for Turbofan Engines NASA Contractor Report CR-1373* 1969.

[12] Karlsson, M. and Åbom, M., *Aeroacoustics of T-junctions-an experimental investigation.* Journal of Sound and Vibration, 2010. **329**: p. 1793-1808.

[13] Holmberg, A., Karlsson, M. and Åbom, M., *Aeroacoustics of rectangular T-junctions subject to combined grazing and bias flows - An experimental investigation.* Journal of Sound and Vibration, 2015. **340**: p. 152-166.

[14] Shah, S.A., Bodén, H., Boij, S. and D'elia, M.E., *Three-port Measurements for Determination of the Effect of Flow on the Acoustic Properties of Perforates*, in *AIAA AVIATION 2021 FORUM*. 2021: Virtual Event.

[15] Temiz, M.A., Tournadre, J., Arteaga, I.L. and Hirschberg, A. , *Non-linear acoustic transfer impedance of micro-perforated plates with circular orifices.* Journal of Sound and Vibration, 2016.

[16] Auregan, Y. and Pachebat, M. , *Measurement of the nonlinear behavior of acoustical rigid porous materials.* Physics of Fluids, 1999. **11**.

[17] Renou, Y. , *Impédance des traitements acoustiques absorbants en conduit : effets de l'écoulement rasant et de la couche limite*, in *Laboratoire d'Acoustique de l'Université du Mans*. 2010, Le Mans University.

[18] Elnady, T. and Bodén, H. *On the modelling of the acoustic impedance of perforates with flow*. in *9th AIAA/CEAS Aeroacoustics Conference*. 2003.

[19] Shah, S., Bodén, H. and Boij, S., *Experimental study on the acoustic properties of perforates under flow using three-port technique*, in *27th International Congress on Sound and Vibration*. 2021: Prague.

[20] Guess, A.W., *Calculation of Perforated Plate Liner Parameters from Specified Acoustic Resistance and Reactance.* Journal of Sound and Vibration, 1975. **40**: p. 119-137.

[21] Betts, J.F., *Experiments and Impedance Modeling of Liners Including The Effect of Bias Flow*. 2000, Virginia Polytechnic Institute and State University.

[22] Dean, P.D., *An In-Situ method of wall acoustic impedance measurements in flow ducts.* Journal of Sound and Vibration, 1974. **34**: p. 97-130.

[23] Dokumaci, E., *A Note on Transmission of Sound in a Wide Pipe with Mean Flow and Viscothermal Attenuation.* Journal of Sound and Vibration, 1997. **208**: p. 653-655.

[24] Flügge, S. , *Handbuch der Physik*. 1955: Springer.

PAPER C

An experimental study on three-port measurements for acoustic characterization of a perforate

Shail A. Shah[a], Hans Bodén[a], Susann Boij[a]

[a] *The Marcus Wallenberg Laboratory for Sound and Vibration Research, Department of Engineering Mechanics, KTH Royal Institute of Technology, Stockholm, SE-10044, Sweden*

Abstract

Multiple analytical, experimental, and numerical studies have been carried out on perforates to study their properties under operating conditions, resulting in varying hypothesis and models to predict their performance. The ongoing effort of providing experimental results using multiform test setups is continued in this study. Incorporating the three-port technique, the passive acoustic response of a perforated plate is studied under acoustic excitation from three directions in presence of grazing flow and high-level excitation. Similar to the in-situ method, usage of the three-port technique has an advantage of being a direct method for impedance determination and is not bound by any boundary conditions traditionally considered in presence of grazing flow. Extending the observations of previous studies, a semi-empirical model is determined for the real part of the transfer impedance of a perforate, where the characterisation of the determined impedance on the testing parameters like the Strouhal number, particle velocity, flow velocity and shear number is displayed.

Keywords: Perforate, Three-port technique, Resistance, Grazing flow, Non-linear effects

1. Introduction

Perforated plates are an integral component of passive noise control solutions, e.g., aircraft liners and mufflers. Majority of the applications of a perforated plate involve an exposure to grazing flow and high-level acoustic incidence [1]. Aero-acoustic characterization of perforates is hence necessary and has been studied in detail over the last few decades [2, 3, 4, 5, 6]. The current scientific discussion involves the effect of relative propagation and mean flow directions on the passive acoustic property of perforates. Various impedance eduction techniques on liners have shown differing results when the propagation is from either the upstream or downstream direction [6, 7]. Many of these techniques implement the Myers boundary condition [8] to explain the flow-acoustic interaction along the perforated surface, however, other studies like Renou and Auregan [9] also contradict this boundary condition. Hence there is a requirement of experimental results acquired without implementing any boundary condition to further the study of perforates.

Direct methods using impedance tubes as a sidebranch, and the in-situ method have also been popularly used on perforated facesheets by Dickey et al. [10] and Dean [11]. Inspired from these studies, this paper contributes to the ongoing research by providing experimental results of the perforate characteristics, namely the real part of the normalised transfer impedance and the scattering matrix. These characteristics are determined under excitation from three different directions with respect to the grazing flow.

Aero-acoustic characterization of circular and rectangular T-Junctions have been studied using the three-port technique, described in detail by Karlsson and Åbom [12] and Holmberg et al. [13], respectively. When compared against a grazing flow velocity based Strouhal number, an oscillating behaviour of amplification and attenuation of the incoming sound waves is observed. This behaviour is associated with hydrodynamic feedback, as also seen in Testud et al. [14], Moers et al. [15] and Howe [16].In this paper, following Karlsson and Åbom [12] and Holmberg et al. [13], the three-port technique is used to determine the acoustic properties of a perforated plate which is mounted at the intersection of a T-junction. The application of the technique is first carried out in Refs. [17, 18] and is further studied here. In absence of grazing flow the determined resistance of the perforate agrees well with the model proposed by Guess [5], where the model is scaled with respect to the discharge coefficient of the plate, as shown in Refs. [17, 18].

In presence of grazing flow, it was found in Ref. [17] that the Strouhal number at which, for an empty T-Junction the maximum amplification of incoming sound waves is seen, is the fifth harmonic of the Strouhal number at which the resistance of the perforate is minimum. This suggested a resemblance in the behaviour of an empty T-Junction and a perforate. However, the testing parameter range of the grazing flow velocity and the frequency did not experimentally validate this resemblance in Ref. [17]. In order to study if the behaviour of an empty T-junction and a perforated plate is analogous in nature, expansion of the testing conditions was carried out in Ref. [19]. It was found that in case of the perforate, an oscillating behaviour is absent. Instead, the Strouhal number of interest represents a limit till which the nature of the normalised resistance is dependent on both the flow- and the acoustic field, and beyond this Strouhal number, it is mainly depending on the acoustic field. Results from Kooi and Sarin [20], Cummings [21] and Kirby and Cummings [22] suggest that the determined resistance uptill the above-mentioned Strouhal number limit is dependent on the skin-friction velocity of the flow profile. For Strouhal numbers above the limit, Kooi and Sarin [20] suggest that the resistance is equal to the resistance determined in absence of grazing flow. Discussion of the above mentioned points is carried out in section 4.1.

In case of high-level excitation incidence, several studies have been carried out to determine the non-linear behaviour of the resistance, e.g., Refs. [3, 23, 24, 25, 26]. A majority of the existing research separately determines the non-linear part of the impedance and then adds it to the impedance determined in the linear range. A dependence of the non-linear part of the resistance on the in-hole particle velocity is observed in most of these models. In absence of grazing flow, Temiz et al. [27] propose a model for microperforated plates with circular orifices and sharp edges in the transition region where the Strouhal number, determined using the in-hole particle velocity, is close to a value of 1. This model is used as a reference for the three-port measurements as shown in Shah et al. [18], and agrees well for the majority of the frequency range used in the experiments. For a strongly non-linear regime, i.e., Strouhal number $\ll 1$, a deviation from the transition state model is seen and the resistance is found to be linearly dependent on the particle velocity. In presence of grazing flow, models proposed by Elnady and Bodén [28] and Renou [29] show the dependence of the non-linear part of the resistance on the in-hole particle velocity. However, for lower grazing flow speeds, Shah et al. [18] show that the non-linear part of the resistance has a 2^{nd} degree polynomial relationship with the ratio of in-hole particle velocity and the grazing flow velocity. The behaviour of this relationship is studied in further detail in this paper, as shown in section .

Experiments carried out on the perforate in the T-junction attempt to characterize the aero-acoustic field in the T-Junction, by comparing the real part of the normalised transfer impedance and the scattering matrix coefficients. Given that the perforate is studied under a plane wave excitation, the wavelength of the incoming sound waves is very high compared to the thickness of the perforate. Hence only the real part of the transfer impedance, i.e., the resistance is considered in this study. Unlike a traditional liner, a relatively smaller surface area of the perforated plate is studied here. Hence, a negligible disruption of the flow profile is seen across the length of the perforated section. However, the results of the transfer impedance show a similarity with the trends observed in Kooi and Sarin [20], where the experiments were carried out on a lined section significantly larger than the one considered in this study. This suggests that the study of a smaller exposed area does not alter the aero-acoustic properties observed.

Based on the determined results, this paper proposes a semi-empirical model for the resistance in presence of grazing flow and high-level excitation. The proposed model includes the dependence on the flow profile characteristics of Mach number, as well as dimensionless numbers such as the Strouhal and the Shear number. Dependence on the perforate properties of thickness, diameter of perforation and open area are not included in the model and are only used to calculate the linear resistance in absence of grazing flow. This is not to contradict existing research that the resistance of the perforate in presence of grazing flow depends on these factors, but due to the study consisting of experiments on only one perforate sample. In addition, the coefficients describing the resistance of the perforate in Section 4 are determined empirically and can be dependent on the perforate properties.

2. Theoretical Background

The characterisation of the acoustic properties of perforated plates is generally done using the normalised transfer impedance ($\bar{Z}$) where the actual transfer impedance of the perforate is normalised with respect to the characteristic impedance of air. The other characteristic of interest is the three-port scattering matrix (S-Matrix). To avoid the experimental errors related to the standing wave pattern in the ducts, a correlation between the scattering matrix coefficients and the normalised transfer impedance is shown in Ref. [17]. The above-mentioned correlation defines the transfer impedance and is explained and governed by equations given in Section 3. A brief background of the existing research reviewed in this study is explained below.

2.1. Linear Resistance in absence of grazing flow

In Shah et al. [18], as well as in Ref. [17], the experimentally determined real part of normalised transfer impedance, i.e., the resistance ($\Re$) in absence of grazing flow and in the linear range in the three-port setup, agrees well with the model shown in Eq.(1) [5, 28].

$$\Re = \frac{(\sqrt{8\nu\omega})t^{'}}{\sigma c d C_d} + \frac{\rho c d^2}{2\lambda^2},\ t^{'} = t + d, \tag{1}$$

where ν is the kinematic viscosity, ω is the angular frequency, σ is the percentage open area, c is the speed of sound, d is the diameter of the perforation, t is the thickness of the perforate, ρ is the density at room temperature, and λ is the excitation wavelength. The extended thickness ($t^{'}$) is defined as the sum of t and d by Guess [5]. The scaling with respect to the discharge coefficient (C_d) is as proposed by Elnady and Bodén [28]. Determination of C_d is done as shown in Shah et al. [18]. This value of resistance is used as a reference for calculating the resistance in presence of grazing flow as well under high-level excitation.

2.2. Non-Linear Resistance in absence of grazing flow

The non-linear part of the resistance calculated using the three-port measurements is investigated in Shah et al. [18]. The determined resistance at high-level excitation follows the model proposed by Temiz et al. [27]. The model is governed using an empirically defined function F_c, where F_c is determined using dimensionless Strouhal number (St_u) and Shear number (Sh). These dimensionless numbers are defined in Eq.(2).

$$\begin{aligned} Sh &= d\sqrt{\frac{\omega\rho}{4\mu}} \\ St_u &= \frac{\omega d}{u} \end{aligned}, \tag{2}$$

where μ is the dynamic viscosity, and u is the r.m.s. value of the in-hole particle velocity. For most of the frequency range the experimentally determined non-linear part of resistance ($\Re_{NL}$) follows Eq.(3).

$$\begin{aligned} \Re_{NL} &= \frac{F_c(St_u, Sh)\rho u}{2{C_v}^2\sigma} \\ F_c(St_u, Sh) &= \frac{1}{1 + 2St_u[1 + 0.06e^{3.74/Sh}]} \end{aligned}, \tag{3}$$

where C_v is the vena-contracta factor, which is taken to be 0.57 following Shah et al. [18]. The resistance under high-level excitation can be determined with the addition of the non-linear part $\Re_{NL}$, and the resistance calculated in the linear range following Eq. (1). The validity of this model as per Temiz et al. [27] is said to be in the region of St_u $\mathcal{O}$ 1.

2.3. Linear Resistance in presence of grazing flow

Which grazing flow parameter best defines the relationship of the resistance in presence of grazing flow, is contested in the previous studies. Models proposed by Kooi and Sarin [20] and others [21, 22] discuss the dependence of the resistance on the skin friction velocity (u_τ) as well as frequency following Eq. (4).

$$\frac{\Re_{Flow} c}{\omega d} = \frac{\kappa u_\tau}{\omega d} - \zeta, \tag{4}$$

where $\Re_{Flow}$ is the resistance determined in presence of grazing flow and κ, ζ are empirically defined coefficients depending on the thickness of the perforate, and the diameter of the perforations. These constants differ in each reference. On the other hand, models proposed by Rao and Munjal [30] and others [3, 5] show the resistance to be a function of only the grazing flow Mach number (M), and independent of the frequency, following Eq.(5).

$$\Re_{Flow} = \frac{\epsilon M}{\sigma}, \tag{5}$$

where ϵ is also an empirically defined coefficient equal to 0.3 in Ref. [3, 5] and 0.53 in Ref. [30]. In Ref. [17] it is observed that the behaviour of the resistance determined in the three-port setup at different grazing flow velocities converges at a particular flow Strouhal number (St_U) defined using the flow velocity. This suggests a dependence of the resistance on this Strouhal number. To validate, experimental parameters, namely the frequency range and the grazing flow velocities are expanded in this paper and the determined resistance is discussed in Section 4. The definition of the flow velocity based Strouhal number is as per Eq.(6).

$$St_U = \frac{\omega d}{U}, \tag{6}$$

where U is the grazing flow bulk velocity.

2.4. Non-Linear Resistance in presence of grazing flow

The reviewed research, namely Feder and Dean [11], Dean [2], Elnady [28], and Renou [29] decouples the non-linear effects observed in the determined resistance in presence of high-level excitation and grazing flow from the flow parameters. They observe the non-linear effects to be solely dependent on the in-hole particle velocity of the perforate. However Shah et al. [18], based on experimental results at low grazing flow velocities (Mach number ≤ 0.05), shows that there exists a 2^{nd} degree polynomial relation between the non-linear part of the resistance ($\Re_{NL-Flow}$) and the ratio of particle velocity to the grazing flow velocity (u/U). The relationship follows Eq.(7).

$$\Re_{NL-Flow} = \alpha(\frac{u}{U})^2 + \beta(\frac{u}{U}) + \gamma, \tag{7}$$

where α,β,γ are the coefficients governing the relationship and their behaviour is discussed in the Section 4.

3. Experimental Technique

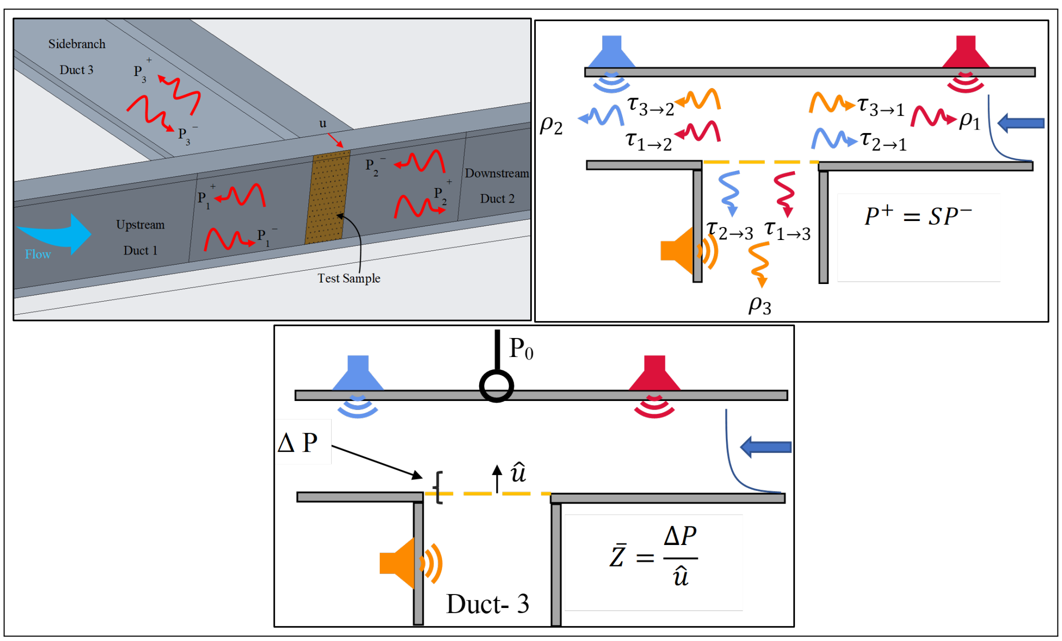

Fig. 1: (a) Schematic of the three-port technique; (b) Calculation of the scattering matrix; (c) Calculation of the transfer impedance

The schematic of the experimental setup is as shown in Fig.1-a. The perforate is flush mounted at the intersection of duct-1,2 and 3, where grazing flow is possible from duct-1 to 2. The end of duct-3 is sealed to have a net zero flow in the duct and avoid leakage. The three-port scattering matrix (S-Matrix) is as defined by Karlsson and Åbom [12]. The S-Matrix consists of reflection (ρ_x) and transmission coefficients ($\tau_{x\rightarrow y}$), and is determined with the help of the decomposed wave pressure amplitudes $P_{x\pm}$. It follows Eq.(8) and the nomenclature is as shown in Fig.1-b.

$$\begin{bmatrix} P_{1+} \\ P_{2+} \\ P_{3+} \end{bmatrix} = \begin{bmatrix} \rho_1 & \tau_{2\rightarrow 1} & \tau_{3\rightarrow 1} \\ \tau_{1\rightarrow 2} & \rho_2 & \tau_{3\rightarrow 2} \\ \tau_{1\rightarrow 3} & \tau_{2\rightarrow 3} & \rho_3 \end{bmatrix} \begin{bmatrix} P_{1-} \\ P_{2-} \\ P_{3-} \end{bmatrix} \tag{8}$$

The determination of the decomposed wave pressures is done using the multi-microphone method [31], where $P_{x\pm}$ are determined in each duct using acoustic pressures measured by three microphones in each duct. The propagating wavenumber (k) is determined using model proposed by Dokumaci [32]. To avoid errors pertaining to background noise a frequency response function between the measured pressure signal and the loudspeaker voltage is used for the analysis. In addition to the three microphones in each duct one more microphone is flush mounted on the wall opposite to the perforate and at the centre of the perforated section, i.e., at the intersection of duct-1, and -2. This microphone is used to acquire pressure P_0,as shown in Fig.1-c, and used to calculate the resistance.

The experimentally determined resistance is defined following Eq.(9). The nomenclature follows that of Fig.1-c.

$$\Re = \frac{1}{\rho c} real(\frac{\Delta P}{\hat{u}}) = real(\frac{P_3 - P_0}{P_{3-} - P_{3+}}), \tag{9}$$

where $\hat{u}$ is the particle velocity determined at the sample surface and is determined using the difference of decomposed pressure wave components in duct-3.

In Ref. [17] it is shown that the difference in the resistance determined using the total acoustic pressure P_0 measured by the microphone and the average of total acoustic pressures in duct-1 and -2, is negligible. Hence, we can assume that P_0 is equal to the average of total acoustic pressures P_1 and P_2. Additionally, assuming anechoic termination, a new formulation of the resistance is proposed that correlates the S-Matrix coefficients and the resistance. The usage of this formulation reduces the errors pertaining to the standing wave pattern created in the three ducts, as the S-Matrix coefficients are independent of the termination reflections. The relation is shown in Eq.(10).

$$\begin{aligned}\Re_1 = &\quad real(\frac{\rho_1 + \tau_{1\to 2} + 1}{2\tau_{1\to 3}} - 1),\\ \Re_2 = &\quad real(\frac{\rho_2 + \tau_{2\to 1} + 1}{2\tau_{2\to 3}} - 1),\\ \Re_3 = &\quad real(\frac{1 + \rho_3}{1 - \rho_3} + \frac{\tau_{3\to 1} + \tau_{3\to 2}}{2(1 - \rho_3)}),\end{aligned} \tag{10}$$

where $\Re_x$ is the resistance determined under excitation from duct-x.

For the determination of the non-linear part of the resistance, the controlling parameter chosen is the in-hole particle velocity, i.e., individual frequencies are chosen and the r.m.s. value of the in-hole particle velocity is increased from ≈ 1 m/s to ≈ 10 m/s. The calculation of the r.m.s. value of the in-hole particle velocity in SI units follows Eq.(11)

$$u = |\hat{u}| \frac{V_{rms}}{\rho c S_i \sigma}; V_{rms} = \sqrt{V_{AS} L_w}, \tag{11}$$

where V_{rms} is the r.m.s. value of the acoustic incidence auto spectra (V_{AS}), corrected with the Hanning window factor (L_w). To convert into the SI units, the sensitivity of the microphones (S_i) is divided. Lastly, to calculate the in-hole value, conservation of mass and isentropic nature is assumed and the value calculated at the surface is scaled with the porosity of the perforate (σ).

It is observed that in case of excitation from ducts-1, and 2, the particle velocity determined in duct-3 is limited due to the range of the loudspeakers used for excitation. Hence the S-Matrix cannot be determined for these higher velocity levels and the chosen frequencies, and the resistance is defined using Eq.(9). Additionally, it should be noted that the non-linear part of the resistance observed at lower in-hole particle velocity levels is found to be independent of incidence direction, as shown in Shah et al. [18]. Hence, only the resistance determined under excitation from duct-3 is studied here. For the linear cases, the controlling parameter is the level of excitation incident on the perforate and the resistance is determined across a wider frequency range, increasing the experimental errors related to the standing wave pattern and hence it follows the definition from Eq.(10), reducing this error.

The sample studied here is a rectangular perforate with circular perforations and square edges, with a 2.54% open area. The diameter of the perforation and the plate thickness are both 1.2 mm and the rectangular T-junction has a cross section of 25 mm by 120 mm. The acoustic pressure was acquired using calibrated flush mounted microphones of type Brüel and Kjær $\frac{1}{4}$- inch 4938. NI 9234 DAQ modules were used for data acquisition at a sampling frequency of 25.6 kHz. Plane wave propagation is assumed and the frequency range of the measurements (100-2250 Hz) as well as the microphone distances were determined following the recommendations of Åbom and Bodén [33]. Static temperature measured by a calibrated K-type thermocouple placed in duct-3 is used for determining the speed of sound and further post-processing of acquired data. The determination of the skin friction velocity and the grazing flow bulk velocity follows the method explained in Ref. [17]. The grazing flow bulk velocity is calculated by integrating the flow profile across half the duct width. The average ratio of the calculated bulk velocity to the maximum grazing flow velocity, i.e., the flow velocity measured at the centre of the duct cross-section is found to ≈ 0.92. Additionally, negligible deviation of the flow profile is observed over the perforated region, as shown in Ref.[17]. During the acoustical measurements, a simultaneous flow profile determination was not possible, hence the bulk velocity which is used for post-processing is calculated by multiplying 0.92 with grazing flow velocity measured at the centre of the cross-section, upstream of the sample. The flow rig was controlled to measure the acoustic properties in the range of the bulk velocity from ≈ 10 m/s to ≈ 60 m/s. Stepped sine excitation was used and a signal-to-noise ratio of at least 20 dB was maintained for all the measurements.

4. Results and Discussion

The following section discusses the behaviour of the resistance of the perforate in presence of grazing flow and high-level excitation. The first subsection discusses the comparison of the resistance in the linear range with existing models [5, 20, 28]. Additionally, beyond the experimental range of Kooi and Sarin [20], deviation of the experimental results from their proposed model is investigated. Then, a semi-empirical model covering the entire operating range is proposed. In subsection 4.2, the experimental results in absence of grazing flow are presented and shown to agree with Temiz et al.'s model [27]. In presence of grazing flow, results from Shah et al. [18] are further studied and the relation between the non-linear part of the resistance and the in-hole particle velocity, grazing flow velocity and the Shear number is discussed.

4.1. Resistance in the linear range

The resistance of the perforate in the linear regime was determined experimentally with and without grazing flow, and the results were compared with some existing models. The comparison is shown in Fig.2. Fig.2-a shows the no grazing flow case, where the determined resistance agrees with the model proposed in Eq.(1). A deviation is observed at $\approx$ 1400Hz. However, the deviation does not represent the property of a sample but is present due to the presence of a pressure anti-node at one of the microphone locations. The anomaly disappears on the addition of grazing flow as the entire standing wave pattern changes. Apart from the deviation a good agreement is observed between the model and the experimental results in absence of grazing flow.

In Fig.2 -b to -f, results determined at different grazing flow velocities are shown, along with the resistance modelled as a function of the skin-friction velocity and the frequency, as per Eq. (4). As mentioned in Section 2, the value of the empirical coefficient κ varies in different studies. Here, to show the comparison of the nature of the resistance, κ is interpolated at each flow velocity to get a good match with the experimental results. For the lower flow velocities, i.e., Fig.2 -b and -c, the frequency at which the model starts differing from the results corresponds to $St_U \approx 0.7$. $St_U \approx 0.7$ matches the limit of $u_\tau/fd \approx 0.2$, beyond which Kooi and Sarin [20] propose that their model is valid. Kooi and Sarin [20] state for higher values of St_U, the flow induced resistance is negligible and that the resistance in presence of grazing flow can be determined following the models proposed for the no grazing flow case, which is not seen here. The resistance for $St_U > 0.7$ is still found to be dependent on the grazing flow Mach number.

Moreover, the model also does not account for the difference observed in resistance when the excitation is in the flow direction ($\Re_1$), and when it is against it ($\Re_2$), as observed at higher flow velocities, e.g., in Fig.2 -e and -f. Lastly, looking at the experimental results in Fig.2 -e and -f, it would be not be an unfair assumption to state that the resistance is independent of the frequency, suggesting the behaviour followed by models in Eq.(5) [3, 5, 30], and the validity of these studies.

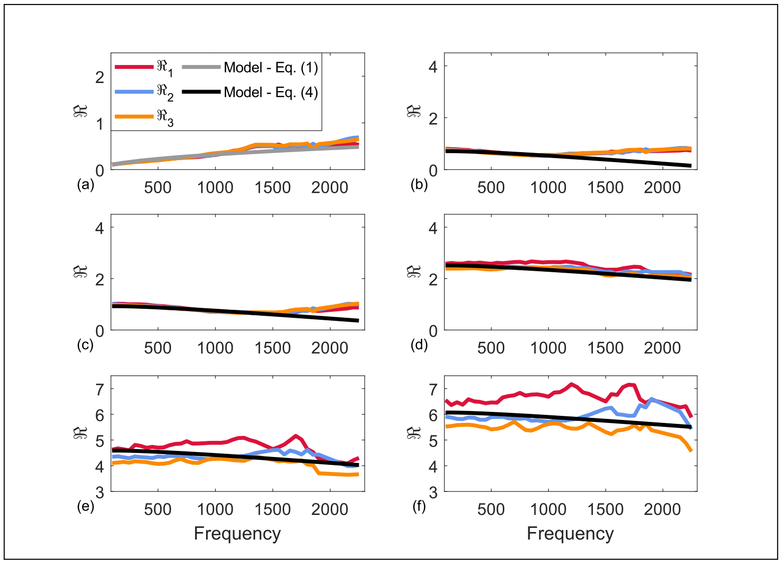

Fig. 2: Comparison of resistance determined following Eq.(10) in the three-port setup, with existing models against frequency. a) No grazing flow; b) Grazing flow $M \approx 0.03$; c) Grazing flow $M \approx 0.04$; d) Grazing flow $M \approx 0.08$; e) Grazing flow $M \approx 0.13$; f) Grazing flow $M \approx 0.17$.

To observe the resistance at a comparable value at all the flow velocities, the scaling of the resistance is applied. It is found that when the resistance is scaled with respect to $M^{1.17}(1 + St_U)^{1.75}$, all the curves at different flow velocities collapse well with each other. Moreover, to account for the difference in the resistance observed with respect to the relative incidence and flow direction, an additional numerical scaling factor can be used to make the resistance independent of the incidence direction. In this study the scaling factors are 0.92 for $\Re_2$ and 0.85 for $\Re_3$. These scaling factors are determined empirically and the combined scaling is done following Eq.(12).

$$\begin{aligned} \Re_1^{'} &= \frac{\Re_1}{M^{1.17}(1 + St_U)^{1.75}}, \; \Re_2^{'} = \frac{\Re_2}{0.92M^{1.17}(1 + St_U)^{1.75}}, \\ \Re_3^{'} &= \frac{\Re_3}{0.85M^{1.17}(1 + St_U)^{1.75}}, \end{aligned} \tag{12}$$

Fig.3 and Fig.4 show the scaled value of resistance at 12 different grazing flow velocities compared against the flow velocity governed Strouhal number (St_U). As observed in Refs. [17, 19], the behaviour of the resistance before

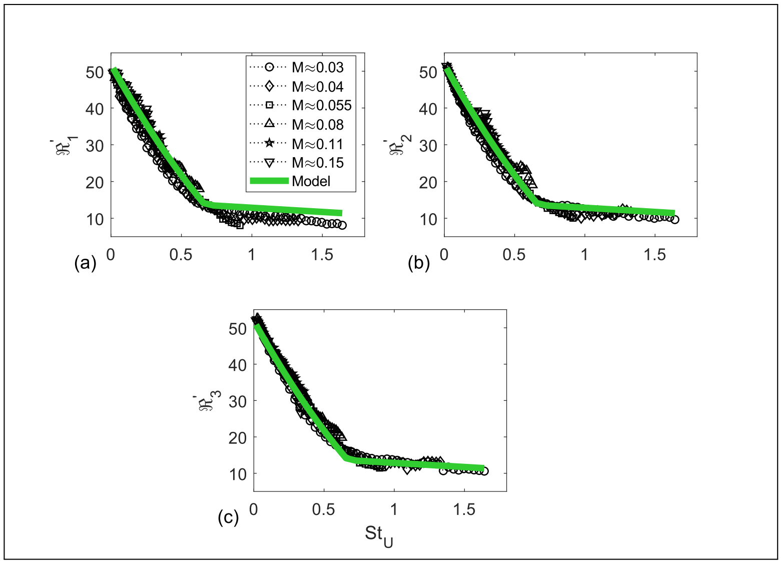

Fig. 3: Comparison of resistance determined in presence of certain grazing flow velocities and scaled following Eq.(12) (black points) with model proposed in Eq.(13) (green lines), against flow velocity governed Strouhal number. Resistance determined under excitation from: (a) duct-1; (b) duct-2; (c) duct-3.

and after the limit of $St_U \approx 0.7$ is completely different. For the lower St_U region, the relation between the scaled value of resistance and St_U is a 2^{nd} degree polynomial. However, after the limit the relation becomes linear with respect to St_U. Moreover, for $St_U > 0.7$, an additional linear dependence on the Mach number is also observed. Hence, a model using empirical defined coefficients can be used to define the resistance in presence of grazing flow in terms of St_U and M. It is displayed in Eq.(13) and the comparison with experimental results is shown in Fig.3 and Fig.4.

$$\Re_x = \begin{cases} when\ St_U < 0.7 & \frac{1}{\psi} M^{1.17}(1+St_U)^{1.75}(17.94{St_U}^2 - 69.22St_U + 51.86) \\ when\ St_U > 0.7 & \frac{1}{\psi} M^{1.17}(1+St_U)^{1.75}((-440M + 10.93)St_U + 311M + 5.8) \end{cases}, \tag{13}$$

where ψ= 1 for $\Re_1$, 0.92 for $\Re_2$, and 0.85 for $\Re_3$.

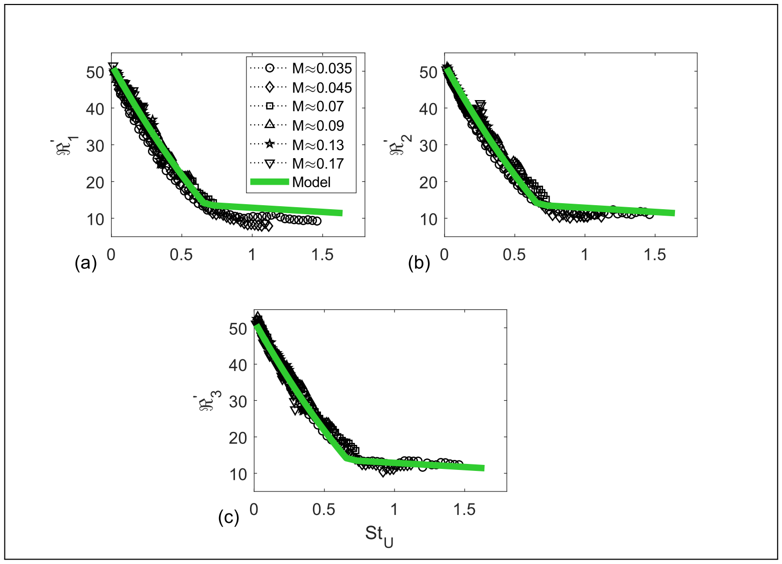

Fig. 4: Comparison of resistance determined in presence of different grazing flow velocities and scaled following Eq.(12) (black points) with model proposed in Eq.(13) (green lines), against flow velocity governed Strouhal number. Resistance determined under excitation from: (a) duct-1; (b) duct-2; (c) duct-3.

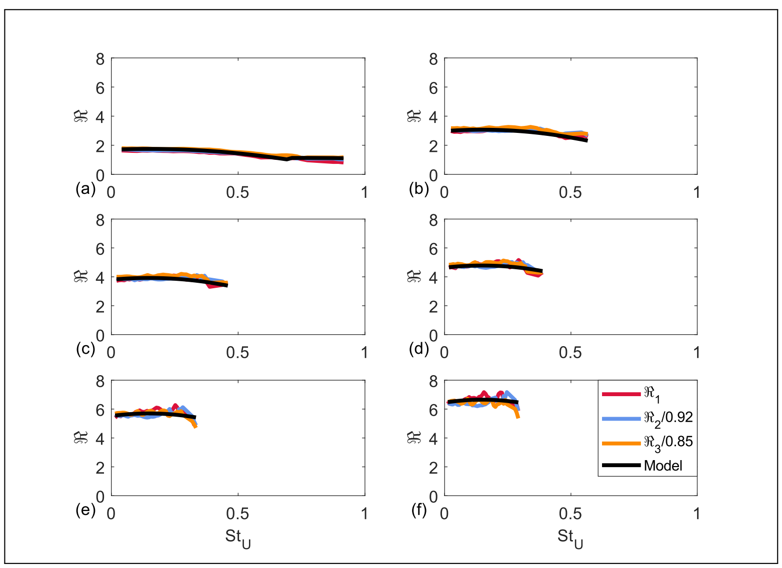

Fig. 5: Comparison of determined resistance, scaled as per the legend, with the model proposed in Eq.(13) against the flow velocity governed Strouhal number. (a) Grazing flow $M \approx 0.055$; (b) Grazing flow $M \approx 0.09$; (c) Grazing flow $M \approx 0.11$; (d) Grazing flow $M \approx 0.13$; (e) Grazing flow $M \approx 0.15$; (f) Grazing flow $M \approx 0.17$.

Fig.5 shows the comparison of the experimentally determined resistance at higher flow velocities ($M > 0.05$) against the Strouhal number. The normalised resistance from different incidence directions is scaled with ψ, following Eq. (13). The experimental results are compared with the model of $\Re_1$ from Eq.(13) and a good agreement can be seen.

4.2. Resistance under high-level excitation

Extending the results of Shah et al.[18] the non-linear part of resistance is studied with and without grazing flow. Comparison between the experimental results with the model proposed by Temiz et al. [27] against $1/St_u$ is as shown in Fig.6. The model is seen to be in good agreement with the results for $1/St_u <\approx 3$. For $1/St_u > 3$, the transition state model no longer matches the results, where the experimental results show the resistance to be linearly dependent on the in-hole particle velocity, as is observed in Melling [4]. In case of 1100 Hz, experimental results deviate from the model at one particle velocity levels. The deviation can be due to the experimental errors as the hardware limits of the loudspeaker were reached in increasing the particle velocity at higher frequencies.

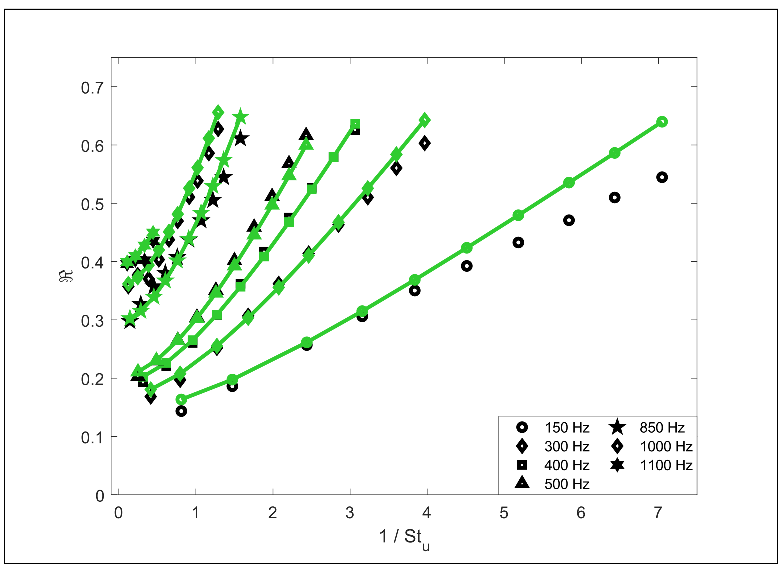

Fig. 6: Comparison of the resistance in absence of grazing flow and under high-level excitation with existing model following Eq.3 (green lines), against the in-hole particle velocity governed inverse Strouhal number.

In presence of grazing flow, the non-linear part of the resistance is determined at flow velocities of $M \approx 0.03$, 0.04 and 0.05. In Shah et al. [18] the behaviour of this resistance is shown to be governed by the ratio of in-hole particle velocity and grazing flow velocity (u/U) and follows Eq.(7). The experimentally determined value of non-linear part of resistance is shown in Fig.8 and Fig.9.

To further study the behaviour of the coefficients in Eq.(7), they are interpolated to match with the experimental results. Fig.7 shows the interpolated value of the coefficients at two different flow velocities, namely when $M \approx 0.03$, and 0.04, compared against the dimensionless ratio of Shear number and grazing flow Mach number (Sh/M). The values of these interpolated coefficients shows a linear relationship with the Sh/M ratio,

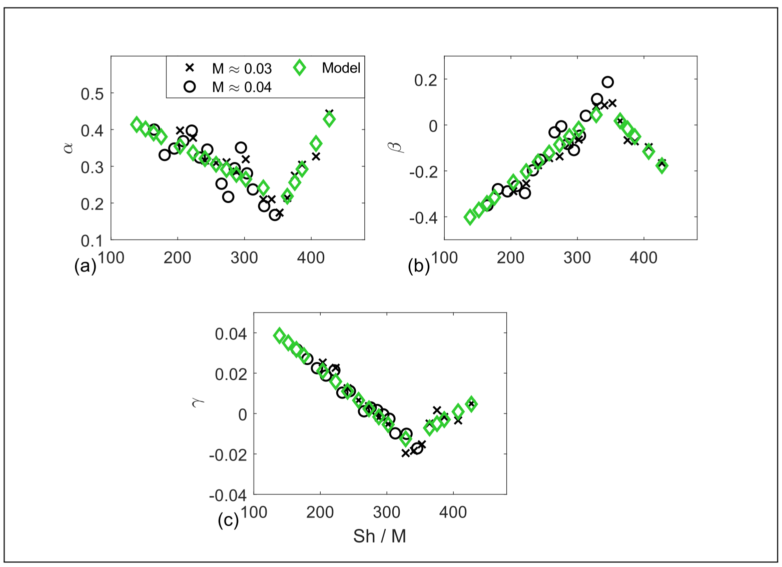

Fig. 7: Comparison of the value of the interpolated polynomial coefficients governing the non-linear part of the resistance in presence of grazing flow with model proposed in Eq. 14, against a ratio of Shear number and grazing flow Mach number. (a) Value of α; (b) Value of β; (c) Value of γ;

It can be observed that the behaviour of the interpolated coefficients completely opposite before and after the ratio of Sh/M reaches a value of ≈ 344. This is also the numerical value of the speed of sound at the in-duct temperatures. This observation, and the definition of Shear number suggests that the onset of the positive $\Re_{NL-Flow}$ values is dependent on the oscillating Stoke layer thickness and the displacement generated by the grazing flow.

This relationship of the α, β, and γ values with Sh/M is quantified in Eq.(14).

$$
\begin{aligned}
&when\ Sh/M <\approx 344; \quad \begin{matrix}\alpha \\ \beta = \\ \gamma\end{matrix} \begin{cases} -9.1X10^{-4}(Sh/M) + 0.54 \\ 2.3X10^{-3}(Sh/M) - 0.73 \\ -2.7X10^{-4}(Sh/M) + 0.076 \end{cases}, \\
&when\ Sh/M >\approx 344; \quad \begin{matrix}\alpha \\ \beta = \\ \gamma\end{matrix} \begin{cases} 3.3X10^{-3}(Sh/M) - 0.99 \\ -3.1X10^{-3}(Sh/M) + 1.15 \\ 1.9X10^{-4}(Sh/M) - 0.075 \end{cases}
\end{aligned}
\tag{14}
$$

Incorporating these coefficients in Eq.(7), the non-linear part of resistance is determined in presence of grazing flow and compared with the proposed model in Fig.8 and Fig.9. A good agreement between the model and the experiments is observed at lower flow velocities.

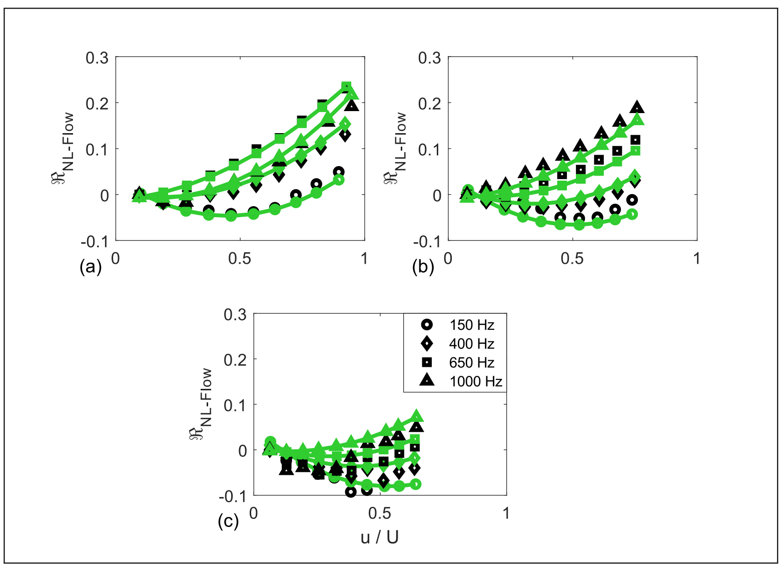

Fig. 8: Comparison of the experimentally determined non-linear part of resistance at selected frequencies (black points) in presence of grazing flow with proposed model following Eq.(7) (green lines), against ratio of in-hole particle velocity and grazing flow bulk velocity. (a) Grazing flow $M \approx 0.03$; (b) Grazing flow $M \approx 0.04$; (c) Grazing flow $M \approx 0.05$

The outlier in Fig.9 is the case of 850 Hz and the grazing flow velocity of $M \approx 0.05$. For that frequency, the value of the non-linear part of the resistance remains almost constant at lower values of u/U and the deviation is not repeated at other frequencies or flow velocities, suggesting a presence of an experimental error due to the shifting of the standing wave pattern and the presence of antinodes at the microphone location.

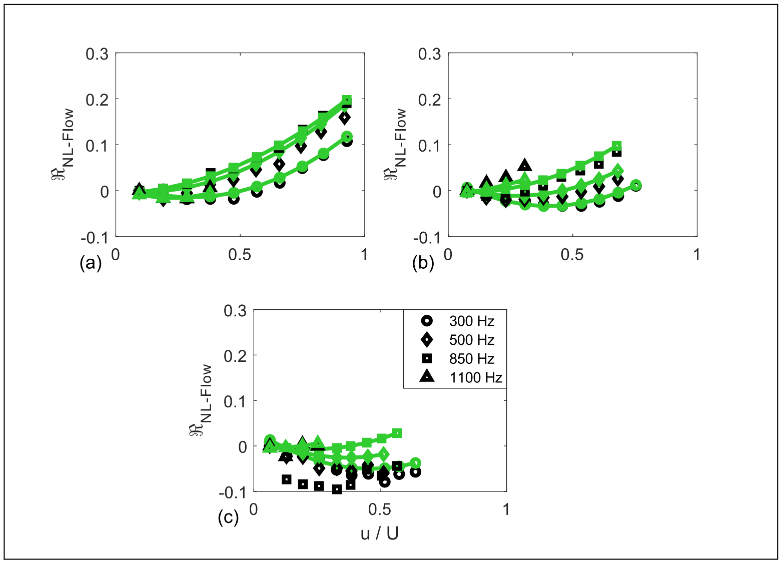

Fig. 9: Comparison of the experimentally determined non-linear part of resistance at different frequencies (black points) in presence of grazing flow with proposed model following Eq.(7) (green lines), against ratio of in-hole particle velocity and grazing flow bulk velocity. (a) Grazing flow $M \approx 0.03$; (b) Grazing flow $M \approx 0.04$; (c) Grazing flow $M \approx 0.05$

Combining the effects of grazing flow (Eq.(13)) and high-level excitation (Eq.(7) and Eq.(14)), an entire model can be proposed for the resistance of the perforate. In Fig.10, the results following such a model are compared with the experimentally determined resistance at three grazing flow velocities and two in-hole particle velocity levels.

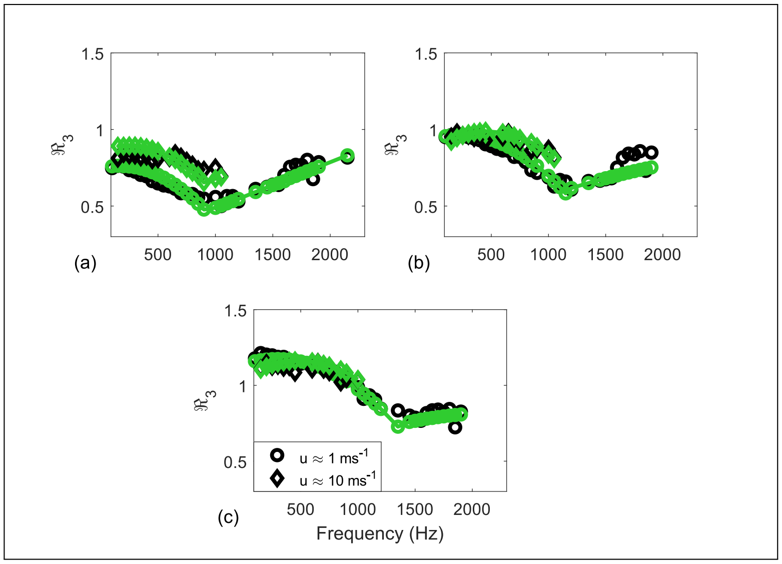

Fig. 10: Comparison of the resistance under excitation from duct-3 in presence of grazing flow at different in-hole particle velocity levels with combined model (green lines), against frequency. (a) Grazing flow $M \approx 0.03$; (b) Grazing flow $M \approx 0.04$; (c) Grazing flow $M \approx 0.05$

5. Concluding Remarks

This paper provides an insight into the usage of a novel direct method for the transfer impedance determination of a perforate, namely the three-port technique. The normalised resistance, a passive acoustic property of the perforate in presence of grazing flow and high-level excitation is studied, and experimental results are provided. Behaviour of the determined resistance is classified into two regions based on the grazing flow velocity Strouhal number. Based on the results a model is proposed which correlates the resistance with the Strouhal-, and the Mach number. The empirically determined coefficients of the equation and their dependence on the perforate properties like porosity, thickness and perforation diameters can be further studied. Under high-level excitation, dependence of resistance on the in-hole particle velocity, grazing flow velocity and shear number is shown and a relation to calculate the non-linear effect at low grazing flow velocities is shown. Lastly, experimental results under both grazing flow and high level excitation are compared with the models and agreement is shown.

Acknowledgments

This work is part of the Marie Skłodowska-Curie Initial Training Network Pollution Know-How and Abatement (POLKA). We gratefully acknowledge the financial support from the European Commission under call H2020-MSCA-ITN-2018 (project number: 813367).

References

[1] H. Bodén, L. Zhou, J. Cordioli, A. Medeiros, A. Spillere, On the effect of flow direction on impedance eduction results, in: in 22nd AIAA/CEAS Aeroacoustics Conference, 2016.

[2] P. Dean, An in-situ method of wall acoustic impedance measurements in flow ducts, Journal of Sound and Vibration 34 (1974) 97–130.

[3] E. Rice, A model for the acoustic impedance of a perforated plate liner with multiple frequency excitations, Report NASA TM-X-67950, NASA Technical Memorandum (1971).

[4] T. Melling, The acoustic impedance of perforates at medium and high sound pressure levels, Journal of Sound and Vibration (1973).

[5] A. Guess, Calculation of perforated plate liner parameters from specified acoustic resistance and reactance, Journal of Sound and Vibration 40 (1975) 119–137.

[6] M. Jones, W. Watson, B. Howerton, S. Busse-Gerstengarbe, Comparative study of impedance eduction methods, part 2: Nasa tests and methodology, in: 19th AIAA/CEAS Aeroacoustics Conference, 2013.

[7] L. Zhou, H. Bodén, C. Lahiri, F. Bake, E. L, E. T., Comparison of impedance eduction results using different methods and test rigs, in: in 20th AIAA/CEAS Aeroacoustics Conference, 2014.

[8] M. Myers, On the acoustic boundary condition in the presence of flow, Journal of Sound and Vibration 71 (1980) 429–434.

[9] Y. Renou, Y. Aurégan, Failure of the ingard–myers boundary condition for a lined duct: An experimental investigation, The Journal of the Acoustical Society of America 130 (2011) 52–60.

[10] N. Dickey, A. Selamet, M. Ciray, An experimental study of the impedance of perforated plates with grazing flow, Journal of Acoustical Society of America 110 (2001) 2360–2370.

[11] E. Feder, L. W. Dean, Analytical and experimental studies for predicting noise attenuation in acoustically treated ducts for turbofan engines nasa contractor report cr-1373, Report, NASA Technical Memorandum (1969).

[12] M. Karlsson, M. Åbom, Aeroacoustics of t-junctions-an experimental investigation, Journal of Sound and Vibration 329 (2010) 1793–1808.

[13] A. Holmberg, M. Karlsson, M. Åbom, Aeroacoustics of rectangular t-junctions subject to combined grazing and bias flows - an experimental investigation, Journal of Sound and Vibration 340 (2015) 152–166.

[14] P. Testud, Y. Aurégan, P. Moussou, A. Hirschberg, The whistling potentiality of an orifice in a confined flow using an energetic criterion, Journal of Sound and Vibration 325 (2009) 769–780.

[15] E. Moers, D. Tonone, A. Hirschberg, Strouhal number dependency of the aero-acoustic response of wall perforations under combined grazing-bias flow, Journal of Sound and Vibration 389 (2017) 292–308.

[16] M. Howe, The dissipation of sound at an edge, Journal of Sound and Vibration 70 (1980) 407–411.

[17] S. Shah, H. Bodén, S. Boij, M. D'elia, Three-port measurements for determination of the effect of flow on the acoustic properties of perforates, in: AIAA Aviation 2021 Forum, 2021.

[18] S. Shah, H. Bodén, S. Boij, Nonlinear three-port measurements for the determination of high-level excitation effects on the acoustic properties of perforates, in: 28th AIAA/CEAS Aeroacoustics Conference, 2022.

[19] S. Shah, H. Bodén, S. Boij, Flow acoustic interaction in a rectangular t-junction with mounted perforate using acoustic three-port measurements (to be published), in: 51st International Congress and Exposition on Noise Control Engineering, 2022.

[20] J. Kooi, S. Sarin, An experimental study of the acoustic impedance of helmholtz resonator arrays under a turbulent boundary layer, in: 7th AIAA Aeroacoustics Conference, 1981.

[21] A. Cummings, The effects of grazing turbulent pipe-flow on the impedance of an orifice, Acoustica 61 (1986) 233–242.

[22] R. Kirby, A. Cummings, The impedance of perforated liners subjected to grazing flow and backed by porous media, Journal of Sound and Vibration (1998).

[23] I. Sivian, Acoustic impedance of small orifices, Journal of the Acoustical Society of America 7 (1935).

[24] U. Ingård, H. Ising, Acoustic nonlinearity of an orifice, Journal of the Acoustical Society of America 42 (1967).

[25] H. Bodén, One-sided multi-port techniques for characterisation of in-duct samples with nonlinear acoustic properties, Journal of Sound and Vibration 331 (2012).

[26] J. Betts, Experiments and impedance modeling of liners including the effect of bias flow, Thesis, Virginia Polytechnic Institute and State University (2000).

[27] M. Temiz, J. Tournadre, I. Arteaga, A. Hirschberg, Non-linear acoustic transfer impedance of micro-perforated plates with circular orifices, Journal of Sound and Vibration (2016).

[28] T. Elnady, H. Bodén, On the modelling of the acoustic impedance of perforates with flow, in: 9th AIAA/CEAS Aeroacoustics Conference, Vol. AIAA 2003-3304, 2003.

[29] Y. Renou, Impédance des traitements acoustiques absorbants en conduit : effets de l'écoulement rasant et de la couche limite, Thesis, Le Mans University (2010).

[30] N. Rao, M. Munjal, Experimental evaluation of impedance of perforates with grazing flow, Journal of Sound and Vibration (1986).

[31] A. Holmberg, M. Åbom, H. Bodén, Accurate experimental two-port analysis of flow generated sound, Journal of Sound and Vibration 330 (26) (2011) 6336–6354.

[32] E. Dokumaci, A note on transmission of sound in a wide pipe with mean flow and viscothermal attenuation, Journal of Sound and Vibration 208 (1997) 653–655.

[33] M. Åbom, H. Bodén, Error analysis of two-microphone measurements in ducts with flow, The Journal of the Acoustical Society of America 83 (1988).